YEAR-END TECHNICAL REPORT

May 18, 2011 to May 17, 2012

Rapid Deployment of Engineered Solutions for Environmental Problems at Hanford

Submitted on June 18, 2012

Principal Investigators:
Leonel E. Lagos, Ph.D., PMP®
Dave Roelant, Ph.D.

FIU Applied Research Center Collaborators:
Leonel E. Lagos, Ph.D., PMP® (Project Manager)

Yelena Katsenovich, Ph.D.

Ravi Gudavalli, M.S.

Claudia Cordona, M.S, DOE Fellow

Carol Moreno, DOE Fellow

Paola Sepulveda, B.S., DOE Fellow

FIU Department of Chemistry Collaborator:
Guangliang Liu, Ph.D.

PNNL Collaborator:
Dawn Wellman, Ph.D.

Prepared for:
U.S. Department of Energy
Office of Environmental Management
Under Grant No. DE-EM0000598

Addendum:

This document represents one (1) of five (5) reports that comprise the Year End Reports for the period of May 18, 2011 to May 17, 2012 prepared by the Applied Research Center at Florida International University for the U.S. Department of Energy Office of Environmental Management under Cooperative Agreement No. DE-EM0000598.

The complete set of FIU's Year End Reports for this reporting period includes the following documents:

1. Chemical Process Alternatives for Radioactive Waste
   Document number: FIU-ARC-2012-800000393-04b-211
2. Rapid Deployment of Engineered Solutions for Environmental Problems at Hanford
   Document number: FIU-ARC-2012-800000438-04b-208
3. Remediation and Treatment Technology Development and Support
   Document number: FIU-ARC-2012-800000439-04b-210
4. Waste and D&D Engineering and Technology Development
   Document number: FIU-ARC-2012-800000440-04b-212
5. DOE-FIU Science & Technology Workforce Development Initiative
   Document number: FIU-ARC-2012-800000394-04b-059

Each document has been submitted to OSTI separately under the respective project title and document number as shown above.

TABLE OF CONTENTS

LIST OF FIGURES

LIST OF TABLES

EXECUTIVE SUMMARY

The reprocessing of irradiated fuel in Hanford's 200 Area to obtain plutonium for the atomic weapons has left a legacy of uranium contamination in the vadose zone (VZ). This contamination created a potential future source for groundwater contamination and risk to receptors through water uptake from contaminated wells or discharges to surface water. The investigation under task 1.1 targets uranium (U) contamination in the VZ of the 200 Area that may affect potential discharges to the Columbia River via groundwater migration. Injection of reactive gases such as NH_3 is an innovative technology that targets uranium (U) contamination in the vadose zone to reduce the potential for radionuclides mobility in subsurface. The vadose zone at Hanford is composed of sediments containing a complex of mineral phases rich in quartz, feldspar, mica, clays, and calcium carbonate common in layers and lenses of caliche. The silica content in the 200 Area sediment compositions was found in a much higher value than the other elements, followed closely by aluminum. The injection of ammonia gas in a vadose zone causes the formation of NH_4OH following a subsequent increase in pH. The alkaline conditions can greatly enhance the solubility rates of most Al- and Si-containing minerals by many orders of magnitude. The following decrease in pH will cause uranium co-precipitation during the recrystallization of minerals. Little is known about the effect of Si, Al, Ca and bicarbonate ions on the U co-precipitation process. Hence, this research was conducted to improve our understanding of the possible mechanisms for U removal from the solution mixture imitating porewater composition. For simplicity, the early stage of experiments was limited to only four elements: Si, Al, U, and inorganic C in the form of bicarbonate. Later, Ca was included into the solution mixture. The study involves a series of batch experiments to evaluate the effect of concentration ratios of silicon and aluminum, in the presence of various bicarbonate concentrations and calcium ion, on the co-precipitation process of U(VI) in the conditions mimicking vadose zone pore water composition.

Research under task 1.2 investigates the effect of bicarbonate on the autunite mineral microbial dissolution by the *Arthrobacter* G968 strain, soil bacteria previously isolated from Hanford Site soil. Previous assessment showed that the G968 strain has a lower ability to tolerate U(VI) toxicity compared to G975, the most tolerant strain found during the assessment of three microorganisms obtained from the Subsurface Culture Collection. Besides being the most tolerant to U(VI) toxicity, G975 strain U(VI) accumulation capacity was found to be almost triple the value obtained for G968, used in the current study.

Last year's report presented data on autunite mineral dissolution by the *Arthrobacter* G975. The results on this study were published in *Chemical Geology* (Katsenovich, Y. P., Carvajal, D.A., Wellman, D. M., and L. E. Lagos, 2012) in an article entitled, "Enhanced U(VI) release from autunite mineral by aerobic *Arthrobacter* sp. in the presence of aqueous bicarbonate," (*Chemical Geology*, 308-309, 1-9).

In addition, results on the effect of bicarbonate and Ca ions on the biosorption of uranium by G975 cells, previously summarized in the progress report, are included in the Appendix. The presence of calcium and bicarbonate ions in synthetic groundwater affects the sorption behavior of U(VI) due to the formation of highly soluble and stable uranyl-carbonate and calcium uranyl carbonate complexes that reduce adsorption of U(VI). In the presence of bicarbonate, when highly soluble and mobile carbonate complexes dominate the aqueous speciation of U(VI), the

viability of cells treated with U(VI) was noted to increase. The manuscript on this study was submitted for peer-review.

The report also includes results and findings for Task 1.3, Effect of Bicarbonate on the Dissolution of Meta-Autunite, which were not incorporated in the 2010 Year End Report. The results of the experiments provide an additional understanding on the effect of bicarbonate ions on the uranium rate of release from autunite mineral, which may add value to remediation efforts at Hanford.

ACRONYMS

AFM- atomic force microscope

µg/L- parts per billion (ppb)

atm- atmosphere

bgs- below ground surface

C- Celsius

CFU- colony forming units

DIW- deionized water

DOE- U.S. Department of Energy

EDS- energy-dispersive spectroscopy

FTIR- Fourier Transform Infrared Spectroscopy

HEPES-Na-2-(2-hydroxyethyl)-1-piperazine ethanesulfonic acid sodium salt hydrate

HMDS- hexamethyldisilazane

ICP-OES- inductively coupled plasma optical emission spectroscopy

KPA- Kinetic Phosphorescence Analyzer

mg/L- parts per million (ppm)

Na_2EDTA- ethylenediaminetetra-acetic acid disodium salt

NH_3 - ammonia gas

SEM- scanning electron microscopy

SGW- synthetic groundwater

SMCC- Subsurface Microbial Culture Collection

SPW- synthetic pore water

XPS- X-ray photoelectron spectroscopy

XRD- X-ray diffraction

INTRODUCTION

The Hanford Site was the first nuclear production facility in the world serving a key role in the nation's defense for over 40 years. Now, the Hanford Site has become the second largest cleanup project. Located on the Columbia Plateau of southeastern Washington State, the site was built in 1943 as part of the Manhattan Project for the production of plutonium for the first atomic weapons. From 1944 to1980, the facilities of the Hanford Site were involved in the production of nuclear fuel (Young and Fruchter 1991). The fabrication of natural and slightly enriched uranium into fuel elements for nuclear reactors in Hanford's 300 Area, and the reprocessing of irradiated fuel in Hanford's 200 Area to obtain plutonium and other useful radioisotopes, generated large amounts of radioactive waste containing uranium, among other constituents. This waste was stored in underground storage tanks (USTs). There are 149 underground single-shell tanks (SST) used to store radioactive mixed waste; sixty-seven of these SSTs have been classified as assumed/confirmed leakers, which have leaked contaminants into the surrounding soil, producing waste streams depositing into the subsurface. Approximately 200,000 kg of uranium was released into the ground at the 200 East and 200 West Areas. These leakages influenced the vadose zone by creating a potential future source for groundwater contamination and risk to receptors through water uptake from contaminated wells or discharge to surface water. Despite extensive remediation efforts initiated in the early 1990s, uranium groundwater plumes identified in multiple locations around the site have persisted for many years. The protection of water resources from contaminated groundwater resulting from operations at the Hanford Site is a key element of the overall Hanford cleanup program.

Due to the complex chemistry of uranium, a predictive understanding of its mobility in the subsurface is limited. In neutral or basic pH conditions, uranium undergoes hydrolysis in aqueous solution and can readily complex with a wide variety of ligands (Grenthe et al. 1992, Langmuir 1997). These complexation reactions often result in the formation of mobile aqueous species or precipitation of U-bearing minerals. Environmental factors, such as pore water ion composition have tremendous effect on both uranium and its mineral phases. Additional research is necessary to understand the effect of these factors on the behavior of U(VI) in groundwater and sediments.

Pore water in the vadose zone is under the influence of carbon dioxide partial pressures that exceed atmospheric (P_{CO2}=10^-3.5atm) (Karberg et al. 2005). In the oxidized carbonate-buffered environments, the behavior of uranium is greatly affected by the presence of carbonates since U(VI) tends to form complexes with carbonate ions. Their mobility in aquifers under circumneutral pH conditions is explained by the formation of highly soluble and stable uranyl-carbonato complexes, $UO_2CO_3^0$, $UO_2(CO_3)_2^{2-}$ and $UO_2(CO_3)_3^{4-}$(Langmuir 1978, Guillaumont et al. 2003). At high pH between 9 and 11, most actinides reside as negatively charged hydroxide or carbonate (CO_3^{2-}) species, such as $(UO_2)_2(OH)_5^-$ and the tris(carbonato) complex $UO_2(CO_3)_3^{4-}$. The structure of the latter mononuclear complex exhibits the hexagonal uranyl coordination where the three carbonate ligands in a bidentate coordination are located in the equatorial plane of the uranyl moiety (Schlosser 2010) (Figure 1). The surfaces of most solids are negatively charged at these pH values and are unlikely to adsorb ionic species, which can explain why the formation of negatively-charged, highly soluble U(VI)-carbonate species typically suppress U(VI) sorption in circumneutral and alkaline conditions (Um et al. 2007a).

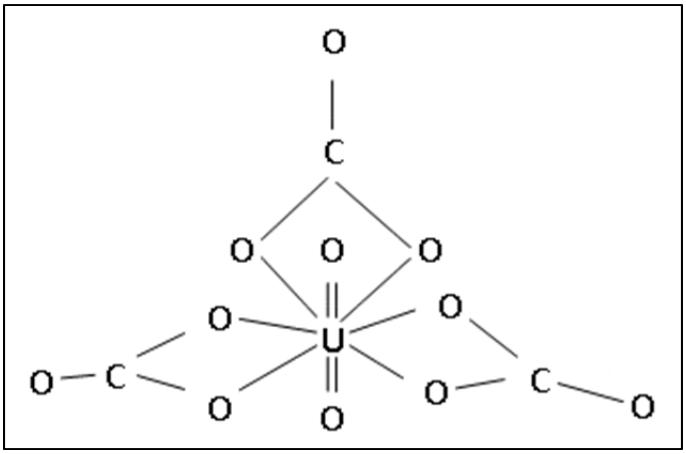

Figure 1. The structures of uranyl carbonate complexes $[UO_2(CO_3)_3]^{4-}$.

Calcium (Ca) is a common aqueous cation found in equilibrium with calcite in porewater and groundwater at many sites contaminated with U. Ca can complex with U(VI) in bicarbonate solutions to form calcium-uranyl-carbonate species such as $Ca_2UO_2(CO_3)_3^{o}(aq)$ and $CaUO_2(CO_3)_3^{2-}$. Their large formation constants (Guillaumont et al. 2003) suggest that Ca can affect U(VI) fate and transport due to the formation of soluble and stable calcium-uranyl-carbonate complexes in aqueous solution. Generally, high soil pH and increased potential for complexation with carbonate and calcium indicate high possibility for U(VI) mobility in the soil.

During fiscal year 2011, FIU ARC conducted two subtasks under Task 1 of this project: Task 1.1, Sequestering Uranium at the Hanford 200 Area by In-Situ Subsurface pH Manipulation Using Ammonia (NH_3) Gas Injection, and Task 1.2, Investigation on Microbial-Meta-Autunite Interaction: the Effects of Bicarbonate and Calcium Ions. Results on the effect of bicarbonate and Ca ions on the biosorption of uranium by G975 cells, previously summarized in the progress report, are included in the Appendix.

This report also includes results and findings for Task 1.3, Effect of Bicarbonate on the Dissolution of Meta-Autunite, which were not included in the 2010 Year End Report.

TASK 1.1 SEQUESTERING URANIUM AT THE 200 AREA BY IN SITU SUBSURFACE PH MANIPULATION USING NH_3 GAS

TASK 1.1 BACKGROUND

Injection of reactive gases such as NH_3 is an innovative technology used to decrease uranium mobility in subsurface contaminated with radionuclides. This task investigates the mechanisms and effectiveness of NH_3 gas injection on the removal of uranium (VI). The injection of ammonia gas in a vadose zone causes the formation of NH_4OH following a subsequent increase in pH that can potentially induce the dissolution of silica and aluminum from soil minerals. The subsequent decrease in pH to natural conditions would lead to precipitation of aluminosilicates that could possibly coat sequestered contaminants in a process called co-precipitation (Szecsody et al. 2010). This technology has significant uncertainness at the 200 Area site vadose zone specific conditions and requires additional testing in the laboratory to understand the effect of various factors on the formation and precipitation of uranium-bearing mineral phases. Particularly what requires clarification are the roles of major pore water constituents and the time for the formation of precipitates after the NH_3 injection. This task also involves the characterization studies of silica-aluminum precipitates created after NH_3 gas injection.

Silicate Chemistry and Its Interaction with Aluminum, Calcium and Uranium

Silicates are one of the most abundant compounds found in the earth's crust. The soluble form of silica is monomeric with one silicon atom formulated as $Si(OH)_4$, which is generally called monosilicic acid. The structure is based on SiO_4-tetrahedra and involves silicon surrounded by four oxygen atoms; the silicon atom shares an electron with each of the four oxygen atoms.

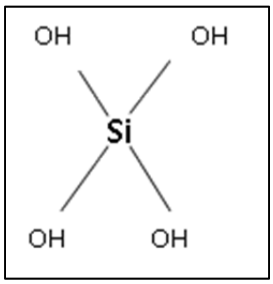

Having two valence electrons, oxygen can form an additional bond with another metal atom or a bond with a second silicon. This possibility leads to polymerization reactions by the linkage of SiO_4^- tetrahedra through Si – O – Si (siloxane) bonds. Therefore, silica can be regarded as a polymer of silicic acid, consisting of interlinked SiO_4 tetrahedral:

$$– Si – OH + OH – Si = H_2O + –Si – O – Si–$$

These reactions produce the hydrated silica polymers with molecular weights of up to ~100,000 consisting of dense spherical particles less than about 50A in diameter. The highly polymerized species form colloidal particles with the size larger than 50A. It is known that dissolved monosilicic acid is stable for a long period at concentrations less that 0.007-0.1% (Iler 1979). When the concentration of $Si(OH)_4$ exceeds this amount, the monomers polymerize rapidly,

initially forming polysilicic acids of low molecular weight and then larger polymeric species or colloidal silica particles. Under alkaline conditions from pH 9 to 10.7, the solubility of amorphous silica is increased due to the formation of silicate ion in addition to the monomer that are in equilibrium with the solid phase. Silica polymerization is a reversible process. At pH above 10.7, the amorphous silica dissolves to form soluble silicate, and no amorphous solids remain in equilibrium, making orthosilicic acid the dominant silica species (Iler 1979).

The removal of silica from water may occur by deposition, adsorption or precipitation reactions that involve the formation of solid silica as a coating or a solid surface or as crystals. The deposition of monomeric silica forms an impervious glass-like film on the surface, whereas colloidal particles can produce a porous film. The deposition of silica from supersaturated solutions is often brought about by lowering the pH of the aqueous solution of a soluble silicate below ~10.7. Regardless of the type of material on which silica is deposited, after more than a monolayer of silica has been absorbed, further deposition of silica is always on a silica surface. If the concentration of monomeric silica is too high, it polymerizes by itself, forming silica particles or nuclei on which silica is deposited. These particles have a very high specific surface area and much of the soluble silica is then deposited on these colloidal particles. At pH 11, all the silica will be dissolved as soluble silicate; therefore, the pH cannot exceed this value. Iler (1979) has described the deposition of an impervious film of silica on a wide variety of surfaces.

The formation of amorphous silica particles by polymerization of $Si(OH)_4$ involves some aspects of the theory of nucleation. Nucleation implies the formation of critical clusters called nuclei after which crystal growth occurs spontaneously (Stumm and Morgan 1996). The presence of impurities such as $Al(OH)_3$ colloids or aluminum silicates, playing the role of nucleation clusters, can accelerate these reactions. When Si and Al are present together at high pH, the prominent species in solution would include $Si(OH)_4$, $SiO(OH)_3^-$, $SiO_2(OH)_2^{2-}$, and $Al(OH)_4^-$. The reaction between the uncharged silica species $Si(OH)_4$ and the charged alumina species $Al(OH)_4^-$ will form aluminosilicate chains joined by shared oxygen atoms as follows:

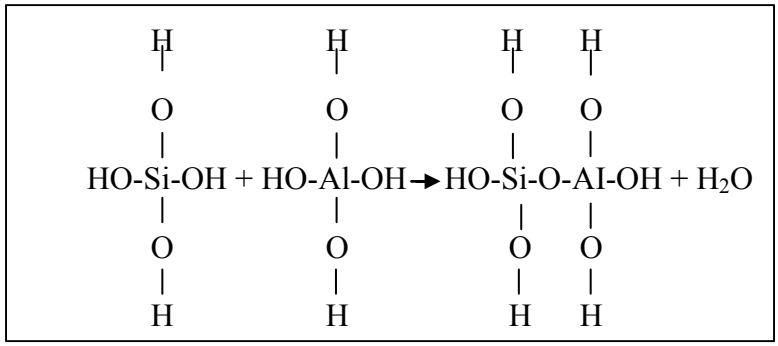

The silica species $Si(OH)_4$ is considered to be the important species for this reaction given that the other two Si species, $SiO(OH)_3^-$ or $SiO_2(OH)_2^{2-}$, are negatively charged, preventing them from coming into contact with $Al(OH)_4^-$.

At pH above 8-9, the predominant aluminum species in solution is the aluminate ion, $Al(OH)_4^-$ (Arnson 1982). Aluminate ions make important modifications to the silica surface. Geometrically, the aluminate ion $Al(OH)_4^-$ is depicted by a regular tetrahedron, with the

aluminum atom located in the center and the hydroxide ions forming the corner points (Gasteiger et al. 1992). Polymerization reactions of aluminum and silicon tetrahedra create an alumino-silicate anion; excess silica must be present at the reaction (Iler 1979). The alumina- modified colloidal silica are negatively charged in a wide range of pH down to 3, compared to pure silica, which is negatively charged by the adsorption of hydroxyl ions above pH 7 but loses the charge in acidic solutions. In the precipitation process, coagulation forces drive particles aggregation. Silica is not precipitated from solution at any pH in the absence of a coagulant (Iler 1979). Calcium is one of the metals that can cause Si aggregation reactions to convert it to calcium silicate.

TASK 1.1 OBJECTIVES

The objective of this task is to assess the roles of major pore water constituents and time on the formation of precipitates after NH_3 injection to the vadose zone of the Hanford Site 200 Area. This task examined the effect of concentration ratios of silicon and aluminum, in the presence of various bicarbonate concentrations and calcium ion, on the co-precipitation process of U(VI) under conditions imitating the pore water of the 200 Area vadose zone. Parallel studies have focused on the detailed characterization of the uranium-bearing precipitates created after ammonia gas injection. Mineralogical and morphological characterization experiments of U(VI)-bearing precipitates were initiated by means of X-ray diffraction (XRD), scanning electron microscope energy-dispersive spectroscopy (SEM-EDS), fourier transform infrared spectroscopy (FTIR) and some samples with X-ray photoelectron spectroscopy (XPS). Future studies will examine the solubility of uranium precipitates over the pH range of 6 to 11 in the presence of bicarbonate, calcium, and major pore water anions and cations to evaluate the migration potential of radionuclides that still reside in the vadose zone.

TASK 1.1 MATERIALS AND METHODS

The composition of pore water has been previously characterized in terms of concentrations of major cations (Al, Ba, Ca, Fe, K, Mg, Na, Si, Sr), anions (NO_3, F, NO_2, Cl, SO_4, PO_4, HCO_3), and pH (Serne et al. 2008). The concentrations of ions and uranium for different sediment layers were averaged and the summary was presented in the FY2010 report. For the initial experiments, the complicated pore water composition was simplified to have only four components in the test solutions: uranium, silica, aluminum, and bicarbonate. In addition, calcium was used in the later stages of the experiments. At first, two relatively low concentrations of U(VI) were tested: 0.5 ppm and 2.0 ppm. Due to similarities between results on the U(VI) removal for both U(VI) concentrations, the following experiments were continued with only 2 ppm U(VI).

Past observations showed that the concentration of Al released during the dissolution from soil by 1 mol L^{-1} NaOH is relatively small, resulting in 5.1 mM of Al in the soil solution (Qafoku et al. 2003). Because of increasing soil pH, the concentration of Si in pore water was observed to be as high as 10 g L^{-1} (Szecsody 2010). For these reasons, the tests were carried out with varied Si concentrations such as 5 mM, 50 mM, 100 mM, 150 mM, 200 mM, and 250 mM to study different Si:Al molar ratios. The experiments were run by limiting Si concentration to a maximum of 250 mM (7.0 g L^{-1}) since the increase in Si concentration up to 10g L^{-1} doesn't show a difference on the results of U(VI) removal. The Al concentrations tested were 2.8 mM

and 5 mM. The 2.8 mM Al concentration represents a value that is between the highest observed Al concentration in the pore water of the Hanford Site 200 Area, which is about 0.8 mM Al, and the concentration of Al released during the dissolution from soil by 1 mol L-1 NaOH reported by Qafoku et al. (2003), which was 5.1 mM Al. The initial experiments with 2.8 mM of Al were initiated last year and the experimental results for three tested sets of 0 mM, 2.9 mM and 25 mM of HCO_3 were presented in the last Year End Report. This report extends to demonstrate the complete range of data for U(VI) removal in the presence of 2.8 mM (batches 4 through 6, Table 1) and 5 mM of Al across all Si and HCO_3 concentrations tested. In addition, 5 mM of Ca ion was included in the water composition to evaluate its effect on the U(VI) removal.

Sample Preparation Procedures

Sample preparation procedures at different molar ratios of Si:Al have included mixing a measured volume of the silicate stock solution with a measured volume of the aluminum stock solution. This mixture has then been added to the test solution with a measured volume of the appropriate bicarbonate stock solution (unless no bicarbonate was used). The pH of the resulting solution was adjusted to 8.0 by titration with concentrated nitric acid; deionized water (DIW) was added to each test solution so that each test solution had a total final volume of 50 mL. The pH value of 8.0 was previously observed in the pore water at the Hanford Site 200 Area vadose zone (Serne et al. 2008). After that, NH_3 gas (5% NH_3 in 95% N_2) was injected into each solution through 20 µm pores of a metal gas sparger (Mott Corporation) until the pH of the solution reached a value of approximately 11 (Figure 2).

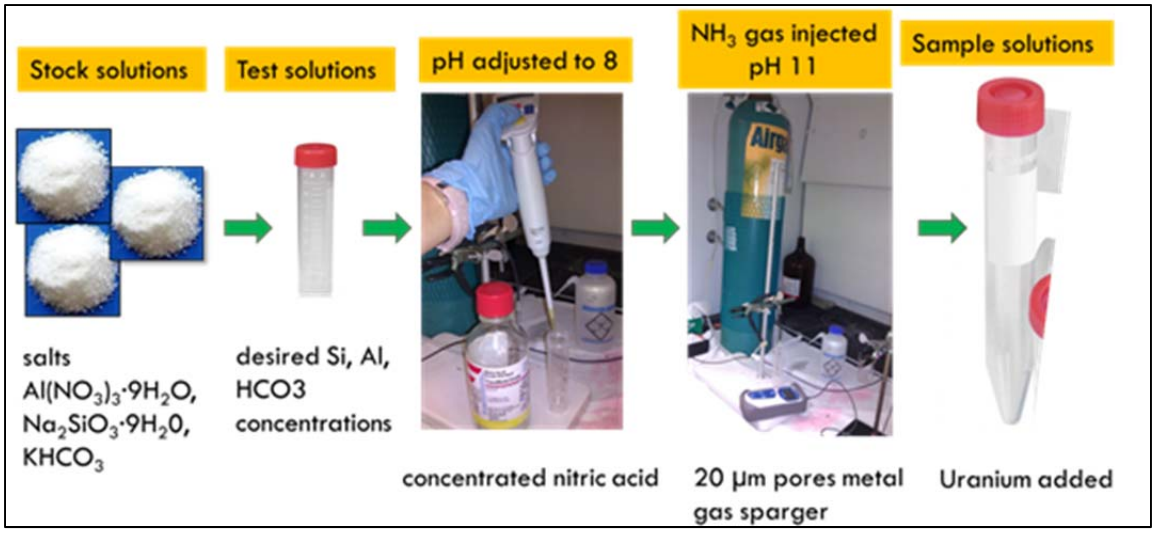

Figure 2. Experimental procedure.

Then, duplicate samples, each with a volume of 5 mL, were extracted from each test solution and added to individual polyethylene 15-mL tubes to amend with a U(VI) concentration of 0.5 ppm or 2 ppm. Control samples were prepared in DIW amended with U(VI) at concentrations of 0.5 ppm and 2 ppm U(VI) to test for U(VI) losses from the solutions due to sorption to tube walls and caps. All control and experimental tubes were kept in an incubator/shaker at 100 rpm and at a temperature of 25 °C. After two days, the solutions were centrifuged for 15 minutes at 4000

rpm and analyzed for U(VI), Si, and Al. Preliminary experiments showed that the removal efficiency of U(VI) reached a plateau level after two days of agitation on the shaker.

There were three remaining bicarbonate concentrations in the experimental sets of 2.8 mM of Al, six sets for 5 mM of Al and six sets for 5 mM of Al amended with 5 mM of Ca. A set with 2.8 mM of Al was prepared with two different U (VI) concentrations, 0.5 ppm and 2 ppm. The following sets were continued with only 2 ppm of U (VI) tested. Each set had six different test solutions prepared in duplicate with a different Si:Al molar ratio, for a total of about 200 sample solutions, including control samples. Table 1 presents a description of the experimental matrix.

Si/Al molar ratios for the solution mixtures amended with 2.8 mM of Al and Si concentrations of 5 mM, 50 mM, 100 mM, 150 mM, 200 mM, and 250 mM (Table 1) correspond respectively to 1.8, 17.6, 35.2, 52.8, 70.4, 88.0. Si/Al molar ratios for 5 mM of Al and the same Si concentrations match to 1, 10, 20, 30, 40, 50, respectively.

In addition, the effect of Si on the formation of U precipitates was evaluated in the experimental runs, prepared without Si when only Al, bicarbonate and U(VI) were present in the solution. Several analogous controls prepared without Al in the solution mixture helped to evaluate its effect on the removal of U(VI).

Table 1. Experimental Matrix

Batch number	**HCO_3, mM**	**Initial Si concentrations in the solution mixture, mM**					
1	0	5	50	100	150	200	250
2	2.9	5	50	100	150	200	250
3	25	5	50	100	150	200	250
4	50	5	50	100	150	200	250
5	75	5	50	100	150	200	250
6	100	5	50	100	150	200	250
Batch number	**HCO_3, mM**	**Si:Al molar ratio (Al=2.8mM)**					
1	0	1.8	17.6	35.2	52.8	70.4	88.0
2	2.9	1.8	17.6	35.2	52.8	70.4	88.0
3	25	1.8	17.6	35.2	52.8	70.4	88.0
4	50	1.8	17.6	35.2	52.8	70.4	88.0
5	75	1.8	17.6	35.2	52.8	70.4	88.0
6	100	1.8	17.6	35.2	52.8	70.4	88.0
Batch number	**HCO_3, mM**	**Si:Al molar ratio (Al=5mM)**					
1	0	1	10	20	30	40	50
2	2.9	1	10	20	30	40	50
3	25	1	10	20	30	40	50
4	50	1	10	20	30	40	50
5	75	1	10	20	30	40	50
6	100	1	10	20	30	40	50

Stock solutions of Al (50 mM), Si (422 mM), and HCO_3^- (400 mM) were first prepared in deionized water (DIW) from the salts $Al(NO_3)_3 \cdot 9H_2O$, $Na_2SiO_3 \cdot 9H_20$, and $KHCO_3$, respectively (Table 2), the final volume of these solutions being 50 mL in order to reach desired concentrations. The 100 ppm stock solution of uranyl nitrate dissolved in DIW was prepared from uranyl nitrate hexahydrate 1000 ppm stock (Fisher Scientific).

Table 2. Stock Solutions Used to Prepare Various Si/Al Molar Ratios

Stock Solution	Salt Used	Molecular Weight of Salt (g/mol)	Stock Solution Concentration (mM)	Amount to prepare 50 mL (g)
Bicarbonate	$KHCO_3$	100.114	400.00	2.002
Metasilicate	$Na_2SiO_3 \cdot 9H_2O$	284.196	422.24	5.998
Aluminum	$Al(NO_3)_3 \cdot 9H_2O$	375.129	50.00	0.938
Calcium	$CaCl_2 \cdot 2H_2O$	147.01	1250.0	9.188

Analytical Procedures

Samples of the supernatant from each vial were analyzed to determine the remaining U(VI) concentration in each solution using a Kinetic Phosphorescence Analyzer KPA-11 (Chemcheck Instruments, Richland, WA) instrument, and to determine the remaining Al, Si, and Ca concentrations in each solution, using inductively coupled plasma-optical emission spectroscopy (ICP-OES) (PerkinElmer). In addition, the accuracy of the initial Al, Si, and Ca stock solutions, prepared by weight, were tested with ICP-OES.

For analysis with the KPA machine, an aliquot was extracted from the supernatant of each test sample and diluted with 1% nitric acid between 5 to 100 times. For analysis with the ICP-OES machine, an aliquot extracted from the supernatant of each test sample was diluted between 100 to 200 times with DIW in conical polypropylene tubes. Total organic carbon (TOC) of supernatant solutions was analyzed using a Shimadzu TOC analyzer with an autosampler (TOC-V CSH). Each analysis was repeated until the standard deviation was less than 3%.

Speciation Modeling

Equilibrium speciation modeling was performed by means of Visual MINTEQ (v. 3.0, maintained by J.Gustafsson at KTH, Sweden, available at http://www.lwr.kth.se/English/OurSoftware/vminteq/ updated with the Nuclear Energy Agency's thermodynamic database for uranium) to identify the predominant uranium species. The software was used to calculate uranium speciation in the presence of Si, Al, HCO_3 and Ca ions and 2ppm of U. The example in Table 3 presents elemental concentration data for utilized silica, bicarbonate, 5 mM Al and 5 mM Ca ion concentrations with the addition of 2 ppm of U(VI). All concentrations were entered for the model calculations to give the most important species with respect to uranium complexation. The temperature was set to 25^oC and the CO_2 pressure was fixed to atmospheric pressure ($3.9 \cdot 10^{-4}$ bar) as the samples were in contact with air during the experiment. Table 4 presents elemental concentration data considered for speciation. The resulting charge difference in the anion and cation balance was no more than 7%.

Table 3. Stock Solutions Considered for Speciation Modeling of 2 ppm U

Stock Solution	Concentration (mM)					
	HCO_3+ *Si + 5 Al + 5 Ca + 2ppm U					
$KHCO_3$	0	3	25	50	75	100
$Al(NO_3)_3$	5	5	5	5	5	5
$Na_2SiO_3 \cdot 9H_2O$	*5-250	*5-250	*5-250	*5-250	*5-250	*5-250
$CaCl_2 \cdot H_2O$	5	5	5	5	5	5
$UO_2(NO_3)_2 \cdot 6H_2O$	0.0084	0.0084	0.0084	0.0084	0.0084	0.0084
HNO_3	Calculated from difference between anions and cations					
5% NH_3+ 95% N_2 GAS	Adjusted in each case to reach pH~11					

*Si concentrations: 5, 50, 100, 150, 200, and 250 mM

Table 4. Input Components for Speciation Modeling with Ca Ions

Minteq components input	Concentration (mM)								
	H^{+1}	*Si (H_4SiO_4)	Al^{+3}	$CO_3^{-}_2$	K^{+1}	Cl^{-1}	Ca^{+2}	**Na^{+1}	U(VI) (UO_3)
* Si + 0mMHCO_3 + 5mM Al + 5 mM Ca + 2ppm U	0	*5-250	5	0	0	10	5	*10-500	0.084
*Si + 3 mM HCO_3 + 5mM Al + 5 mM Ca + 2ppm U	3	*5-250	5	3	3	10	5	*10-500	0.084
*Si +25 mM HCO_3 + 5 mM Al + 5 mM Ca + 2ppm U	25	*5-250	5	25	25	10	5	*10-500	0.084
*Si +50 mM HCO_3 + 5 mM Al + 5 mM Ca + 2ppm U	50	*5-250	5	50	50	10	5	*10-500	0.084
*Si +75 mM HCO_3 + 5 mM Al + 5 mM Ca + 2ppm U	75	*5-250	5	75	75	10	5	*10-500	0.084
*Si+100 mM HCO_3 + 5 mM Al + 5 mM Ca + 2ppm U	100	*5-250	5	100	100	10	5	*10-500	0.084
NH_3 GAS	Adjusted in each case to reach pH~ 11								

*Si concentrations: 5, 50, 100, 150, 200, and 250 mM **Na^{+1}: 10,100, 200, 300, 400, and 500 mM

Methods for Mineralogical and Morphological Characterization of U(VI)-bearing Precipitates

In the parallel experiments, dried uranium-bearing precipitates, created after NH_3 gas injection, were characterized via SEM-EDS, FTIR, XRD, and some samples with XPS analysis. The analytical results in combination with the thermodynamic speciation modeling of the

experimental systems allowed to identify mineral phases, structural features of the amorphous precipitates and the oxidation stage of U(VI) co-precipitated with the polymerized silica gel.

Sample preparation procedures for the characterization studies of the U(VI)-bearing precipitates followed the same routine as for the U(VI) removal experiments. Table 5 presents the concentrations of aluminum, silica and bicarbonate in the testing solutions used throughout the study. In set #1, the test samples were each amended with a U(VI) concentration of 2.0 ppm. In set #2 four new test samples were each amended with a U(VI) concentration of 30 ppm. For set #3 four new test samples were each amended with 130 ppm U(VI). In each set, control samples were prepared in DIW amended with U(VI) at concentrations of 2.0 ppm, 30 ppm, and 130 ppm to account for U(VI) losses from the solutions due to sorption to the tube's walls and caps. All control and experimental tubes were kept for 2 days in an incubator/shaker at 100 rpm and temperature of 25°C. Then, the solutions were centrifuged for 5 minutes at 4000 rpm and analyzed for U(VI), Si, and Al. There were a total of three experimental sets to conduct precipitate characterization studies, each with a specific U(VI) concentration and variations of aluminum, silica and bicarbonate concentrations (Table 5). From each test solution, the supernatant was decanted. The residue, in the form of a gel, was transferred into small plastic sample cups. The sample cups were placed in the incubator for drying at a temperature of 30°C for about one week. The dry, solidified pellets were subsequently used for SEM-EDS, FTIR, and XRD. Only four samples were tested for XPS due to the low value of U atomic percentage found in the previous samples.

Table 5. Experimental Sets

	Set#1	Set#2	Set#3
SEM/EDS	100 mM Si + 5 mM Al + 0 mM HCO3 + 2 ppm U	100 mM Si + 2.8 mM Al + 25 mM HCO3 + 30 ppm U	100 mM Si + 5 mM Al + 3 mM HCO3 + 130 ppm U
	100 mM Si + 5 mM Al + 3mM HCO3 + 2 ppm U	100 mM Si + 2.8 mM Al + 50 mM HCO3 + 30 ppm U	100 mM Si + 5 mM Al + 50 mM HCO3 + 130 ppm U
	100 mM Si + 5 mM Al + 100 mM HCO3 + 2 ppm U	100 mM Si + 5 mM Al + 3 mM HCO3 + 30 ppm U	50 mM Si + 5 mM Al + 3 mM HCO3 + 130 ppm U
		100 mM Si + 5 mM Al + 25 mM HCO3 + 30 ppm U	50 mM Si + 5 mM Al + 50 mM HCO3 + 130 ppm U
FTIR	100 mM Si + 5 mM Al + 3mM HCO3 + 2 ppm U (gel)	100 mM Si + 2.8 mM Al + 50 mM HCO3 + 30 ppm U	50 mM Si + 5 mM Al + 3 mM HCO3 + 130 ppm
	100 mM Si + 5 mM Al + 3mM HCO3 + 2 ppm U		100 mM Si + 5 mM Al + 3 mM HCO3 + 130 ppmU
	100 mM Si + 5 mM Al + 50mM HCO3 + 2 ppm U		
	250 mM Si + 5 mM Al + 50mM HCO3 + 2 ppm U		
XRD	100 mM Si + 5 mM Al + 3mM HCO3 + 2 ppm U		
	250 mM Si + 5 mM Al + 50mM HCO3 + 2 ppm U		
XPS			100 mM Si + 3 mM HCO3 + 5 mM Al + 130 ppm U
			100 mM Si + 50 mM HCO3 + 5 mM Al + 130 ppm U
			50 mM Si + 3 mM HCO3 + 5 mM Al + 130 ppm U
			50 mM Si + 50 mM HCO3 + 5 mM Al + 130 ppm U

Speciation Modeling for Characterization of Precipitates

The concentrations of the elements used in the solutions preparation (Table 6) were entered so that model calculations could provide information about the most important species with the respect to uranium complexations at U(VI) concentration of 130 ppm.

For each sample's speciation, the H^{+1} concentration value entered comes from the concentration of the $KHCO_3$ added. The Si (H_4SiO_4) concentration entered comes from the concentration of the Na_2SiO_3 - $9H_2O$ added. The Al^{+3} concentration entered comes from the concentration of Al $(NO_3)_3$. The concentration of CO_3^{-2} entered comes from the concentration of $KHCO_3$ added. The concentration of K^+ entered comes from the concentration of $KHCO_3$ added as well. The Na^+ entered concentration comes from multiplying the concentration of $Na_2SiO_3 \cdot 9H_2O$ times 2. The concentration of U(VI) (UO_3) added comes from the uranium concentration used in the specific set. Finally, the N (NO_3^-) concentration entered was calculated by subtraction, in order to obtain the same concentration of anions and cations for the speciation in total.

Table 6. Stock Solutions Considered for Speciation Modeling of 130 ppm U

Stock Solution	**Concentration (mM)**			
	100 mM Si + 3 mM HCO_3 + 5 mM Al + 130 ppm U	100 mM Si + 50 mM HCO_3+ 5 mM Al + 130 ppm U	50 mM Si + 50 mM HCO_3 + 5 mM Al + 130 ppm U	50 mM Si + 50 mM HCO_3 + 5 mM Al + 130 ppm U
$KHCO_3$	3	50	3	50
$Al(NO_3)_3$	5	5	5	5
Na_2SiO_3 - $9H_2O$	100	100	50	50
UO_2 $(NO_3)_2$ - $6H_2O$	0.55	0.55	0.55	0.55
HNO_3	Calculated from difference between anions and cations			
5%NH_3+ 95%N_2 **GAS**	adjusted in each case to reach pH 11			

Table 7. Input Components for Speciation Modeling

Minteq components input	**Concentration (mM)**			
	100 mM Si + 03 mM HCO3 + 5 mM Al + 130 ppm U	100 mM Si + 50 mM HCO3 + 5 mM Al + 130 ppm U	50 mM Si + 50 mM HCO3 + 5 mM Al + 130 ppm U	50 mM Si + 50 mM HCO3 + 5 mM Al + 130 ppm U
H^{+1}	3	50	3	50
Si (H_4SiO_4)	100	100	50	50
Al^{+3}	5	5	5	5
$CO3^{-2}$	3	50	3	50
K^{+1}	3	50	3	50
Na^{+1}	200	200	100	100
N (NO_3^-)	108.5	155.5	58.5	105.5
U (VI) (UO_3)	0.55	0.55	0.55	0.55
NH_3 GAS	adjusted in each case to reach pH 11			

Since ammonia is a gas injected into each sample and the amount of gas injected depends on the pH each sample had at the moment of injection, the concentration entered for this compound varies for each sample. This variation was based on obtaining a pH of 11 in the speciation predictions and in obtaining the least charge difference possible. Besides ammonia, the other gas taken into account for the speciation calculations was CO_2, which was fixed at $3.9 \cdot 10^{-4}$ bar for all the samples as suggested by the speciation program for the atmosphere-open systems.

Scanning Electron Microscope-Energy Dispersive Spectroscopy

The samples' surface composition was analyzed after precipitate solidification via Scanning Electron Microscopy and Energy-Dispersive-Spectrometry (SEM-EDS). Two instruments were employed for this analysis. The uranium-containing dry precipitate samples were mounted on aluminum stubs with double-sided sticky carbon tape and then coated for 30 seconds with a thin layer of gold to increase conductivity.

For sets #1 and #2, the surface composition of gold-coated samples (Pelco SC-7, Auto sputter coater) was analyzed using a JOEL, JSM-6330F SEM SEM-Energy-Dispersive-Spectrometry (SEM-EDS) Noran System Six Model 200 at 15 kV at magnifications of 2000-5000. For set #3, electron microscopy was performed using a JEOL JIB 4500 multibeam system. EDS analysis was accomplished using a Thermo Scientific NSS ultra dry system. All micrographs were backscattered electron compositional images acquired at either 10 KV or 20 KV accelerating potentials. X-ray spectra were acquired using objective lens aperture 3 (50 μm dia) and a spot size (condenser lens) setting of 65.

X-Ray Photoelectron Spectroscopy

Previous studies have shown that XPS can be a valuable spectroscopic tool when studying possibly occurring redox reactions. XPS spectra were obtained using a Physical Electronics 5400 series XPS spectrometer. For this experiment, the Al anode was utilized at a power of 400 W.

The instrument was operated in the fixed analyzer transmission (FAT) mode with a pass energy of 35.75 eV for high-resolution scans. The analysis pressure was kept 8-9 Torr. All data analysis performed on the XPS spectra was carried out with the help of AugeScan Software.

X-Ray Diffraction

X-ray diffraction analyses were performed on the dried precipitates at 40 kV and 40 mA via Bruker 5000D XRD instrument. Diffraction patterns were obtained using copper Cu Kα radiation source (λ=0.154056 nm) with a tungsten filter. A powder sample was deposited onto the surface of an aluminum plate and analyzed over a 2-theta (2θ) range of 8° to 90° with a 0.02° step size and 1.5 s counting per step.

Fourier Transform Infrared Spectroscopy

Fourier Transform Infrared Spectroscopy (FT-IR) is a qualitative technique complementary to XRD for identifying the presence of amorphous materials as well as functional groups within the solid phases. The FTIR spectra were recorded on a JASCO FT-IR-4100 spectrometer. The solid dried precipitate was ground in an agate mortar for about 3 minutes; approximately 10 mg of sample were deposited on a KBr plate (Pike Technologies). A drop of Nujol oil was added on top

of the sample, and then a second KBr plate above it sandwiched the sample. The spectra were recorded over a range of 4000 to 800 cm^{-1} using Spectra Manager software. Each spectrum was the accumulated average of 128-256 scans. The peaks recorded were then identified by the use of Knowitall software, and values found in literature.

TASK 1.1 RESULTS AND DISCUSSIONS

As outlined in the experimental matrix in Table 1, three trials using two uranium concentrations, 0.5 ppm and 2 ppm, and three different bicarbonate concentrations, 50 mM, 75 mM and 100 mM, were continued to finalize experiments initiated last year. Presented results are based on the percent removal of the elements of interest: U(VI), Al and Si. Figure 3 represents the percent removal of Si in solutions amended with 2.8 mM of Al, 0.5 ppm and 2 ppm of U(VI). The HCO_3^- concentrations ranged between 0 to 100 mM. The initial Si concentrations of 5 mM, 50 mM, and 100 mM, 150 mM, 200 mM, and 250 mM used to prepare a solution mixture correlate to Si/Al ratios of 1.8, 17.6, 35.2, 52.8, 70.4 and 88.0, respectively (Table 1).

In this experiment, comparisons between results for each data set prepared with different U(VI) concentrations were conducted using graphs with the initial Si concentrations on the x-axis vs. percent removal of the element of interest on the y-axis. A reduction in Si concentrations was observed for the most of the initial Si concentrations tested (Figure 3).

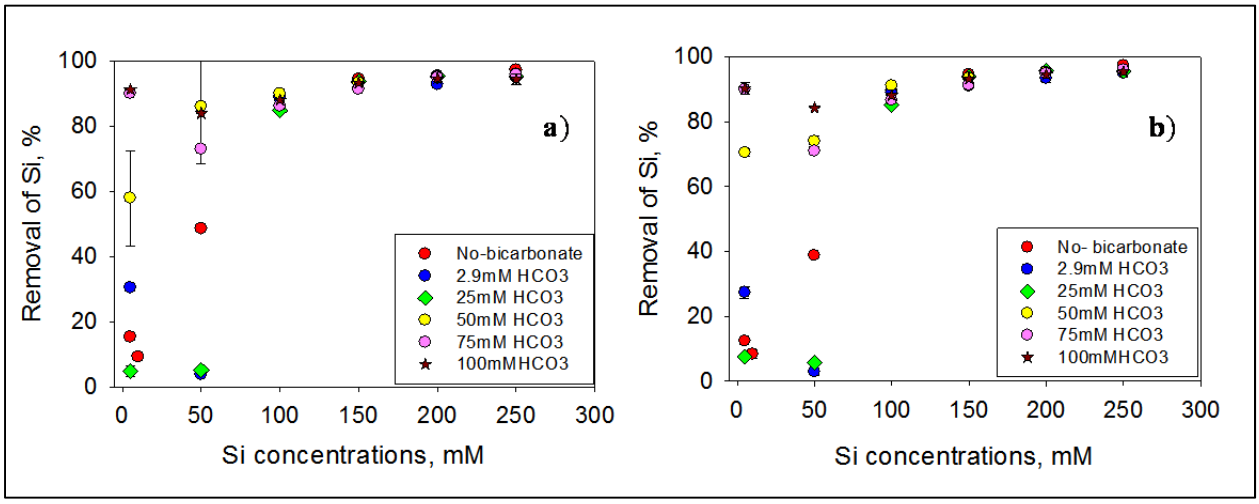

Figure 3. Reduction of Si in 2.8 mM Al amended solutions for U(VI) a) 0.5ppm b) 2ppm.

At bicarbonate concentrations between 0 mM – 25 mM and initial Si concentrations below 100 mM, the removal efficiency of Si showed relatively low values ranging between 0 and 50%. However, the increase in bicarbonate (HCO_3^-) concentrations up to 100 mM correlated with the enhanced Si removal reaching 91%. The experimental runs with the greater Si content of 200 mM and 250 mM resulted in relatively high Si removal efficiencies reaching up to 97%. Concentrations of HCO_3^- up to 100 mM did not appear to alter the efficiency of Si removal at higher initial concentrations. These results suggest that the percent removal of Si increases with the higher HCO_3^- and Si concentrations in the solution until it stabilizes to a constant value (Figure 3).

Figure 4 corresponds to the percent removal of Al in test solutions with U(VI) concentrations of 0.5 ppm and 2.0 ppm. The percent of Al removal (Figure 4) was found to be consistent with data for Si removal (Figure 3) over the various initial Si concentrations tested. Solutions with higher concentrations of bicarbonate tended to have higher removal efficiencies for Si and Al. For an example, at initial Si concentration of 5 mM, the removal of Al from solutions was greater at HCO_3^- concentrations 50-100 mM. Figure 3 and Figure 4 both suggest that the addition of NH_3 to test solutions and subsequent increase in the pH up to 11 resulted in the removal of Si and Al from the supernatant solutions. Figure 5 presents experimental results for the percent removal of U(VI) from the test samples at two different concentrations of U(VI), 0.5 ppm and 2 ppm, over the range of HCO_3^- concentrations tested. Results showed similar trends, indicating that the chosen range of initial U(VI) concentration did not appear to affect the efficiency of U(VI) removal.

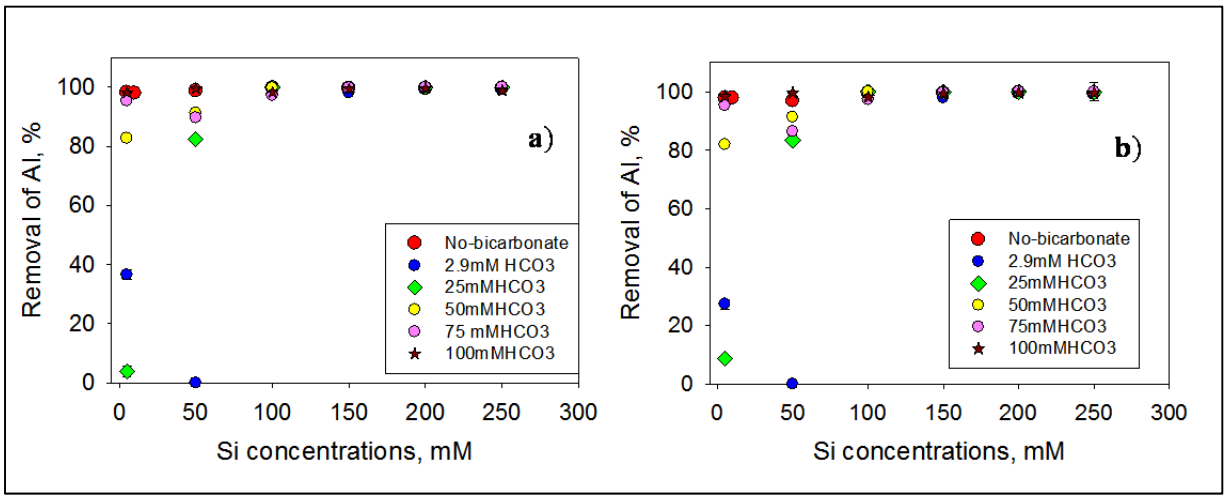

Figure 4. Reduction of Al in 2.8 mM Al amended solutions for U(VI) a) 0.5 ppm b) 2 ppm.

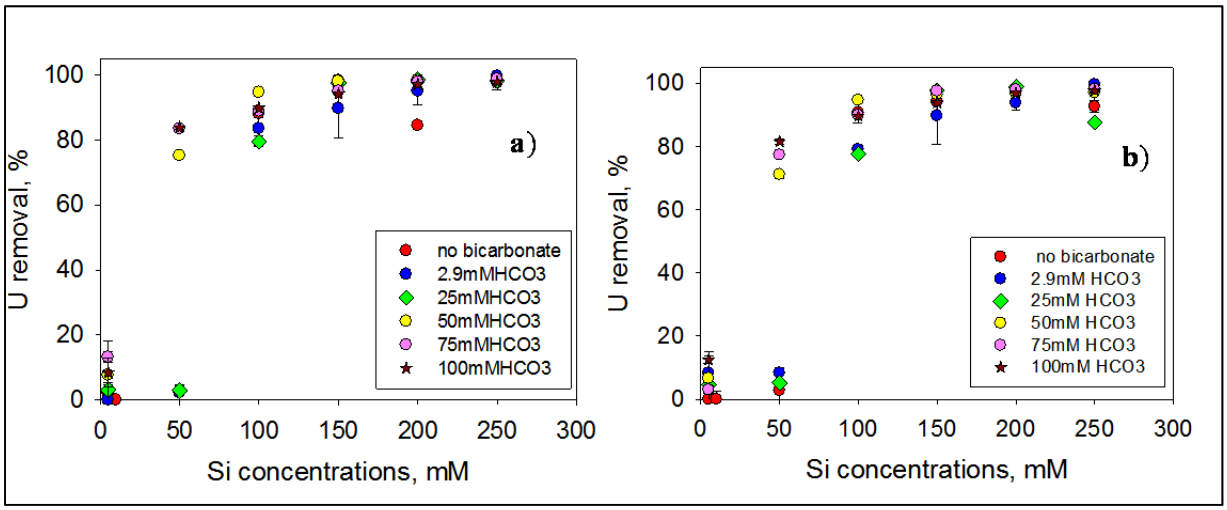

Figure 5. Reduction of U(VI) in 2.8 mM Al amended solutions a) 0.5 ppm b) 2 ppm.

Data analysis of U(VI) reduction in the supernatant solutions, presented in Figure 5, shows that the maximum percent removal of U(VI) was close to 98% for the initial Si concentration over

150 mM. At low Si concentrations, 5 mM and 50 mM, there were no observed reduction in the U(VI) concentrations in the supernatant solutions; therefore, the process of U(VI) removal does not seem to be efficient when the concentration of Si is less than 50 mM or 10-20 times higher than the concentration of Al used in solution. The increase in HCO_3^- concentrations appeared to alter the efficiency of Si removal at lower Si concentrations. Samples containing HCO_3^- higher than 50 mM revealed considerable changes in the percent removal of U(VI) compared to samples amended with 25 mM or less in HCO_3^-. In those samples the reduction in the U(VI) concentrations in the supernatant solutions was increased to 80-99% and was not affected by the different HCO_3^- concentrations tested. Experimental runs for both concentrations of U(VI) followed the same trend: no observed reduction of U(VI) concentrations in solutions containing initial Si concentration between 5 mM-50 mM. Then a percent removal of U(VI) increased ranging between 78% -94% at a Si concentration of 100 mM, and then the highest percent removal of U(VI) 95-99% at Si concentrations between 150 mM-250 mM. U(VI) removal from the solutions mixture followed a similar trend as the removal of Si. Figure 6 illustrates the comparison between the sets amended with 2.8 mM of Al. It is evident that results on the U(VI) removal for the twelve experimental sets conducted with 0.5 ppm and 2 ppm of U(VI) followed a similar path with relatively small deviations between triplicate samples. The interesting fact of these experiments is the increase in the removal of U(VI) noted at 50 mM of Si when the solution mixture contained HCO_3^- concentrations higher than 50 mM.

Based on the modeling predictions, at pH 11 negatively charged U(VI) species become predominant. In the absence of carbonate in the solution, U(VI) major species appear as uranyl-hydroxide $UO_2(OH)_3^-$ and $UO_2(OH)_4^{-2}$. The addition of 2.9 mM of HCO_3 cause the formation of anionic uranyl carbonate complexes, $UO_2(CO_3)_2^{-2}$ and $UO_2(CO_3)_3^{-4}$, which are highly soluble. In alkaline conditions at $HCO_3 \geq 25$ mM, the $UO_2(CO_3)_3^{-4}$ species account for 99.9%, which should be present in solution as a dissolve uranyl carbonate. However, our data did not support this explanation and instead showed the contrary result with the increase in the U(VI) removal when bicarbonate concentration in the solution became higher.

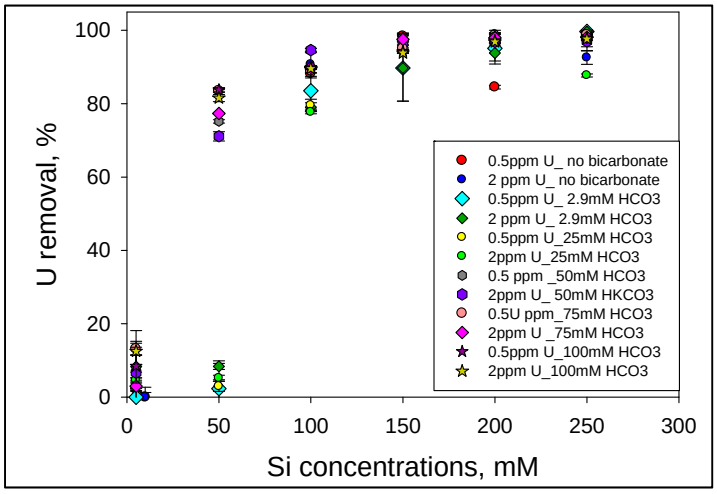

Figure 6. Removal of U(VI) in 2.8 mM Al amended solutions for initial U(VI) concentrations of 0.5 and 2 ppm.

The following experiments explored the effect of higher concentrations of Al and the effect of Ca ions; only 2 ppm of U(VI) was employed to investigate the removal of U(VI). The

concentration of Al in the subsequent experiments was increased up to 5 ppm and the removal efficiency of U(VI) from the Si-Al-HCO_3^- mixture was evaluated across all HCO_3^- concentrations tested.

The Si removal from the solution mixture in the presence of 5 mM and 2.8 mM of Al showed a similar trend (Figure 3). However, 5 mM of Al produced more stable results for Si removal at low Si/Al ratio 10 (50 mM of Si) compared to values obtained for 2.8 mM of Al (Figure 7). Generally, the Si removal was found between 75-89% at Si/Al ratio 10, which is 50 mM of initial Si in the solution; the only set amended with 25 mM HCO_3^- showed a relatively low 6.2% removal of Si. On the contrary, the removal of Si obtained for 2.8 mM of Al at the same initial Si in the solution was much lower, especially for the range 0-25 mM HCO_3^-. Figure 3 and Figure 7 show a similar pattern for the U(VI) removal at Al/Si ratio 1 (5 mM of Si) with the higher removal obtained at 75 mM HCO_3 and 100 mM HCO_3^- amended solutions. The concentrations of Al were none- detectable in the supernatant when Si was higher than 100 mM (Figure 4 and Figure 8).

In the presence of 5 mM of Al, a fair agreement was found between the removal of U(VI) and Si when Si initial concentrations in the solution were 50 mM and higher. In the set amended with 25 mM of HCO_3^-, the low decline in Si correlated with 7.5% removal of U(VI) (Figure 9). For the rest of the bicarbonate concentrations tested, the removal of U(VI) ranged between 71% and 98.5% showing a good link with the 90-95% reduction of Si concentrations in the supernatant solutions (Figure 9).

The effect of Al on the removal of 2 ppm of U(VI) was compared in the series of experiments using solutions prepared with and without Al when only three constituents combined the solution mixture- Si, HCO_3^-, and U(VI). For this assessment, two distinct concentrations of bicarbonate were used in the experiments, 2.9 mM and 50 mM. The concentration of Al tested were 0, 2.8, and 5 mM.

As shown on Figure 10, the U(VI) removal was delayed when the solution mixture for both HCO_3^- concentrations were missing Al. At 2.9 mM HCO_3^-, the U(VI) removal of 82% was observed at Si ≥150 mM. Similar solution mixtures containing 2.9 mM HCO_3- and Al at 2.8 mM exhibited 79% U(VI) removal starting from 100 ppm of Si. The increase in Al concentration up to 5 mM, resulted in 9.5%-16% higher U(VI) removal compared to values obtained with 2.8 mM of Al. At 50 mM HCO_3^- and no Al in the solution, U(VI) removal was shown at Si ≥ 100 mM. In the mixture with the same HCO_3^- and 5 mM of Al, the U(VI) removal of 70% was observed at 50 mM of Si (Figure 10). Hence, the higher Al and HCO_3^- concentrations contributed to the enhanced removal of U(VI) from the solution mixture.

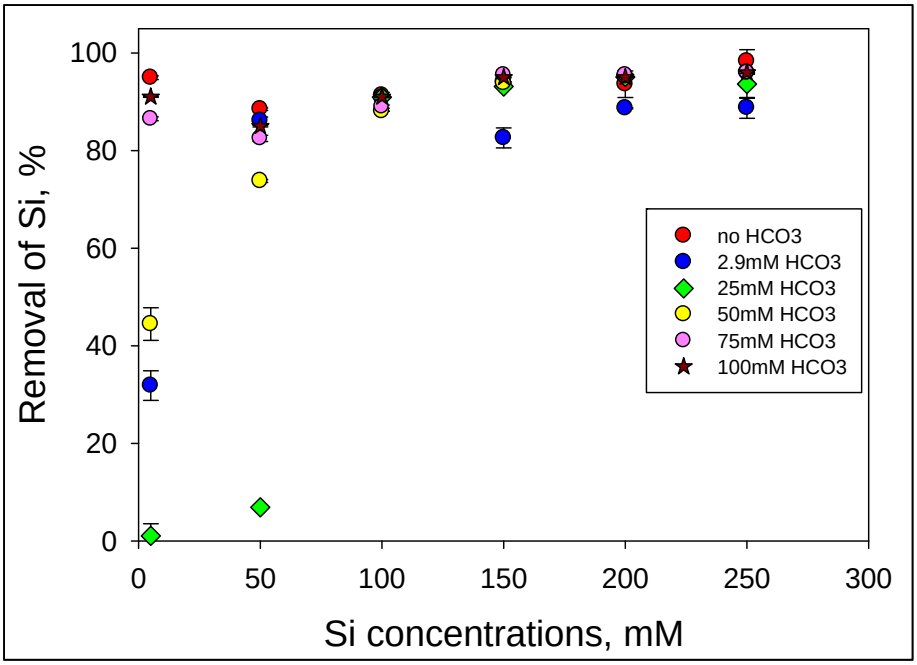

Figure 7. Removal of Si concentrations in the solution mixture prepared with 5 mM of Al.

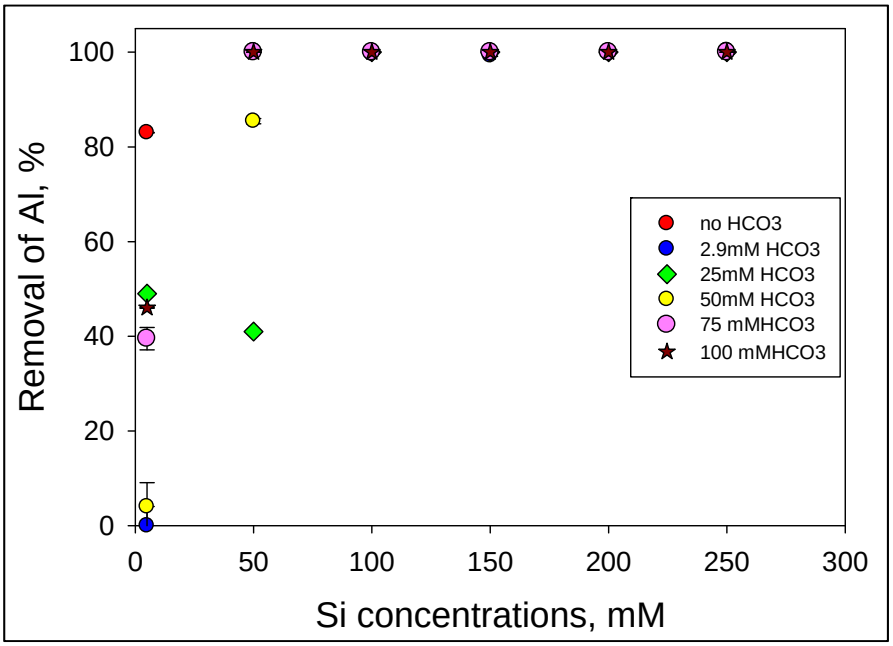

Figure 8. Removal of Al concentrations in the solution mixture prepared with 5 mM of Al.

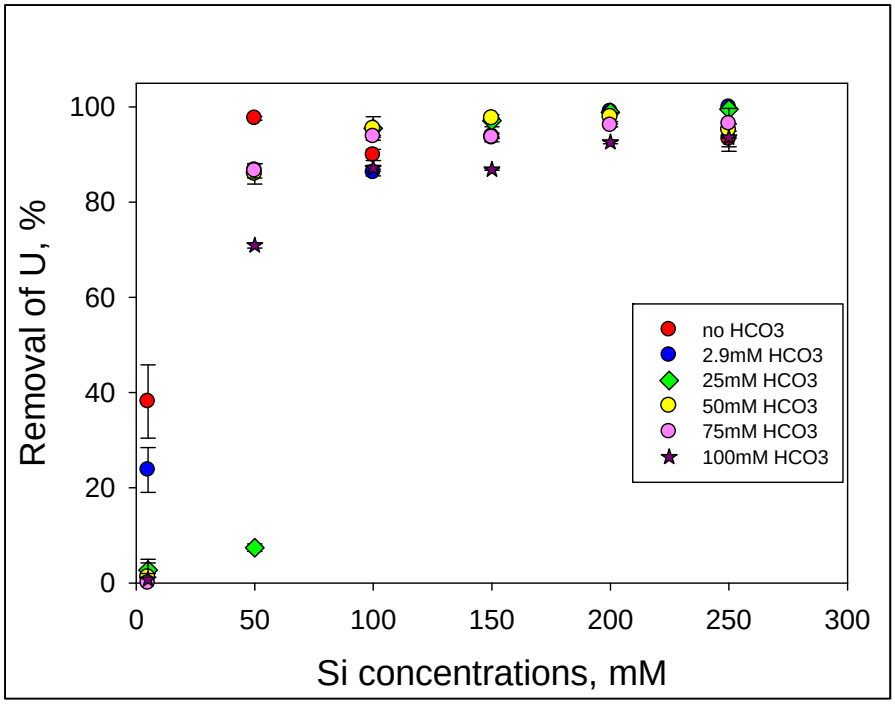

Figure 9. Removal of U(VI) in the solution mixture prepared with 5 mM of Al.

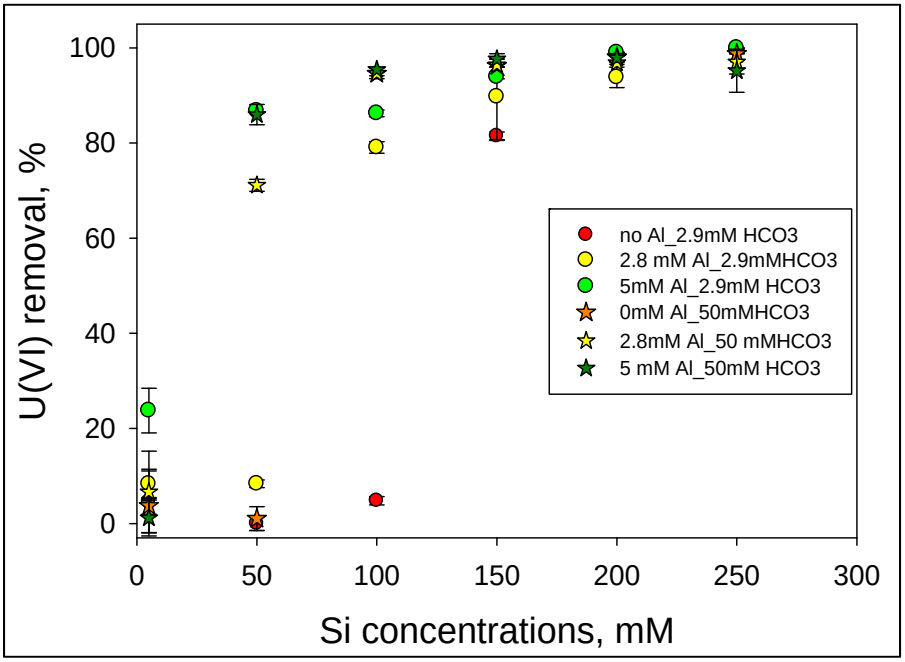

Figure 10. The effect of Al and HCO_3 concentrations on the removal of U(VI).

In contrast, when the solution mixture contained 2.8 mM of Al and no Si present, the uranium percent removal exponentially declined as the concentration of HCO_3^- increased in the solution (Figure 11). This phenomenon might be explained by the competitive adsorption of HCO_3^- and U(VI) on A1 hydroxide created in the solution (Su and Suarez 1997).

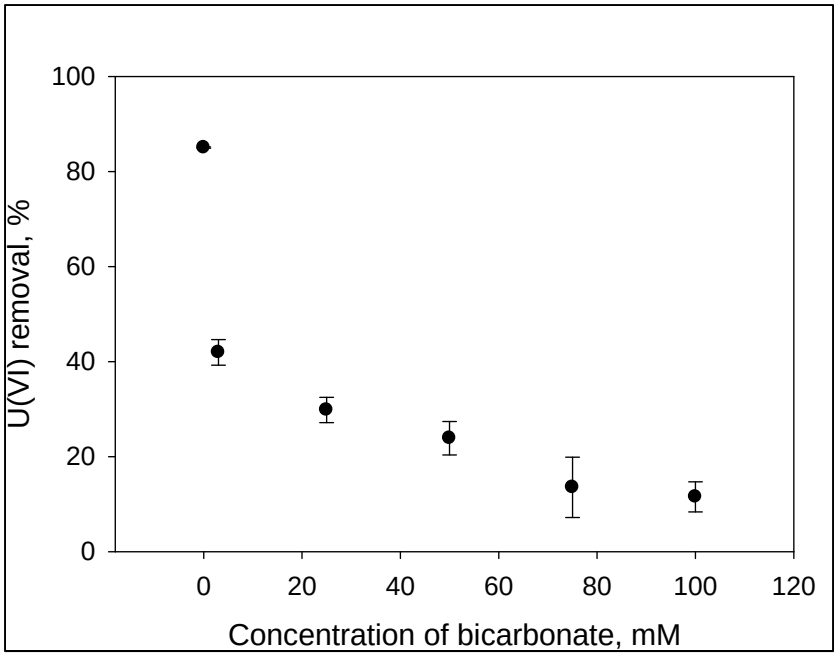

Figure 11. Removal of U(VI) in the solution mixture with no Si.

Su and Suarez (1997) proposed a ligand exchange reaction to describe the interaction of bicarbonate and carbonate ions with the surface functional groups of A1. These reactions could potentially limit the competitive adsorption of U(VI) on the surface of A1 hydroxide. In addition, U(VI) adsorption decreased in the presence of carbonate due to the formation in the solution of negatively charged uranyl carbonate complexes (Zheng et al. 2003, Um et al. 2007).

Overall, the formation of Si gel always correlated with the removal of U(VI), Si, and Al from the solution. If no Si polymerization and gel formation was observed, there was no U removal from the supernatant solution. The efficiency of U(VI) removal was affected by the Si, Al and bicarbonate concentrations supplemented into the solution.

Several important aspects should be considered to explain these findings. One of them is the formation of aluminosilicate chains upon mixing monosilicic acid and $Al(OH)_3$. Aluminosilicate impurities act as nuclei or "seeds" accelerating Si polymerization reactions. The formation of aluminosilicate impurities is accompanied by the dissociation of bicarbonate ions provoking a local decrease in pH. In this condition, the silica speciation shifts towards a higher degree of protonation that in turn triggers silica polymerization reactions. As a result, silica polymerizes around the developing nano size clusters forming coating layers. The adsorption of alkali metals onto the silica polymer chain with the release of hydrogen atom is another possible mechanism that contributes to heterogeneous nucleation (Iler 1975). Several studies confirmed the tendency of silica-mediated deposition at high pH on the amorphous calcium carbonate grains (García-Ruiz 1998, García-Ruiz et al. 2009, Kellermeier et al. 2010, Lakshtanov and Stipp 2010). Ammonia gas injection through altering the pH in the soil pore water can potentially induce the dissolution of Si, Al and other elements from soil minerals. This study has shed light on the effect of Si, Al, and bicarbonate ions dissolved from soil minerals on U co-precipitation process in alkaline conditions.

The Effect of Ca Ions on the Removal of U(VI)

This study further elucidated the effects of 5 mM of Ca on the removal efficiency of U(VI) in the Si− Al− HCO_3^- solution matrix. The concentrations of Al and U(VI) used in the experiments and speciation modeling was 5 mM and 2 ppm, respectively. Prior to experiments, Visual MINTEQ calculated the aqueous speciation of U(VI) in the solution matrix composed of Si− Al− HCO_3^- and Ca^{2+} ions. Concentrations of elements used in the solutions preparations detailed the information for the U(VI) speciation analysis. The results from the calculations are presented in Table 8. In solutions containing no bicarbonate, the major species predicted were $UO_2(OH)_3^-$ and $UO_2(OH)_4^{-2}$. As the concentration of bicarbonate ions in the solution increased, the dominant species remained $UO_2(CO_3)_3^{-4}$, $Ca_2UO_2(CO_3)_3$ (aq), and $CaUO_2(CO_3)_3^{-2}$. Calcium- uranium-carbonates were previously identified as stable and mobile complexes with high potential to contaminate soil and groundwater (Kalmykov and Choppin 2000).

Experiments to study U(VI) removal from the solution mixture were conducted with Si/Al molar ratios of 1, 10, 20, 30, 40, 50 that corresponded to Si concentrations of 5 mM, 50 mM, 100 mM, 150 mM, 200 mM, and 250 mM, respectively (Figure 12).

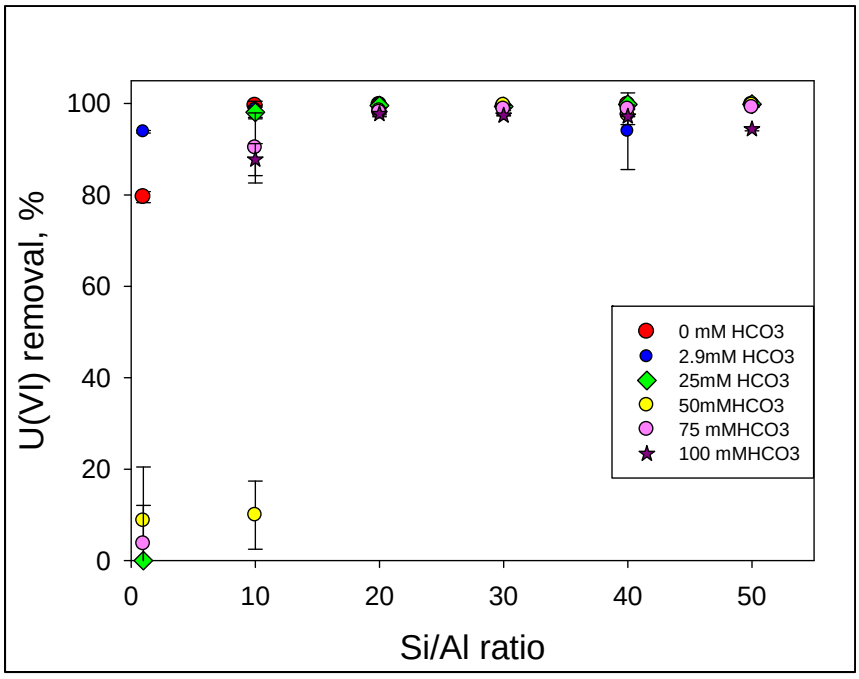

Figure 12. Removal of U(VI) in the solution mixture prepared with 5 mM of Ca.

In the presence of Ca, the removal of U(VI) at Si/Al ratio 10 was increased up to 87-99%, compared to 71-98% (Figure 9) without Ca ions in the solution mixture. Besides, starting from the Si/Al ratio 20 (Si ≥100mM), the removal of U(VI) yielded 98%-99%, which seemed to have overshadowed previous results without Ca ions introduced in the solution (Figure 12). According to the modeling predictions, U(VI) is present in the solution dominantly as $Ca_2UO_2(CO_3)_3$ and $CaUO_2(CO_3)_3^{-2}$. Ca-UO_2-CO_3 ternary complexes constitute ~65%-90% of uranyl species. The remaining amount of uranium forms cationic uranyl carbonato-complex $UO_2(CO_3)_3^{-4}$. Visual Minteq modeling predicted the formation of aragonite and calcite in addition to aluminosilicate solid phases created out of components present in the solution.

Table 8 Distribution of U(VI) Species in the Presence of Ca^{2+} Ion

Si (mM)	HCO_3^- (mM)	$UO2^{+2}$ species in the presence of various bicarbonate and silica concentrations,%						
		$UO_2(OH)_3^-$	$UO_2(OH)_4^{-2}$	$UO_2(OH)_2$	$(UO_2)_3(OH)_7^{--}$	$UO_2(CO_3)_3^{-4}$	$Ca_2UO_2(CO_3)_3(aq)$	$CaUO_2(CO_3)_3^{-2}$
5	0	91.203	8.648	0.103	0.046			
	3	0.111				0.359	71.253	28.266
	25	2.164				2.164	31.129	66.706
	50					16.116	10.644	73.238
	75					19.686	8.4	71.905
	100					36.135	3.252	60.612
50	0	89.318	10.573	0.081	0.028			
	3	0.146	0.01			0.21	77.123	22.51
	25					4.837	28.97	66.189
	50					12.74	13.165	73.643
	75					23.936	6.471	69.591
	100					32.222	4.033	63.743
100	0	87.86	12.052	0.069	0.02			
	3	0.59	0.051			0.206	76.91	22.241
	25					4.018	32.285	63.688
	50					10.976	15.676	73.345
	75					21.649	7.43	70.917
	100					29.671	4.649	65.677
150	0	86.829	13.094	0.62	0.016			
	3	1.706	0.172			0.207	75.785	22.128
	25	0.017				3.622	34.162	64.196
	50					10.069	16.925	72.99
	75					20.421	8.019	71.555
	100					28.229	5.044	66.723
200	0	86.069	13.861	0.057	0.013			
	3	3.922	0.445			0.208	73.547	21.872
	25	0.034				3.396	35.324	61.241
	50					9.536	17.736	72.718
	75					19.696	8.4	71.905
	100					27.353	5.302	67.339
250	0	85.487	14.447	0.054	0.012			
	3	7.625	0.945			0.207	69.944	21.271
	25	0.06				3.254	36.084	60.593
	50	0.013				9.19	18.292	72.5
	75					19.207	8.661	72.119
	100					26.778	5.48	67.734

The rapid nucleation of $CaCO_3$ with the formation of clusters in the alkaline silica-rich solutions induces dissociation of bicarbonate and the release of protons according to the following reaction (Kellermeier et al.2010):

$$HCO_3^- \leftrightarrow CO_3^{2-} + \boldsymbol{H}^+ \xrightarrow{Ca^{2+}} CaCO_3 \downarrow \quad (1)$$

The reaction results in the decrease in pH around the surface of growing particles. Concomitant decrease in local pH triggers a reduction in silica solubility and polymerization reactions (García-Ruizet et al. 2009). The evaluation of results showed that the removal of Si correlated with the removal of U(VI) from the solution (Figure 13). In addition, the increase in bicarbonate concentration tended to decrease Si removal. This finding is opposite to the results obtained in the previous tests without Ca when higher bicarbonate concentrations correlated with higher yield in Si and U removals.

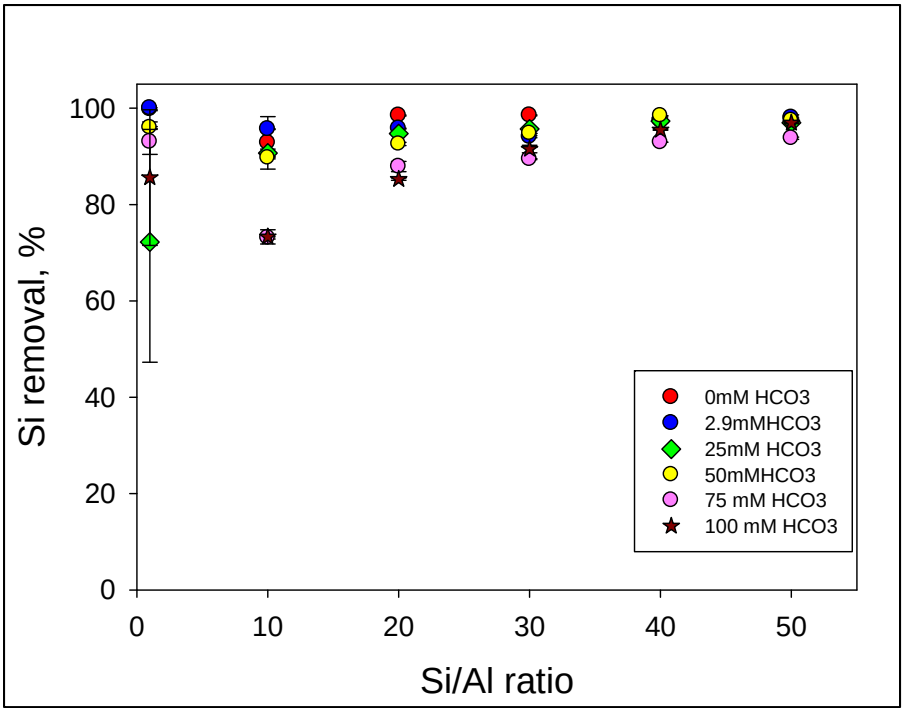

Figure 13. Removal of Si in the solution mixture prepared with 5 mM of Ca.

Under alkaline conditions, $Al(OH)_4^-$ is the dominant species for Al. It was almost undetectable in all samples tested starting from Si/Al ratio ≥10 except couple of outliers at Si/Al 20 and Si/Al 40 (Figure 14).

According to speciation modeling, the dominant Ca species in the solution are $CaNH_3^{+2}$, $Ca(NH_3)_2^{+2}$, and $CaCO_3$. Ca-ammonia compounds are soluble and their dissociation results in the release of charged hydrogen ions that promote the reduction of pH. The removal of Ca^{2+} ion from the solution apparently is due to the precipitation of calcium carbonate; however, Visual Minteq predicted a lower percentage of $CaCO_3$ to be formed than was observed in experiments. The difference between observed and predicted is higher for Si/Al ratios ≥20 in the bicarbonate range of 50-100 mM. The variances between speciation modeling predicted and experimental results on Ca removal are probably due to co- precipitation of Ca compounds with Si gel (Figure 15).

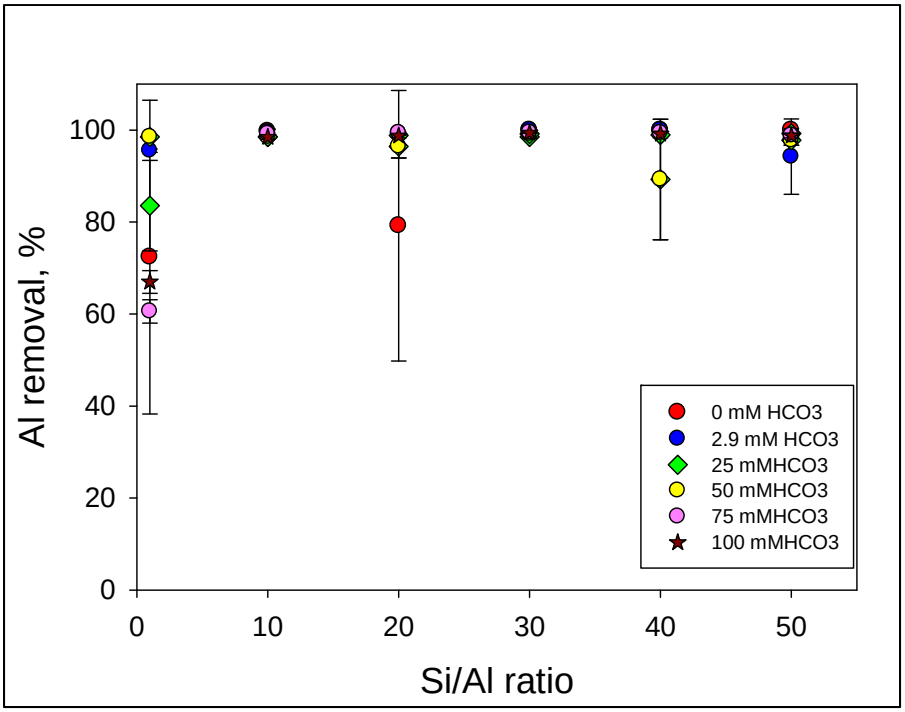

Figure 14. Removal of Al in the solution mixture prepared with 5 mM of Ca.

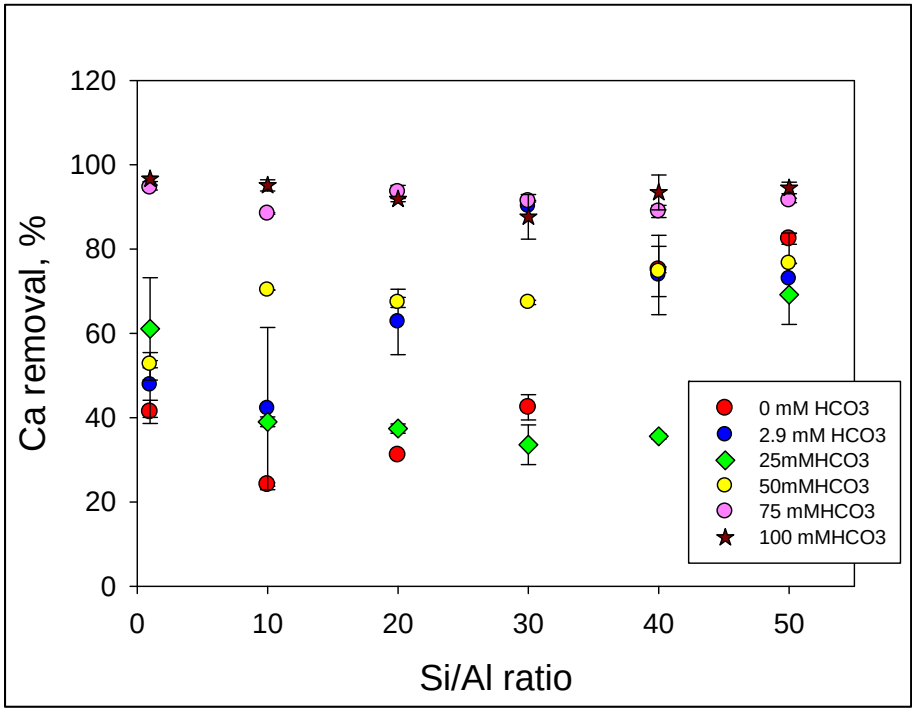

Figure 15. Removal of Ca in the solution mixture prepared with 5 mM of Ca.

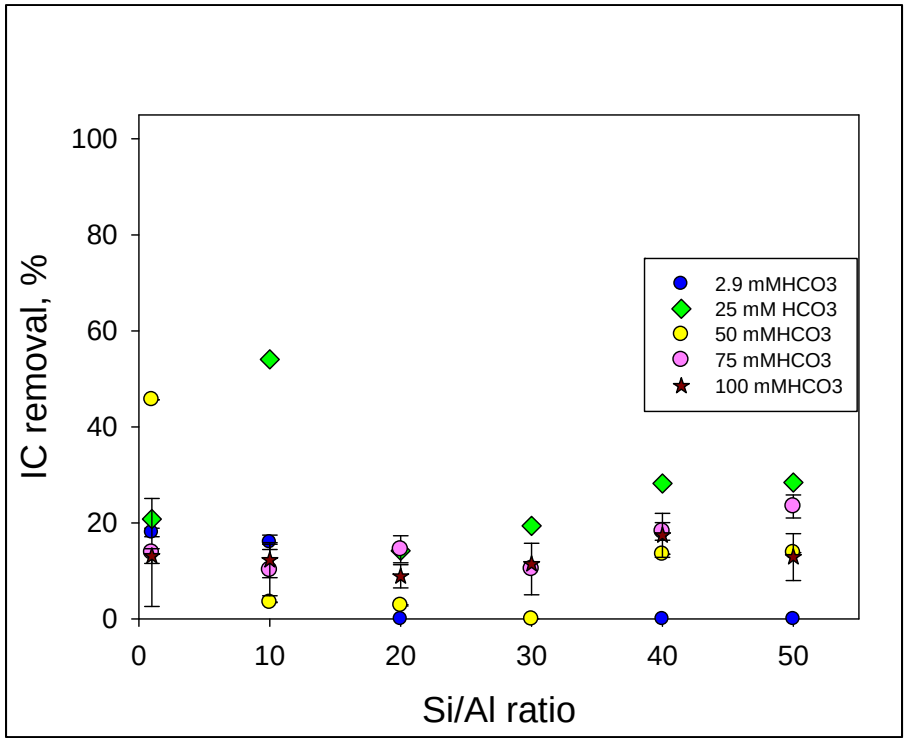

Figure 16. removal of inorganic carbon from the solution mixture prepared with 5 mM of Ca.

The precipitation of calcium carbonate controls the removal of inorganic carbon from the aqueous solution. Speciation modeling suggested that calcium carbonate accounts for 18.5-48.4%, 14.3-4.7%, and 1-5 % of the total bicarbonate concentrations present initially in the solution at the 3 mM, 25 mM and 50-100 mM range, respectively. Experimental results showed that the removal of inorganic carbon is approximately in the 10-25% range (Figure 16). Perhaps Si gel co-precipitated some bicarbonate ions (HCO_3^-), their percentage according to the speciation modeling predictions was calculated in the 2.5-13% range for all Si/Al ratios and bicarbonate concentrations tested.

Mineralogical and Morphological Characterization of U(VI)-Bearing Precipitates

Identification of U(VI)-containing solid phases is a difficult task because no two precipitates are identical. Scanning electron microscopy (SEM) with energy dispersive spectrometry (EDS) was used for the analysis of morphology and surface elemental composition of the precipitated solids; however, the use of coating materials in sample preparation for SEM/EDS can conceal some peaks or cause others to overlap (Buck, et al. 2004). Some of these problems can be overcome by using X-ray (XRD) diffraction, as it is capable of providing qualitative and quantitative information about the compounds present in a solid sample. In addition, FTIR provides a powerful tool for identifying the presence of functional groups because it provides information specific to the group itself, on the interaction of the group with other parts of the molecule, and on the spatial properties of the group (Coates 2000). Also, using XPS provides the ability to narrow the possibilities and even approach quantification of uranium valence states in complex materials (Ilton and Bagus 2011). Combining results from multiple analytical techniques increases the potential for solid phases' accurate identification and interpretations.

Speciation modeling for characterization of U(VI)-bearing precipitates

For hazardous materials contaminated soil and groundwater, the only conceivable transport medium is the aqueous phase. It is important to predict the reactions that are likely to occur between the dissolved uranium and other constituencies in order to estimate the quantity of uranium that can be transported in the aqueous phase. This information is provided by speciation modeling, which is based on the thermodynamic properties of dissolved uranium species (Langmuir 1978, Grenthe, et al. 1992)**.**

The modeling package Visual-MINTEQ was used to calculate distributions of aqueous species and mineral saturation indices by entering elemental concentration data. Visual-MINTEQ provides an extensive database of mineral and aqueous species for interpretation purposes. In order to obtain the speciation data, input files were calculated based on the elements that were added to each sample. Since these models provide an insight into the general features of natural phenomenon, rather than specific details (Ekwere and Edet 2012), it is possible to interpret structural motifs in the amorphous precipitates and relate them to the stable phases and uranium species based on possible bonding paths outlined by the speciation calculations.

The predicted percentage distribution among absorbed and dissolved species shows that the predominant complex of the uranyl group in the samples is found predominantly in the form of $UO_2(CO_3)_3^{-4}$, followed by the $UO_2(OH)_3^-$form (Table 9). The higher the bicarbonate concentration, the more $UO_2(CO_3)_3^{-4}$ is formed, making the uranyl complex less available for forming $UO_2(OH)_3^-$. The uranium species distribution in the solutions composed of 130 ppm U was plotted in Figure 17. U species distribution in the solutions composed of 130 ppm U and various bicarbonate and silica concentrations for the following compositions: a)50 mM Si, 3 mM HCO_3, 5 mM Al, and 50 mM Si, 50 mM HCO_3, 5 mM Al; b)100 mM Si, 3 mM HCO_3, 5 mM Al, and 100 mM Si, 50 mM HCO_3, 5 mM Al. Additionally, the speciation predictions for the concentrations of aqueous inorganic species shows that uranium's main species in the samples is $UO_2(CO_3)_3^{-4}$ (Figure 7). Thus, from both the concentration values and the component's percentage distribution, we could hypothesize that the more bicarbonate is present in the samples, more $UO_2(CO_3)_3^{-4}$ becomes available as an aqueous inorganic species, making the percentage distribution to be represented almost solely by $UO_2(CO_3)_3^{-4}$. Since this percentage distribution accounts for dissolved species, it might be possible that the more $UO_2(CO3)_3^{-4}$ available, the higher the probability that the main form of uranium found in the precipitate is this one.

Table 9. Distribution of U(VI) Species in the Presence of Various HCO_3^- and Si Concentrations

U Species	Molar % distribution for 50 mM Si		Molar % distribution for 100 mM Si	
	3 mM HCO_3^-	50 mM HCO_3^-	3 mM HCO_3^-	50 mM HCO_3^-
$(UO_2)_3(OH)_7^-$	1.617	-	4.061	-
$UO_2(OH)_4^{-2}$	3.493	-	4.939	-
$UO_2(OH)_3^-$	20.837	0.012	28.527	0.053
$UO_2(OH)_2$ (aq)	0.019	-	0.025	-
$UO_2(CO_3)_2^{-2}$	0.041	0.031	0.038	0.051
$UO_2(CO_3)_3^{-4}$	73.993	99.956	62.41	99.893

Mineral saturation indices were calculated as part of the output from the modeling program; the results for uranium containing minerals are shown (Table 11). Saturation indices are useful for indicating what minerals might be dissolving or precipitating into or from the solution, or controlling the solution's composition. The solution is considered to be in equilibrium with regards to a particular mineral if the saturation index (SI)=0. It is considered to be under saturated if SI<1 and oversaturated if the SI>1 (Ekwere and Edet 2012). Modeling data predicted the formation of Rutherfordine UO_2CO_3, Shoepite $(UO_2)_8O_2(OH)_{12}\cdot 12H_2O$, and Gummite, which are found in nature as alteration products of uraninite (UO_2). However, speciation calculations showed that at the studied U(VI) concentration of 130 ppm, solutions were under saturated with respect to all U-bearing minerals phases (Table 11).

Table 10. Concentrations of Uranium Containing Aqueous Inorganic Species in the Presence of Various HCO_3^- and Si Concentrations

Aqueous Inorg. Species	Concentration (mol/L) for 50 mM Si		Concentration (mol/L) for 100 mM Si	
	3 mM HCO_3^-	50 mM HCO_3^-	3 mM HCO_3^-	50 mM HCO_3^-
(UO2)2(OH)2+2	1.75E-17	3.30E-24	3.34E-17	6.30E-23
(UO2)2OH+3	6.11E-25	2.77E-32	1.23E-24	5.24E-31
(UO2)3(CO3)6-6	1.64E-13	7.38E-17	1.64E-13	3.19E-16
(UO2)3(OH)4+2	1.39E-18	2.01E-28	3.61E-18	1.69E-26
(UO2)3(OH)5+	1.32E-11	4.45E-21	3.30E-11	3.78E-19
(UO2)3(OH)7-	2.94E-06	9.74E-16	7.39E-06	8.45E-14
(UO2)4(OH)7+	8.92E-13	2.30E-25	3.03E-12	8.65E-23
UO2(CO3)2-2	2.24E-07	1.71E-07	2.06E-07	2.78E-07
UO2(CO3)3-4	4.04E-04	5.46E-04	3.41E-04	5.46E-04
UO2(OH)2 (aq)	1.03E-07	8.21E-11	1.38E-07	3.62E-10
UO2(OH)3-	1.14E-04	6.45E-08	1.56E-04	2.88E-07
UO2(OH)4-2	1.91E-05	4.52E-09	2.70E-05	2.03E-08
UO2+2	4.79E-17	1.19E-20	6.78E-17	5.13E-20
UO2CO3 (aq)	4.29E-11	1.94E-12	4.65E-11	5.16E-12
UO2H3SiO4+	6.06E-11	4.68E-14	1.64E-10	4.05E-13
UO2NO3+	1.75E-18	2.38E-21	4.32E-18	1.48E-20
UO2OH+	1.14E-11	6.59E-15	1.56E-11	2.88E-14

Table 11. Mineral Saturation Indices Based on Solution Compositions from 130 ppm U and Various Bicarbonate and Silica Concentrations

Minerals	Saturation indices for 50 mM Si		Saturation indices for 100 mM Si	
	3 mM HCO_3^-	50 mM HCO_3^-	3 mM HCO_3^-	50 mM HCO_3^-
Gummite	-2.49	-5.607	-2.359	-4.963
Rutherfordine	-5.529	-6.892	-5.491	-6.468
Schoepite	-0.209	-3.326	-0.077	-2.681
$UO_2(NO_3)_2(s)$	-31.694	-34.07	-31.048	-33.116
$UO_2(NO_3)_2{:}2H_2O(s)$	-24.398	-26.773	-23.751	-25.819
$UO_2(NO_3)_2{:}3H_2O(s)$	-22.937	-25.312	-22.29	-24.358
$UO_2(NO_3)_2{:}6H_2O(s)$	-21.593	-23.969	-20.946	-23.015
$UO_2(OH)_2$ (beta)	-0.43	-3.547	-0.298	-2.902
$UO_3(s)$	-2.519	-5.636	-2.387	-4.991

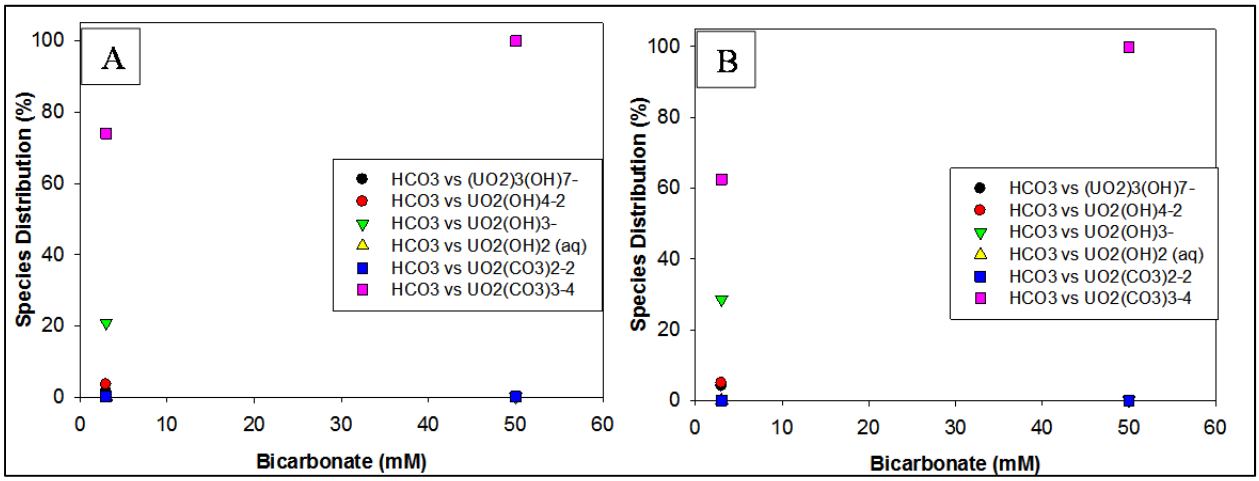

Figure 17. U species distribution in the solutions composed of 130 ppm U and various bicarbonate and silica concentration.

Predictions of the speciation modeling were compared to experimental data on characterization of U-bearing precipitates.

SEM/EDS

SEM/EDS specified solid phase's surface localized precipitation of uranium. The first samples prepared with 2 ppm and 30 ppm of U(VI) were analyzed using SEM equipped with an EDS, and resulted in very low atomic percentages for U. The uranium atomic percentages for sets #1 and #2 samples are shown in Figure 18, Figure 19, Figure 20 and Figure 21.

Calculated elemental composition of mineral phases based on the EDS showed the presence of Na_2SiO_3. However, low U(VI) atomic percentage makes XRD, FTIR and XPS analyses ineffective in identification of U solid phases in these samples. A uranium atomic percentage above 0.1 is necessary to consider these samples for XRD, FTIR and XPS analysis. In order to increase the atomic percentage of U(VI) in the solid phase, the concentration of U(VI) in the solution mixture was increased to 130 ppm. These samples provided more information on elemental composition of mineral phases than previous ones prepared with 2 ppm and 30 ppm of

U(VI). The two most interesting results are depicted in Figure 22, Table 12, Table 13, and Figure 23.

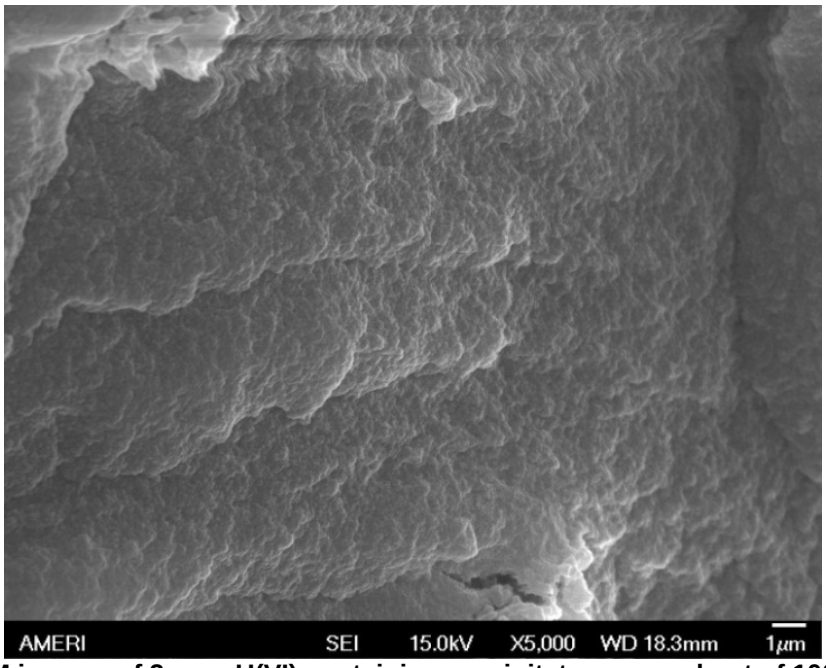

Figure 18. SEM images of 2 ppm U(VI) containing precipitate prepared out of 100 mM Si+5 mM Al+0mM HCO_3+ 2 ppm U(VI).

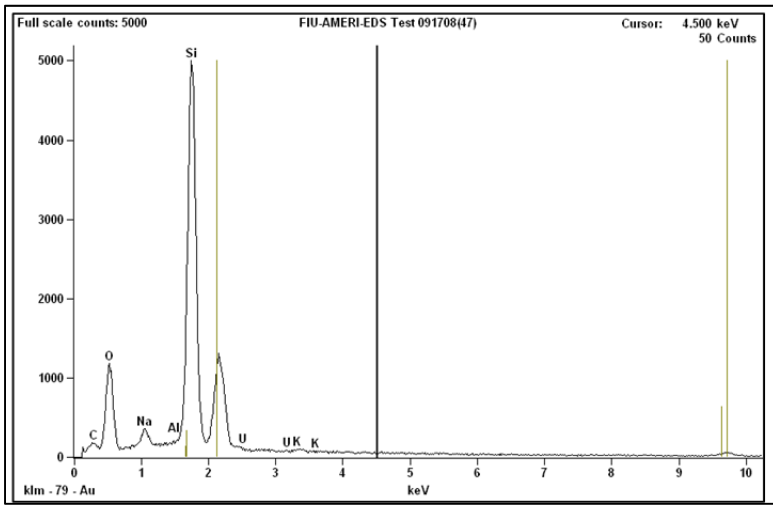

Element Line	Weight,%	Atom, %
C	29.63	41.50
O	36.21	38.08
Na	2.00	1.46
Al	0.79	0.49
Si	30.62	18.34
K	0.23	0.1
U	0.52	0.04
Total	100	100

Figure 19. EDS results for precipitate prepared out of 100 mM Si+5 mM Al+0 mM HCO_3+2 ppm U(VI).

Observations showed that uranium distribution is uneven throughout the sample. SEM/EDS images indicated lighter aggregates on the surface of the precipitate with higher uranium concentration. However, we are not able to assess whether this happens similarly in the interior of the solids. The maximum atomic percentage of 1.27% was found on the lighter surface aggregates in the sample composed of 50 mM Si, 3 mM HCO_3, 5 mM Al, and 130 ppm U [Figure 22A, Table 12(A3)].

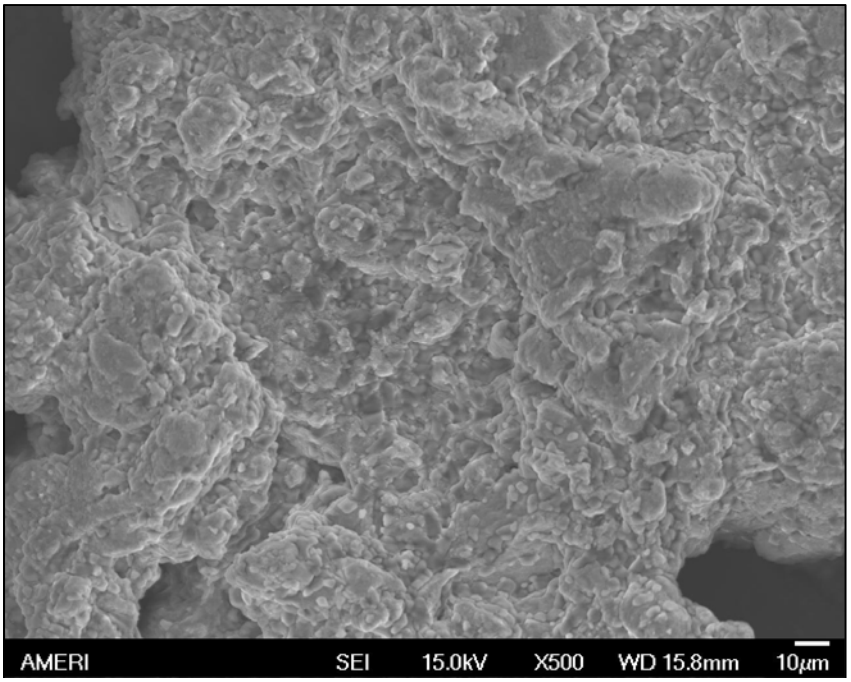

Figure 20. SEM image of 30 ppm U(VI) containing precipitate composed of 3 mM HCO_3+2.8 mM Al+100 mM Si+30 ppm U.

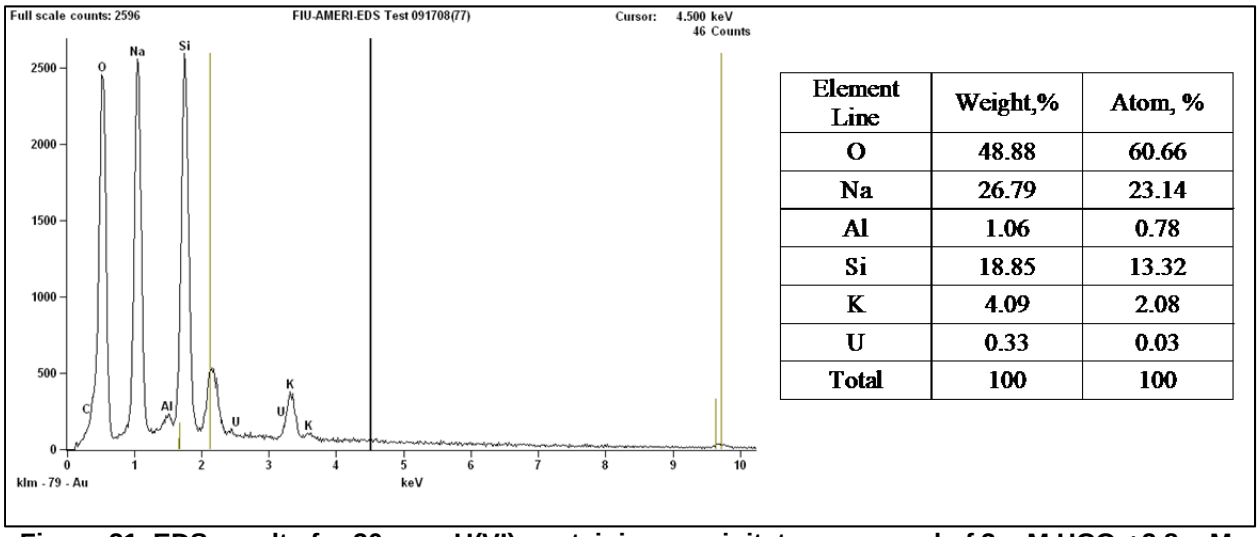

Element Line	Weight,%	Atom, %
O	48.88	60.66
Na	26.79	23.14
Al	1.06	0.78
Si	18.85	13.32
K	4.09	2.08
U	0.33	0.03
Total	100	100

Figure 21. EDS results for 30 ppm U(VI) containing precipitate composed of 3 mM HCO_3+2.8 mM Al+100 mM Si+30 ppm U.

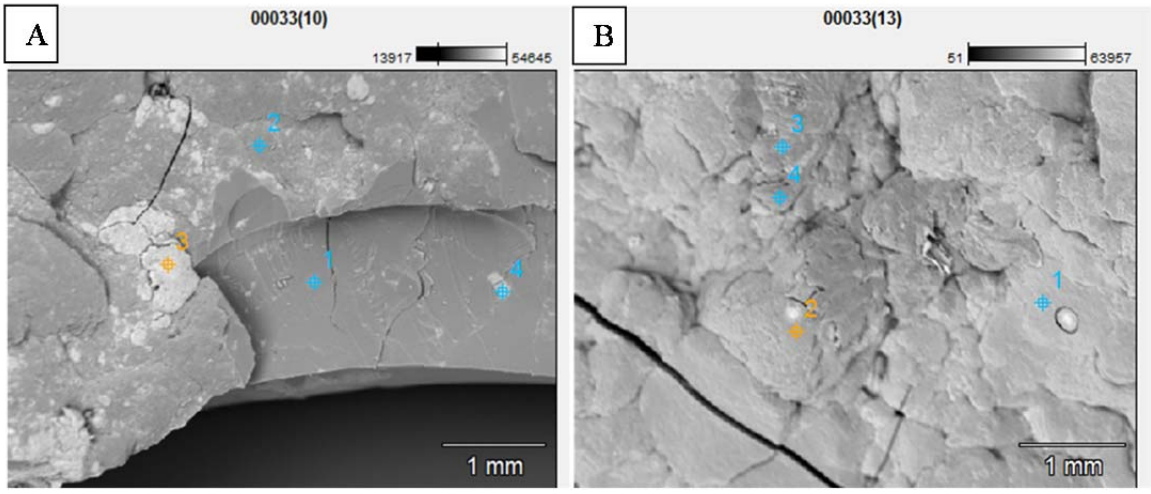

Figure 22. SEM images of uranium bearing percipitates A) 3 mM HCO_3, B) 50 mM HCO_3.

Table 12. EDS Results for A) 50 mM Si + 3 mM HCO3 + 5 mM Al + 130 ppm U

Wed Jan 25 23:44:25 2012
Filter Fit Chi-squared value: 85.994 Errors:+/-1 Sigma
Correction Method: Proza (Phi-Rho-Z)
Acc.Voltage: 20.0 kV Take Off Angle: 54.0 deg
A.1

Element Line	Net Counts	Element Wt.%	Wt.% Error	Atom %	Atom % Error
C K	701	8.96	+/-0.94	14.64	+/- 1.52
N K	137	1.13	+/-0.83	1.59	+/- 1.17
O K	17999	44.32	+/-0.44	54.39	+/- 0.54
Na K	522	0.68	+/-0.13	0.58	+/- 0.11
Al K	5210	3.47	+/-0.13	2.53	+/- 0.09
Si K	54335	36.47	+/-0.22	25.50	+/- 0.15
Si L	0	---	---	---	---
K K	874	0.87	+/-0.07	0.43	+/- 0.03
K L	0	---	---	---	---
U L	0	---	---	---	---
U M	2005	4.10	+/-0.28	0.34	+/- 0.02
Total		100.00		100.00	

Wed Jan 25 23:44:30 2012
Filter Fit Chi-squared value: 142.707 Errors:+/-1 Sigma
Correction Method: Proza (Phi-Rho-Z)
Acc.Voltage: 20.0 kV Take Off Angle: 54.0 deg
A.2

Element Line	Net Counts	Element Wt.%	Wt.% Error	Atom %	Atom % Error
C K	3054	12.49	+/-0.55	18.53	+/- 0.81
N K	333	1.01	+/-0.58	1.29	+/- 0.73
O K	61594	54.93	+/-0.32	61.17	+/- 0.36
Na K	2375	1.36	+/-0.09	1.05	+/- 0.07
Al K	9647	2.75	+/-0.08	1.82	+/- 0.05
Si K	88435	24.80	+/-0.12	15.73	+/- 0.08
Si L	0	---	---	---	---
K K	1411	0.56	+/-0.07	0.26	+/- 0.03
K L	0	---	---	---	---
U L	0	---	---	---	---
U M	2559	2.09	+/-0.14	0.16	+/- 0.01
Total		100.00		100.00	

Wed Jan 25 23:44:33 2012
Filter Fit Chi-squared value: 157.015 Errors:+/-1 Sigma
Correction Method: Proza (Phi-Rho-Z)
Acc.Voltage: 20.0 kV Take Off Angle: 54.0 deg
A.3

Element Line	Net Counts	Element Wt.%	Wt.% Error	Atom %	Atom % Error
C K	2283	11.72	+/-0.55	20.22	+/- 0.96
N K	451	2.10	+/-0.68	3.11	+/- 1.01
O K	25261	40.95	+/-0.40	53.06	+/- 0.51
Na K	1723	1.53	+/-0.14	1.38	+/- 0.12
Al K	8504	3.74	+/-0.12	2.87	+/- 0.09
Si K	51908	22.18	+/-0.16	16.37	+/- 0.12
Si L	0	---	---	---	---
K K	5761	3.24	+/-0.31	1.72	+/- 0.16
K L	0	---	---	---	---
U L	1	---	---	---	---
U M	12554	14.54	+/-0.76	1.27	+/- 0.07
Total		100.00		100.00	

Wed Jan 25 23:44:27 2012
Filter Fit Chi-squared value: 152.960 Errors:+/-1 Sigma
Correction Method: Proza (Phi-Rho-Z)
Acc.Voltage: 20.0 kV Take Off Angle: 54.0 deg
A.4

Element Line	Net Counts	Element Wt.%	Wt.% Error	Atom %	Atom % Error
C K	2081	8.57	+/-0.52	14.47	+/- 0.87
N K	466	1.48	+/-0.54	2.14	+/- 0.78
O K	43937	48.40	+/-0.34	61.34	+/- 0.43
Na K	2604	1.85	+/-0.12	1.63	+/- 0.10
Al K	13224	4.64	+/-0.10	3.49	+/- 0.08
Si K	60397	20.75	+/-0.14	14.98	+/- 0.10
Si L	0	---	---	---	---
K K	3776	1.69	+/-0.06	0.88	+/- 0.03
K L	0	---	---	---	---
U L	0	---	---	---	---
U M	13727	12.63	+/-0.41	1.08	+/- 0.03
Total		100.00		100.00	

Uranium-bearing aggregates of light grey color originated on the surface of solids prepared with 3 mM HCO_3 were not found on the surface of samples composed of 50 mM HCO_3. EDS showed a uniform distribution of uranium throughout the sample. The surface of these samples featured a lower atomic percentage of silica (11.3%) and carbon (15.6%) compared to found in the sample prepared from 3 mM HCO_3, (18.1%) and (16.98%), respectively.

Table 13. EDS Results for A) 50 mM Si + 50 mM HCO_3 + 5 mM Al + 130 ppm U

B.1

Wed Jan 25 23:45:01 2012
Filter Fit Chi-squared value: 171.363 Errors:+/-
Correction Method: Proza (Phi-Rho-Z)
Acc.Voltage: 20.0 kV Take Off Angle: 54.0 deg

Element Line	Net Counts	Element Wt.%	Wt.% Error	Atom %	Atom % Error
C K	2969	8.90	+/-0.54	13.30	+/- 0.82
N K	4632	9.92	+/-0.67	12.72	+/- 0.86
O K	50988	42.76	+/-0.28	47.98	+/- 0.31
Na K	40342	16.36	+/-0.11	12.78	+/- 0.09
Al K	6513	1.62	+/-0.06	1.08	+/- 0.04
Si K	73419	17.08	+/-0.10	10.92	+/- 0.06
Si L	0	---	---	---	---
K K	8287	2.54	+/-0.07	1.17	+/- 0.03
K L	0	---	---	---	---
U L	0	---	---	---	---
U M	1304	0.82	+/-0.14	0.06	+/- 0.01
Total		100.00		100.00	

B.2

Wed Jan 25 23:44:58 2012
Filter Fit Chi-squared value: 231.747 Errors:+
Correction Method: Proza (Phi-Rho-Z)
Acc.Voltage: 20.0 kV Take Off Angle: 54.0 deg

Element Line	Net Counts	Element Wt.%	Wt.% Error	Atom %	Atom % Error
C K	2783	11.96	+/-0.58	18.43	+/- 0.89
N K	435	1.33	+/-0.57	1.75	+/- 0.75
O K	52935	46.54	+/-0.30	53.83	+/- 0.35
Na K	5707	2.65	+/-0.09	2.13	+/- 0.07
Al K	13458	3.26	+/-0.08	2.23	+/- 0.05
Si K	130741	31.67	+/-0.14	20.87	+/- 0.09
Si L	0	---	---	---	---
K K	3940	1.39	+/-0.07	0.66	+/- 0.03
K L	0	---	---	---	---
U L	0	---	---	---	---
U M	1648	1.20	+/-0.15	0.09	+/- 0.01
Total		100.00		100.00	

B.3

Wed Jan 25 23:45:03 2012
Filter Fit Chi-squared value: 20.315 Errors:+/-
Correction Method: Proza (Phi-Rho-Z)
Acc.Voltage: 20.0 kV Take Off Angle: 54.0 deg

Element Line	Net Counts	Element Wt.%	Wt.% Error	Atom %	Atom % Error
C K	2547	4.87	+/-0.23	9.54	+/- 0.44
N K	1199	13.46	+/-2.04	22.62	+/- 3.43
O K	5236	20.36	+/-0.51	29.95	+/- 0.74
Na K	2145	1.83	+/-0.09	1.87	+/- 0.09
Al K	0	---	---	---	---
Si K	2300	0.88	+/-0.06	0.73	+/- 0.05
Si L	0	---	---	---	---
K K	114590	58.61	+/-0.30	35.28	+/- 0.18
K L	0	---	---	---	---
U L	0	---	---	---	---
U M	0	---	---	---	---
Total		100.00		100.00	

B.4

Wed Jan 25 23:44:55 2012
Filter Fit Chi-squared value: 358.066 Errors:+
Correction Method: Proza (Phi-Rho-Z)
Acc.Voltage: 20.0 kV Take Off Angle: 54.0 deg

Element Line	Net Counts	Element Wt.%	Wt.% Error	Atom %	Atom % Error
C K	7506	14.72	+/-0.39	21.04	+/- 0.56
N K	1406	2.27	+/-0.45	2.78	+/- 0.55
O K	114669	55.44	+/-0.26	59.50	+/- 0.28
Na K	8376	2.52	+/-0.07	1.88	+/- 0.05
Al K	16607	2.52	+/-0.06	1.60	+/- 0.04
Si K	140938	20.88	+/-0.09	12.77	+/- 0.05
Si L	0	---	---	---	---
K K	4030	0.84	+/-0.05	0.37	+/- 0.02
K L	0	---	---	---	---
U L	0	---	---	---	---
U M	1890	0.81	+/-0.10	0.06	+/- 0.01
Total		100.00		100.00	

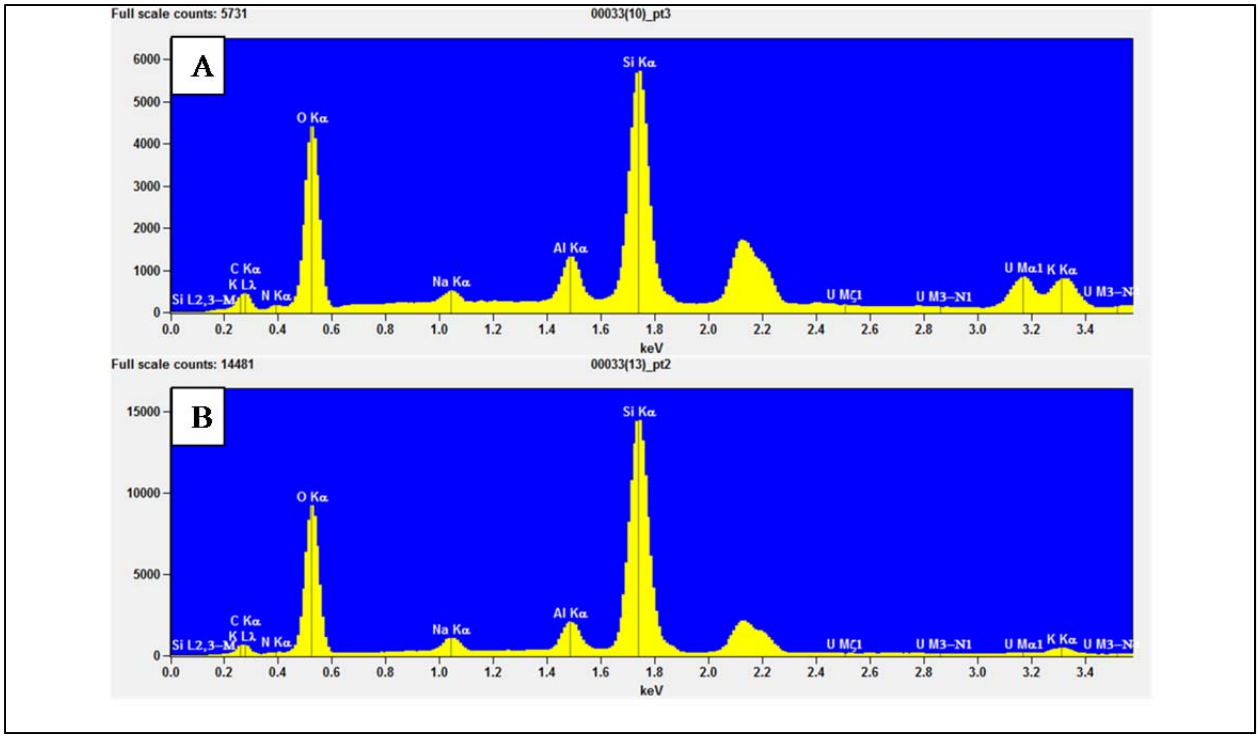

Figure 23. EDS analysis of samples surface composition A) 50 mM Si + 3 mM HCO_3 + 5 mM Al + 130 ppm U; B) 50 mM Si + 50 mM HCO_3 + 5 mM Al + 130 ppm U.

Fourier Transform Infrared Spectroscopy

The qualitative aspects of infrared spectroscopy are one of the most powerful attributes of this diverse and versatile analytical technique. All complex ionic compounds (containing more than one atom) and coordination compounds produce characteristic spectra; therefore, associated group frequencies may be used diagnostically for characterization of an unknown sample (Coates, 2000). Since the preferred format for presenting spectral data for qualitative analysis is in the percentage transmittance format (logarithmic relationship with respect to the linear concentration format-absorbance), the spectral data collected is shown in Percent Transmittance vs. Wavenumber (Figure 24).

From the plotted FTIR spectra, compounds identification was carried out using Knowitall software based on values found in literature. Due to the low atomic percentage of uranium, a subtle band appeared from 800 to 1000 cm^{-1}. This band may represent three possible functional groups: the presence of the uranyl ion was identified by the stretching from 1000 to 800 cm^{-1} (Gorman-Lewis et al. 2008); the asymmetric stretching vibration of O-U-O from 980 to 920 cm^{-1}, or the symmetric O–U–O stretching vibration at 860 cm^{-1} (Cottton 2006). The appearance of this band was found only in the sample spectra belonging to the sample with lower silica concentration 50 mM Si, 03 mM HCO3, 5 mM Al, 130 ppm U; however, it can be seen that in the spectra for the sample composed of higher silica concentration (100 mM Si, 03 mM HCO3, 5 mM Al, 130 ppm U), the band was beginning to appear but it was not strong enough for clear identification. Further research needs to address the main functional groups responsible for the incorporation of U(VI) in the dried precipitates.

Other peaks identified include: strong absorption bands 4000-2500 cm^{-1} from stretching vibrations between hydrogen and some other atoms with a mass of 19 or less. In this range, O-H and N-H stretching frequencies fall in the 3700 to 2500 cm^{-1} region (Sherman Hsu 1997), and the software used for identification at the same time showed that the bond of Si-OH could also be found in this region from 3700 to 3200 cm^{-1}. H_2O bending vibrations were observed from 1700 to 1590 cm^{-1}, structurally incorporated H_2O at ~1630 cm^{-1} as well as surface absorbed H_2O at ~1530 cm^{-1}(Gorman-Lewis et al. 2008). Absorption bands at 1693 and 1649 cm^{-1} indicate C=O from $KHCO_3$, recognized by the software between 1700-1680 cm^{-1} , and 1680-1630 cm^{-1}. Also a peak at 1402 cm^{-1} (Gasc et al. 2009) or 1390 cm^{-1} (Miravete 1993) corresponds to the C-O bond from carbonate. A band at 1654 cm^{-1} is attributed to Si-OH (Voinescu et al. 2008), and a peak at 1382 cm^{-1} originates from SiO_3OH^{3-} (Gorman-Lewis et al. 2008). There is also a slight band for Si-O-Si(C) from 1250 to 1000 cm^{-1} (Yang et al. 2005), which was recognized by the software between 1100-1000 cm^{-1}. In the lower silica concentration spectra, this band was beginning to appear as well but did not seem to be strong. Additionally, a possible Si-CH_3 peak was identified at 1276 cm^{-1}, and the remaining identified silica peaks were more concentrated around the 900-800 cm^{-1}; the asymmetric Si-O-Si stretching was found at 859 cm^{-1}(Voinescu et al. 2008), and the software recognized Si-C at 860-845 cm^{-1} and Si-O at 910-830 cm^{-1}. A small peak that can be found in NO_2 such as in nitrates is between 1660-1500 cm^{-1}. Since the peak belonging to uranium was only found for one sample's spectra, this analysis will be repeated with higher U(VI) concentrations to clarify the presence of a U(VI)- containing functional group in the dried precipitate.

X-Ray Photoelectron Spectroscopy

X-ray photoelectron spectroscopy (XPS) is a surface sensitive technique (i.e., analysis depth 100 Å) used to identify the elemental composition of the analyzed surface. The detection limit is approximately 0.1 atom percent for most elements. Previous studies have shown that XPS is valuable spectroscopic tool when studying the oxidation state of the elements (Fiedor et al. 2003) In this way, XPS can provide a fingerprint of the oxidation of uranium and thus offers a significant contribution in determining uranium speciation.

The oxidation states of primary interest are U(IV), U(V), and U(VI). In reducing environments, uranium (IV) is generally insoluble. In oxidizing conditions, however, uranium U(VI) forming compounds are for the most part fairly soluble and mobile. Knowing whether U is present in the tetravalent or hexavalent state in the subsurface is important, as oxidation state is a primary control on U mobility and hence its ultimate fate and transport in the environment. For uranium, the 4f line is commonly used because it is the most intense, relatively free from interference, and typically narrowest observed in the spectra. The binding energies (BE) for a particular oxidation state are unique and can be used to identify the chemical state of the material being analyzed (Ilton and Bagus 2011).

XPS technique was used to monitor uranium's oxidation state at the precipitate's surface for the four samples prepared with 130 ppm of U(VI). Two out of four tested samples containing U(VI) showed definitive peaks between the BE of 375 and 385 eV. The third sample showed a weaker peak between 380 and 384 eV, while the fourth sample does not provide a peak possibly due to the low atomic percentage of U in the sample as determined previously via EDS analysis (Table 12). Sample 3, containing 50 mM Si, 3 mM HCO_3, 5 mM Al and 130 ppm U(VI), showed a BE

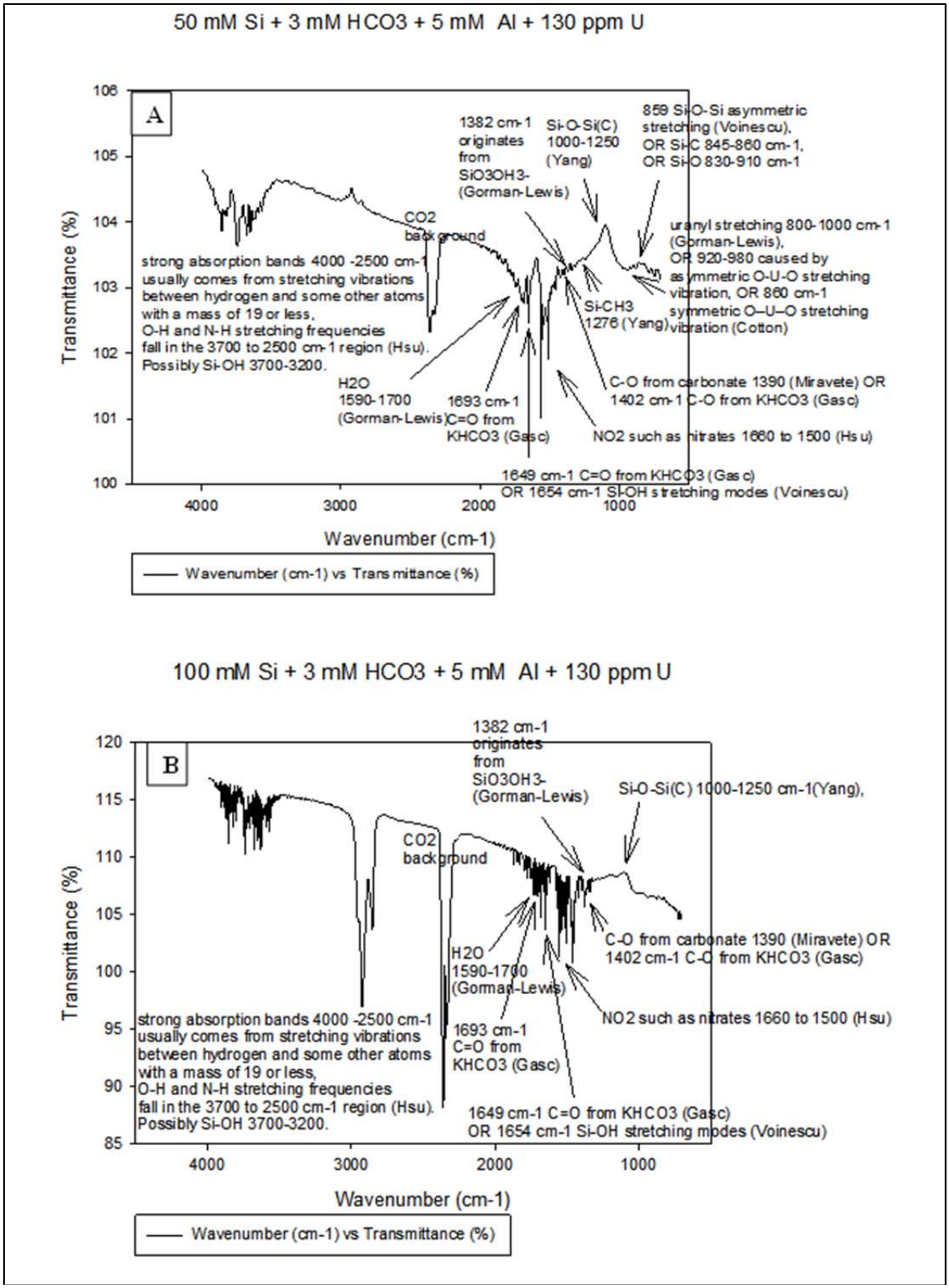

Figure 24. FTIR results for A) 50 mM Si + 3 mM HCO_3 + 5 mM Al + 130 ppm U and B) 100 mM Si + 3 mM HCO3 + 5 mM Al + 130 ppm U.

peak at 382.6 eV, confirming that uranium in the precipitate occurs in the hexavalent state. The sample containing 50 mM Si, 50 mM HCO_3, 5 mM Al and 130 ppm U (Sample 2) and the sample containing 100 mM Si, 50 mM HCO_3, 5 mM Al and 130 ppm U (Sample 4) indicated two peaks of uranium in the range from 375 to 410 eV (U4f7 and U4f5) in both samples containing higher bicarbonate concentrations. XPS scans indicated two peaks that suggest two chemical oxidation states; the peak for 382.4 eV corresponded to U(VI) in form of alkaline earth uranyl carbonates, but the second one was found at about 377.7 eV, which is close to the data on U(IV) presented by a PNNL research team (Ilton and Bagus 2011). Although the oxidation states for U(IV), U(V), and U(VI) are roughly grouped by BE, the BEs of the different oxidation states have a high degree of overlapping. According to Ilton and Bagus (2011), the BEs for K2s are around 377. We have not identified other K peaks in this area that suggest that peak found at 377.3 eV belongs to U.

In addition, XPS scans helped in chemical identification of sample constituencies. Major photoelectron peaks indicated the large peak at 531.5-533.1 eV from the oxygen 1s electron; much smaller peaks for aluminum at 73.9-74.0 eV, and carbon at 285.5 eV (Figure 25). The data for silica provide evidence that silicon present in the samples as SiO2 gel or SiO_2 quartz at BE 103.4- 103.7eV, and aluminum is in the form of $Al(OH)_3$ (gibbsite) at BE 74 eV. In sample 1, measured binding energies for nitrogen correlate to ammonia salt at BE 403.3 eV and in sample 4, a small peak for nitrates appeared at BE 407.3 eV. The incidence of nitrate in the sample 4 is due to the pH adjustment of the testing solutions using nitric acid. The binding energies of U $4f_{7/2}$ taken at 382.1 -382.3 eV correspond to the electronic structure of the alkaline earth uranyl carbonates (Ilton and Bagus 2011, Amayri et al. 2005). The results of XPS analysis correlated with predictions of Visual MINTEQ modeling data. Further analysis is necessary in order to assess U oxidation's state and evaluate the possibility of U(VI) reduction occurring at higher bicarbonate concentrations after ammonia gas injection.

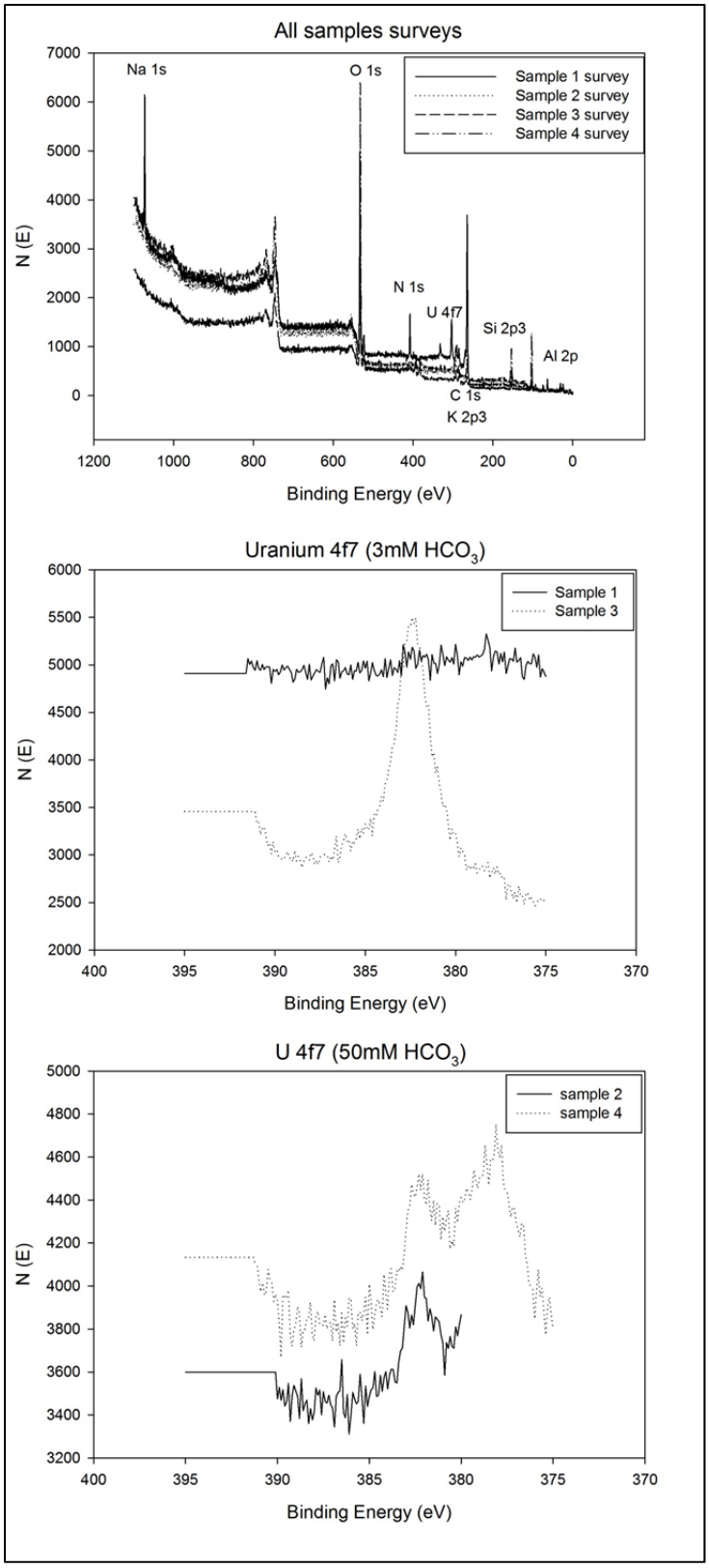

Figure 25. XPS scans for samples 1, 2, 3 and 4.

X-Ray Diffraction

X-ray diffraction (XRD) is a technique that provides detailed information about the atomic structure of crystalline substances and widely used for the identification of soil minerals. It is the only method capable of providing qualitative and quantitative information about the compounds present in a solid sample. Crystalline materials produce well-defined diffraction peaks whose widths are related to the crystalline quality. Crystalline materials produce sharp peaks, while poor-quality crystalline materials yield broader and more diffuse diffraction pattern (Skoog 2007).

XRD analysis were performed on the early stage of experiments with two samples prepared using 250 mM Si + 50 mM HCO_3 + 2.8 mM Al + 2 ppm of U(VI) and 100 mM Si + 3 mM HCO_3 + 2.8 mM Al + 2 ppm of U(VI) (Figure 26). Structural and chemical information has been sought by comparing spectra to those obtained from known phases. A sample holder made of aluminum results in a very high background for aluminum. By removing spectra provided by such an aluminum sample holder, mixtures of solid phases present in the samples produced complex XRD patterns that presented a challenge in mineral identification. Mineral powder diffraction data of solid phases, predicted by MINTEQ, such as aluminum (gibbsite), quartz, aluminosilicate (halloysite), and known uranyl carbonate minerals Cejkaite $Na_4[(UO_2)(CO_3)_3]_2(H_2O)$ and Grimselite $K_3Na[(UO_2)(CO_3)_3](H_2O)$ were obtained for identification of unknown minerals. Diffraction data were taken from American Mineral Crystal Structure Database (http://rruff.geo.arizona.edu/AMS/amcsd.php last visited 05/25/2012). XRD analysis showed no indication of crystal structure and a broad wave extending from angle 10 to 30 indicated that the uranium containing precipitates are amorphous. Relative peak intensities began with d-spacing for the highest intensity peaks for gibbsite, quartz, and halloysite and identified several peaks between 15-40 2θ. However, due to the amorphous nature of the samples, their identification was not accurate. XRD analysis will be repeated using a plastic sample holder. Such analysis will be carried with samples prepared with 200 ppm of uranium and kept in the "mother" solution for a different time interval prior to drying to further explore its crystalline structure. Such analysis would greatly improve the usefulness of the XRD data.

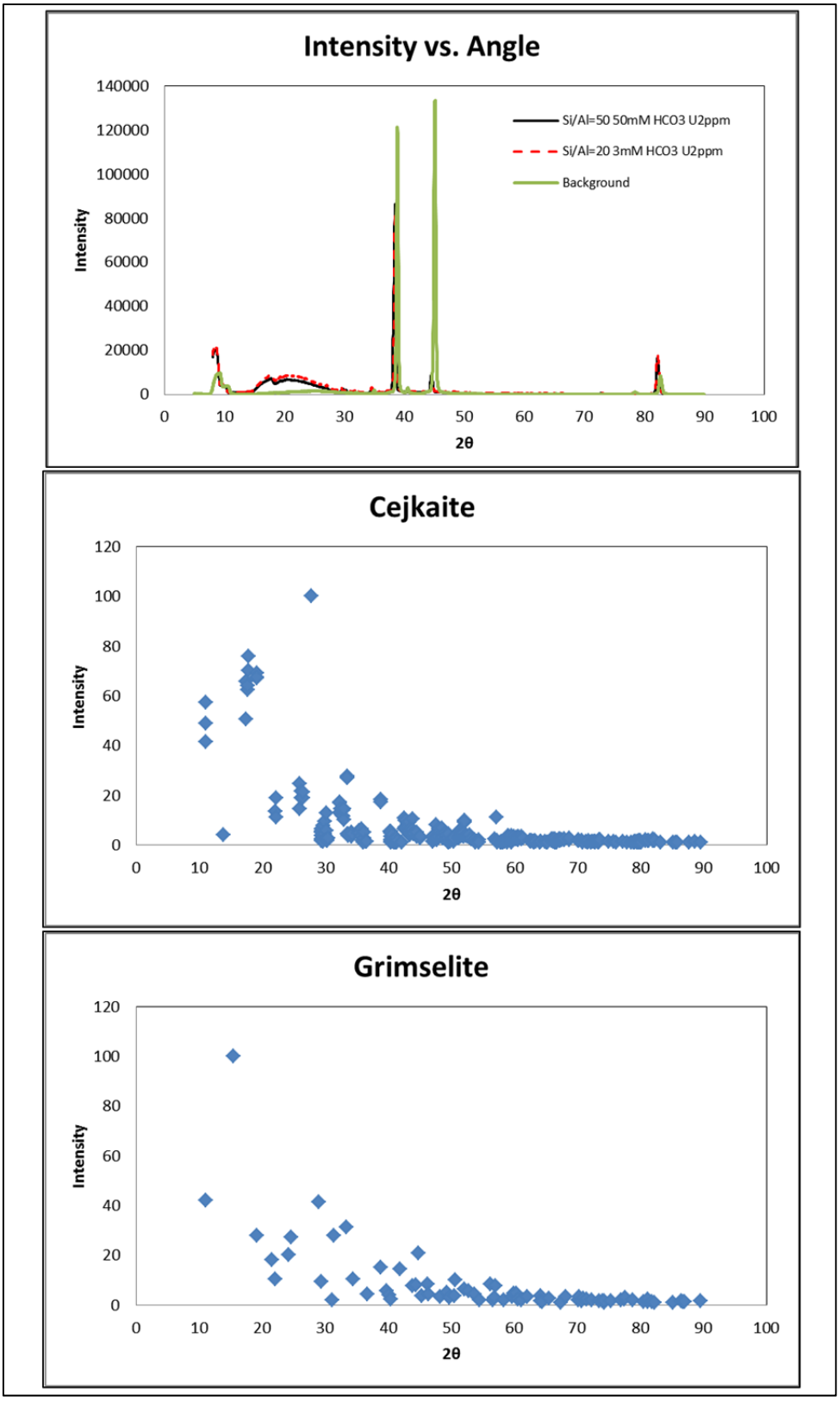

Figure 26. XRD data plots comparing U 2ppm samples with Cejkaite and Grimselite minerals.

TASK 1.1 CONCLUSIONS

Our results provided details on the effect of various silicon, aluminum and bicarbonate concentrations on the removal of uranium and formation of the uranium-bearing precipitates. From the experiments, it is evident that solutions with higher concentrations of Si tended to have greater removal efficiencies of U(VI). The highest percent removal of U(VI) 95-99% was observed at Si concentrations between 150 mM-250 mM. The process of U(VI) removal didn't appear to be efficient when the concentration of Si is less than 50 mM. Solutions with higher concentrations of bicarbonate exhibited bigger removal efficiencies for Si, Al, and U(VI). The increase in Al concentration up to 5 mM, resulted in 9.5%-16% higher U(VI) removal compared to values obtained with 2.8 mM of Al. Overall, the formation of Si gel always correlated with the removal of U(VI), Si, and Al from the solution. If no Si polymerization and gel formation was observed, there was no U removal from the supernatant solution. In the presence of 5 mM of Ca, the removal of U(VI) have overshadowed previous results without Ca ions introduced in the solution. Visual Minteq modeling predicted that U(VI) present in solution dominantly as $Ca_2UO_2(CO_3)_3$ and $CaUO_2(CO_3)_3^{-2}$. Ca-UO_2-CO_3 ternary complexes constitute ~90% of uranyl species.

The solid phase characterization using X-ray diffraction, SEM/EDS, FTIR, and XPS in combination with thermodynamic modeling has allowed evaluating the structural character of the samples' precipitates and relating them to expected uranium species. The progress of the analysis led to increasing uranium concentrations in search for results that would provide valuable information about uranium's conditions in the dried precipitates. XRD showed these precipitates are amorphous phases that would not allow identifying any crystalline structures. The SEM-EDS results showed that the uranium distribution in samples containing low bicarbonate concentrations of 3 mM is uneven throughout a sample and contains varied uranium atomic percentage aggregates of higher uranium concentration. However, EDS indicated more evenly distributed uranium throughout a sample composed of 50 mM HCO_3.

FTIR analysis showed uranium containing functional groups in a sample of lower silica concentration. There was also appearance of the C-O-Si functional group, and if this can be confirmed in future samples, it could be helpful in understanding the structure of the uranium complexes formed. Thus, increasing uranium's concentration and its atomic percentage may increase to the possibility of identifying such functional groups. At the same time, XPS detected the oxidation state of elements and defined that uranium in the sample composed of 50 mM of bicarbonate contains both oxidation states of U (IV) and U (VI). In sample 1, the pattern resulted in very low intensities without any distinct peaks; in this case, increasing uranium's concentration should also clarify results. From the speciation results, we expect most of the uranium to be in the form of $UO_2(CO_3)_3^{-4}$. Future work includes analyzing samples of higher uranium concentration over time and the addition of calcium to investigate how this element affects the precipitate's structure and morphology.

TASK 1.2 INVESTIGATION ON MICROBIAL-META-AUTUNITE INTERACTIONS: THE EFFECTS OF BICARBONATE AND CALCIUM IONS

TASK 1.2 BACKGROUND

The formation of uranyl phosphate complexes in the soil and groundwater has the ability to control actinide behavior due to their low solubility under pH levels between 6.5 and 7.5 (Devivo et al. 1984). Autunite and meta-autunite minerals $\{X^{n+}_{3-n}[(UO_2)(PO_4)]_2\, xH_2O\}$ largely limit the mobility of dissolved U(VI) in soils contaminated by actinides and are an extremely important group of uranyl minerals when considering U sequestration. The autunite structure is composed of phosphate tetrahedrons linked to uranium-oxygen groups that form distorted octahedrons. The phosphates and uranium groups lie in sheets that are weakly hold together by water molecules (Burns et al. 1996). This structure produces the tabular habit, the one perfect direction of cleavage. Autunite minerals precipitation because of polyphosphate injection was identified as a feasible remediation strategy for sequestering uranium in contaminated groundwater and soil *in situ* at the Hanford Site (Vermeul et al. 2009). Autunite stability under vadose and saturated zone environmental conditions can help to determine the long-term effectiveness of this remediation strategy (Wellman et al. 2007).

Aqueous carbonate present in the soil and ground water is a primary species increasing uranium mobility by affecting the dissolution of actinide and promoting the uranium desorption reaction from soil (Langmuir 1978). In a calcium-rich environment, the large formation constants of soluble and stable calcium uranyl carbonate complexes, $[Ca_2UO_2(CO_3)_3^0(aq);\ CaUO_2(CO_3)_3^{2-}]$, influences the speciation of uranium (Langmuir 1978, Bernhard et al. 2001).

In the previous reports, we illustrated the significance of bacteria-uranium interactions by focusing on one of three bacterial strains of *Arthrobacter* sp, isolated from Hanford Site soil. The *Arthrobacter* bacteria are one of the most common groups in soils and are found in large numbers in Hanford soil as well as other subsurface environments contaminated with radionuclides (Boylen 1973, Balkwill et al. 1997, Van Waasbergen et al. 2000, Crocker et al. 2000). Balkwill et al. (1997) reported the predominance of the genus *Arthrobacter* among the culturable aerobic heterotrophic bacteria from the Hanford Site sediments with this group accounting for roughly up to 25% of the subsurface isolates. In addition, *Arthrobacter*-like bacteria were the most prevalent in the highly radioactive sediment samples collected underneath the leaking high-level waste storage tanks and accounted for about of one-third of the total soil isolatable bacterial population (Fredrickson et al. 2004). Furthermore, a previous study conducted using the *Arthrobacter oxydans* G975 strain illustrated a bio-enhanced release of U(VI) from natural Ca-autunite in the presence of various concentrations of bicarbonate. G975 was found the fastest growing and the most uranium-tolerant strain amongst studied microorganisms obtained from SMCC collection. This bacterial strain is ubiquitous in subsurface microbial communities and can play a significant role in the dissolution of minerals and the formation of secondary minerals (Katsenovich et al. 2012a). We wanted to further this research by conducting experiments on the stability of autunite mineral in oxidized conditions pertaining to the Hanford Site and study the environmental fate and transport of uranium in the

subsurface, using the *Arthrobacter* oxydans G968 strain. This strain was found to be less resistant to the U(VI) toxicity. The alteration in surface morphology for G968 was noted at 0.5 ppm; in comparison, G975 shows signs of cell inhibition at the much higher concentration of 19 ppm of U(VI). Additionally, G975 strain accumulated up to 92% of uranium in the studied U(VI) concentration range up to 27 ppm, which is almost triple the value compared to the G968. The results on cell density for G968 determined via hemocytometer showed slightly lower values for the same period compared to G975 (Katsenovich et al. 2012b).

TASK 1.2 OBJECTIVES

The main objective of this investigation was to study the bacterial interactions under oxidizing conditions with uranium (VI); study the potential role of bicarbonate, which is an integral complexing ligand for U(VI) and a major ion in groundwater compositions; and present data from autunite dissolution experiments using *Arthrobacter* strain G968, a less U(VI)-tolerant strain.

TASK 1.2 MATERIALS AND METHODS

Arthrobacter Strains and Growth Culture Conditions

A detailed description of where the *Arthrobacter* strains were obtained is described in the 2010 Year End Report and recent publications (Katsenovich et al. 2012a, Katsenovich et al. 2012b). The strains were cultured in 5% PYTG liquid culture media and agar plates consisting of 5 g/L peptone, 5 g/L tryptone, 10 g/L yeast extract, 10 g/L glucose, 0.6 g/L $MgSO_4.7H_2O$, 0.07 g/L $CaCl_2.2H_2O$. Media was prepared in deionized water (DIW) (Barnstead NANOpure Diamond Life Science (UV/UF), Thermo Scientific), autoclaved at 121^oC and 15 psi for 15 minutes, then allowed to cool down before being used.

To account for viable bacteria, a well-mixed homogeneous aliquot (0.01 mL - 0.1 mL) of the suspension from each test vial was uniformly spread on the sterile Petri dishes containing a 5% PTYG growth media mixed with 15 g/L of agar. Inoculated plates were kept inverted in an incubator at 29^oC. Viable microorganisms were calculated from the number of colony-forming units (CFU) found on a specific dilution. In addition, the agar plating was used to provide a quick visual check for contamination and to maintain colonies from each stage of the enrichment for the duration of the experiment. The cell density (cells/mL) was calculated with the help of a glass hemocytometer (Fisher Scientific, Pittsburg, PA). Cell counts in the samples containing uranium employed INCYTO C-Chip disposable hemocytometers. The hemocytometer is a microscope slide with a rectangular indentation, creating a chamber that is engraved with a grid of perpendicular lines. Having known the area bounded by the lines as well as the depth of the chamber, the cell density in a specific volume of fluid and in a bacterial broth solution was calculated from a sample, homogenously distributed inside the chamber. Once the average cell count was obtained, it was multiplied by the dilution factor and the volume factor, 10^4, in order to calculate the final concentration of cells per mL.

Dissolution of U(VI) from Autunite

Sterile 100 mL glass mixed reactors served as the major bioreactor for initial experimentation. These autunite-containing bioreactors were injected with bacterial cells after the autunite equilibrated with media solution.

Bicarbonate Media Solution Preparation

The media solution to conduct the autunite dissolution experiments was prepared using 0.25 g/L peptone, 0.25 g/L tryptone, 0.5 g/L glucose, 0.6 g/L $MgSO_4$, and 0.07 g/L $CaCl_2 \cdot 2H_2O$. Due to the high phosphorus content, yeast extract was not included in the media. Media was prepared in deionized water (DIW) (Barnstead NANOpure Diamond Life Science (UV/UF), Thermo Scientific), autoclaved at 121°C, 15 psi for 15 minutes, and cooled down to about 30°C. After sterilization, the media was equally distributed between four 200-mL bottles and separately adjusted to contain 0 mM, 3 mM, 5 mM, and 10 mM of $KHCO_3$. The media was adjusted to pH 7.5 with 0.1 mol/L HCl or NaOH and buffered with 0.02 M 2-(2-hydroxyethyl)-1-piperazine ethanesulfonic acid sodium salt hydrate (HEPES-Na) buffer. Each of the individual four bicarbonate media solutions were filtered-sterilized (0.2 μm) and kept refrigerated until time of use.

Autunite bioleaching in bioreactors

Natural Ca meta-autunite, $Ca[(UO_2)(PO_4)]_2 \cdot 3H_2O$ obtained from Excalibur Mineral Corporation (Peekskill, New York), was previously characterized using ICP-OES, ICP-MS analyses, X-ray diffraction and SEM/EDS to confirm the mineral composition, structure, and morphology as 98–99% pure autunite (Wellman et al. 2006). The autunite sample was powdered to have a size fraction of 75 to 150 μm or -100 to +200 mesh with a surface area of 0.88 m^2/g determined by Kr-adsorption BET analysis (Wellman et al. 2006). Autunite microbial bioleaching experiments were conducted with 100 mL foam stoppered glass serum bottles containing 50 mL of sterile media buffered with 20 mM HEPES-Na and 91 mg of meta-autunite to provide an U(VI) concentration of 4.4 mmol/L. The suspensions were slightly agitated at 60-rpm in incubator/shaker at 25 °C. G968 *Arthrobacter* cells in the amount of 10^6 cells/mL were injected into the reactors after 27 days, giving time for the autunite to reach steady state. During the inoculation, reactors kept their sterile foam stoppers to sustain aerobic conditions within the reactors. Abiotic non-carbonate controls were kept without bacterial inoculation to provide a control for the biotic samples.

Analytical Procedures

Every few days, a 0.3 mL sample of the solution was aseptically withdrawn from each bottle, filtered (0.2 μm), and then analyzed for dissolved U(VI) by means of kinetic phosphorescence analyzer KPA-11 (Chemcheck Instruments, Richland, WA). The dilution factors for sample analysis were 100 for low concentrations of bicarbonate, and 200 for high concentrations of bicarbonate. Prior to this analysis, sample aliquots were ashed on a hot plate with the addition of concentrate plasma grade nitric acid and hydrogen peroxide solutions. Wet digestion was continued until a dry white precipitate formed, and then dry ashing was performed in the furnace at 450°C for 15 min. Samples were allowed to cool down at room temperature followed by the dissolution of the precipitate by the addition of 1 M nitric acid (HNO_3). Aqueous concentrations of calcium and phosphorus were determined from the digested samples by

means of Optima 7300 ICP-OES (Perkin Elmer). Uranium calibration standards (SPEX certiPrep), blanks and check standards (95-105% recovery) were analyzed for quality control. After the bioleaching experiment, the samples of cells transferred to the centrifuge tubes were prepared for SEM/EDS analysis. The cells were harvested by centrifugation at 4000 rpm for 5 minutes, washed twice with DIW and then fixed in the 5 ml of 2% glutaraldehyde in 0.1 M HEPES buffer at pH 7.2 for 2h at 4^{o}C. The material was removed by centrifugation and washed with 50 mM HEPES buffer three times for 10 min. The rinsed cells were then dehydrated in ethanol/ water solutions of 35% (v/v), 70% (v/v), and 90% (v/v) each for 10 min, and two times in 100% (v/v) for 10 min. Dehydrated samples were immersed for 10 min in 100% pure hexamethyldisilazane (HMDS); followed by 10 min of air-drying to allow liquid to evaporate from a sample. The dehydrated specimens were then kept in the desiccators until the time of SEM/EDS assay (Katsenovich et al. 2012).

Statistical Analysis

The bioleaching experiment was conducted in triplicates to obtain descriptive statistical analyses such as mean, standard deviation and confidence interval of the mean. Uranium calibration standards (SPEX certiPrep), blanks, and check standards (95-105% recovery) were analyzed for quality control before each experiment utilizing the KPA to check on variability of the machine.

TASK 1.2 RESULTS AND DISCUSSION

Dissolution of U(VI) from Autunite

The release of aqueous U(VI) over time during the autunite dissolution experiments is presented in Figure 27. U(VI) concentrations in the abiotic control that did not contain bicarbonate equilibrated over a period of 27 days and reached an average of 0.46± 0.1137 μm. In bicarbonate-amended reactors, U(VI) release from autunite was strongly enhanced. Prior to strain inoculation, U(VI) concentrations measured at 0.5532±0.1231 μm, 1.0715±0.3371 μm, and 43.9839±7.1645 μm for 3 mM, 5 mM and 10 mM $KHCO_3$, respectively. The uranyl release from autunite in the studied bicarbonate concentrations range prior to G968 inoculation was increased by a factor of 1.2±1.08, 2.3±2.96, 95.6±63.00 compared to the no-bicarbonate control, respectively. After bacteria inoculation, U(VI) measured in the reactors increased 8.9±23.34, 101.0±108.97, 72.1±123.86, 2.3±8.65 fold, respectively, compared to the corresponding bicarbonate-bearing controls at steady state. Even though there is an increased amount of U(VI) leached out into the solution driven by the presence of bacteria, the effect of bacteria on autunite dissolution is reduced as the concentration of $[HCO_3^-]$ increases. This trend is expected since the thermodynamic stability constants for the interactions between carbonate and both the autunite and the bacteria are higher than the autunite-cell interactions. Since the steady-state U(VI) concentration is higher for larger $[HCO_3^-]$, the increase in soluble U(VI) concentration induced by bacteria is dwarfed. Therefore, as $[HCO_3^-]$ increases, a diminishing trend on the effect of bacteria on autunite leaching is observed.

It has been demonstrated that mechanisms of uranium release from autunite minerals is controlled by a surface mediated reaction. Bicarbonate can promote mineral dissolution by binding to surface U(VI) ions causing weaker bonds, which is followed by detachment of the

U(VI) species into solution (Sparks 1999). The figure below illustrates the release of phosphorus from the mineral influenced by the detachment of U(VI) (Figure 28).

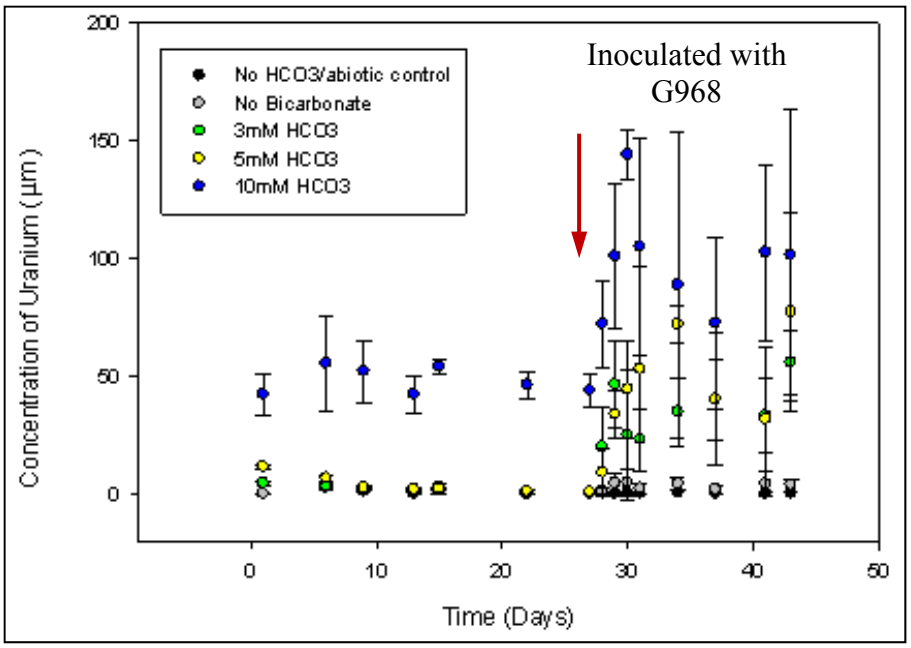

Figure 27. Changes for aqueous U(VI) as a function of time for the natural autunite dissolution experiments inoculated with *Arthrobacter* G968 strain.

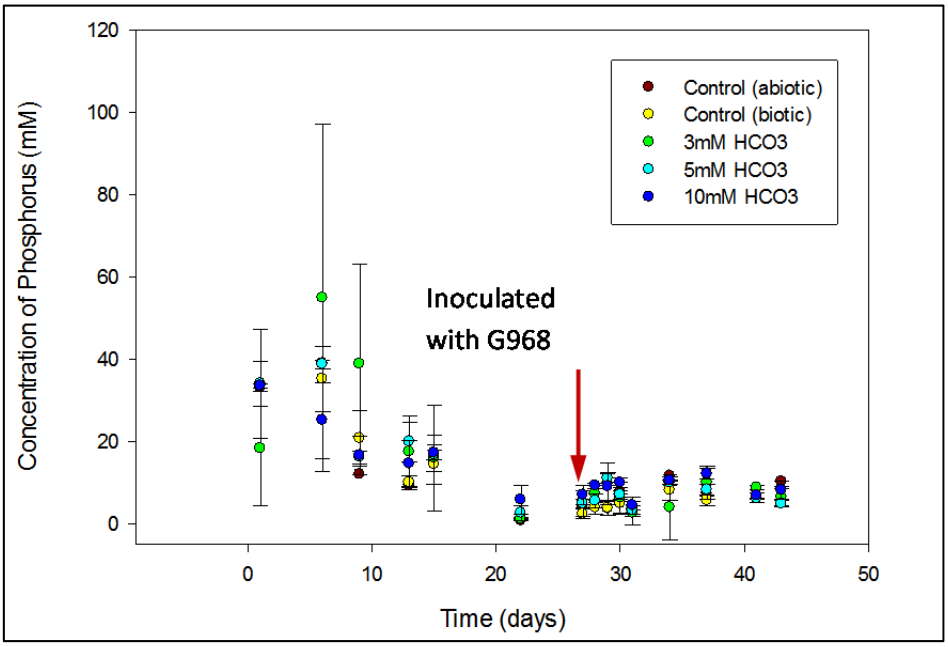

Figure 28. Aqueous P release as a function of time from the natural autunite dissolution experiments inoculated with Arthrobacter G968 strain.

During the autunite dissolution period without bacteria, P concentrations were increased compared to the non-carbonate abiotic control. After inoculation, P concentrations in the biotic

reactors were found to decrease for all studied bicarbonate concentrations. This was correlated with the exponential growth phase of bacteria that were seeded into the reactors. P is an essential nutrient requirement for bacteria for the synthesis of DNA, ATP, polyphosphates, and cell wall phospholipids. Ivanova et al. found that biocatalytic processes involving simultaneous occurring biosynthetic and chemical reactions greatly enhance the rate of efficiency of phosphorous bioleaching. Microorganisms are able to dissolve P-bearing minerals by accessing insoluble phosphate bearing minerals through microbial dissolution (Vazques et al. 2000).

Similar to U(VI), aqueous Ca release over the period of autunite dissolution without bacteria was noted to increase as a function of bicarbonate concentrations, illustrated in Figure 29.

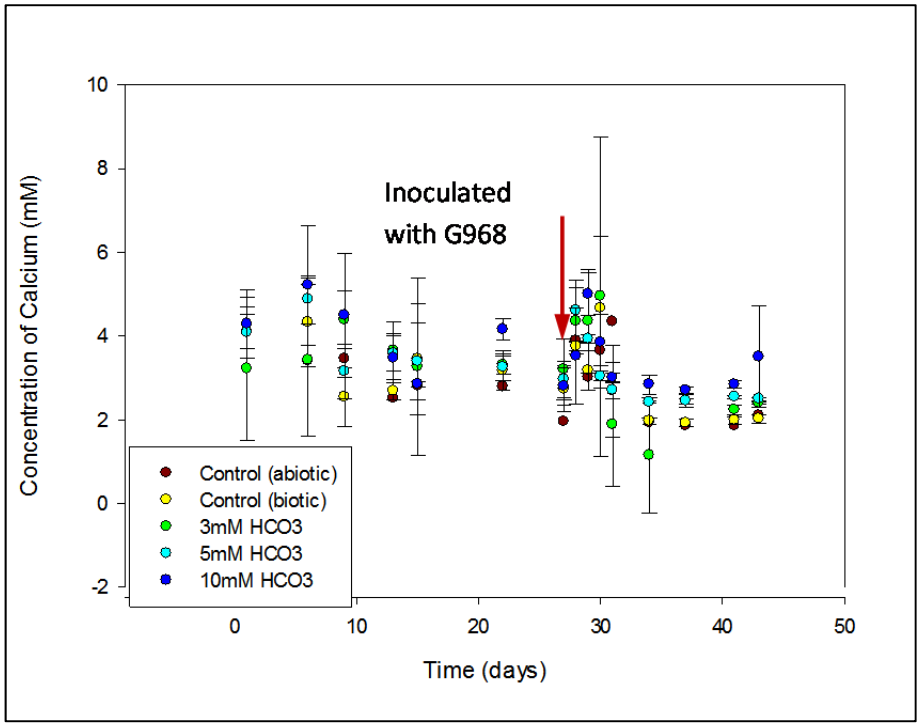

Figure 29. Aqueous Ca release as a function of time for the biotic reactors inoculated with Arthrobacter G968 strain.

Arthrobacter species has the potential of becoming an important component in the dissolution process while forming secondary minerals. The stability of uranyl- phosphate complexes makes them a strong candidate for the remediation efforts to sequester U in the subsurface. The conditions in the Hanford Site, however, are a bicarbonate-rich oligotrophic environment, causing the autunite to have a high liability to dissolution in the presence of bacteria. Autunite, as a P-containing mineral, can attract bacteria to liberate P to meet their needs for nutrients, which may result in U mobilization into the environment.

Comparison

In an assessment of the resistance of Hanford Site *Arthrobacter* isolates to uranium (VI) exposure, presented in 2011, *Arthrobacter* G975 bacterial strain proved to remain viable in the presence of 0.5 ppm of U(VI). After a week, the number of viable colonies was comparable to the control without U(VI). Furthermore, G975 exhibited the highest tolerance towards U(VI) relative to the other *Arthrobacter* strains and remained viable in the presence of 9.5- 19 ppm of

U(VI). A series of tests illustrated that G975 was the fastest growing and the most uranium tolerant strain and can accumulate more than 90% of uranium due to its distinctive surface structure (Katsenovich 2012b). When the cells are exposed to various concentrations of uranium, it is necessary to use an atomic force microscopy (AFM) to oversee the changes at the nanoscale level. Illustrated below the uranium treated samples contain clear crystalline deposits on the cell surface (Figure 31, Figure 33). Figure 30 and Figure 32 present deposits-clear bacterial surfaces of control samples.

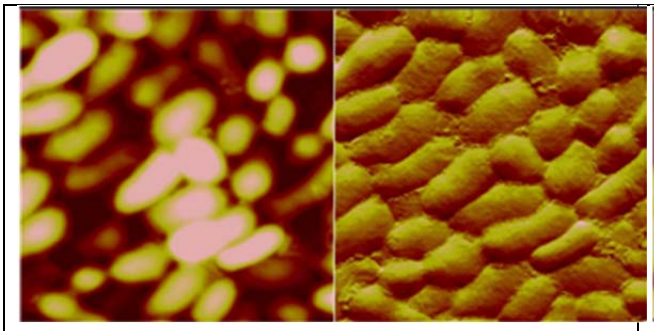

Figure 30. G968 control sample (scan size 10 × 10 µm2). Phase image clearly shows no precipitation on the cell surface.

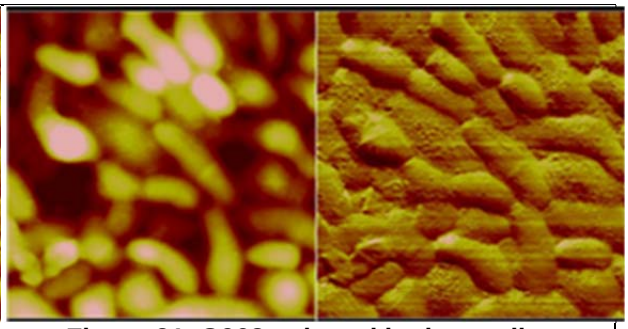

Figure 31. G968 cultured in the media amended with 1ppm of U(VI) (scan size 10 × 10 µm2). Phase image clearly shows crystalline deposits on the cell surface, which can also be visualized in height image on the left.

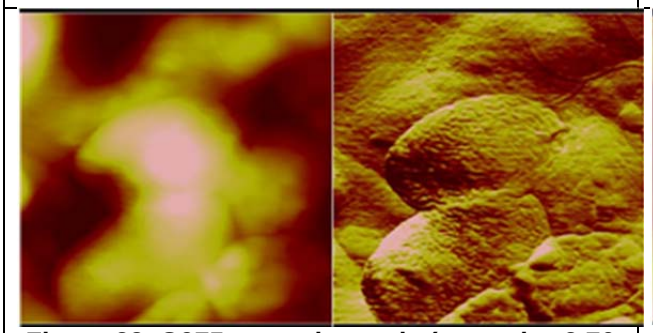

Figure 32. G975 control sample (scan size 3.76 × 3.76 µm2) showing its unusual irregular surface morphology on the right. The topography image on the left (Z range 250 nm) and frictional image (0.3 V) on the right.

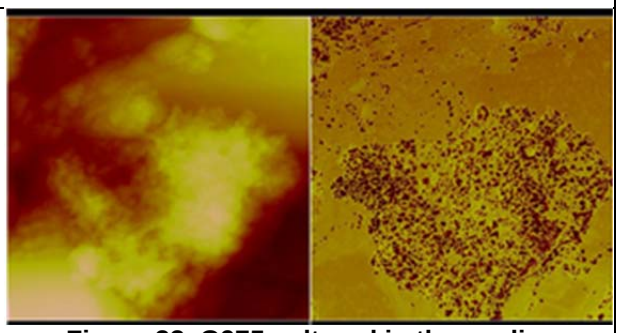

Figure 33. G975 cultured in the media amended with 10ppm of U(VI), (scan size 1.57 × 1.57 µm2; phase angle 60º). Phase image on the right clearly shows crystalline deposition on the cell surface.

Although precipitate was present on all *Arthrobacter* strains, the amount aggregated on the unusually wrinkled surface of G975 surpassed the rest, which is presented in Figure 33. The surface morphology of this strain supports a higher accessibility for the formation of the uranium precipitates.

Despite these morphological differences between the two bacterial strains, they are able to dissolute uranium at the same capacity. The effect of both bacterial strands on autunite dissolution reduces as the concentration of bicarbonate increases while the increase in soluble U(VI) concentration induced by G968 and G975 is dwarfed, for larger [HCO_3^-]. Furthermore, during the autunite dissolution period without bacteria, P concentrations were increased

compared to the non-carbonate abiotic control. After inoculation, P concentrations in the biotic reactors were found to decrease for all studied bicarbonate concentrations. Similar to U(VI), aqueous Ca release over the period of autunite dissolution without bacteria was noted to increase as a function of bicarbonate concentrations for both *Arthrobacter* strains.

Cell Viability

Viability of cells was conducted after 24 hours of cell incubation with the appropriate uranium and bicarbonate concentration treatment. Samples of the smallest and largest concentration of bicarbonate were plated and incubated on 5% PTYG hard media and then counted for colony-forming unites (CFU). The number of cells was greater in sample containing 10 mM bicarbonate compared to 0 mM bicarbonate. As expected, the cells started to reduce after day 41 due to the nutritional exhaustion of the media. Moreover, viable bacteria accounted for more than 94% in the presence of 10 mM bicarbonate.

TASK 1.2 CONCLUSION

The effect of bicarbonate on the autunite mineral microbial leaching experiments was evaluated in mixed reactors comprised of autunite powder and media solution. The *Arthrobacter* G968 strain was used in the experiments. The uranium release from autunite prior to the *Arthrobacter* G968 strain inoculation in mixed reactors was increased by a factor between 1.2±1.08 and 95.6±63.00 compared to the no-bicarbonate control. After bacteria inoculation, U(VI) measured in the reactors increased 8.9±23.34 to 2.3±8.65 fold when compared to the corresponding bicarbonate-bearing controls at a steady state. A diminishing trend on the effect of bacteria on autunite leaching was observed as bicarbonate concentrations were increased in the solution. The aqueous concentrations of U(VI), P, and Ca released during the dissolution of autunite were non-stoichiometric over the range of experimental conditions. After inoculation, P concentrations in the biotic reactors were found to decrease. In the future, a Kirby-Bauer Disk-Diffusion technique will be applied to determine the susceptibility of G968 strain to different concentrations of uranium in sterile Petri dishes. Other future work includes conducting an autunite bioleaching experiment in culture ware with inserts to investigate how the autunite mineral reacts with the bacteria separated from it, and to perform an SEM/EDS microscopy analysis on the strain to test the cell surface composition.

TASK 1.3 EFFECT OF BICARBONATE ON THE DISSOLUTION OF META-AUTUNITE

TASK 1.3 BACKGROUND

The 300 Area of the Hanford Site was used for uranium fuel fabrication, research and development activities. After operations at the 300 Area began in 1943, these activities led to the contamination of streams, soil and groundwater primarily with uranium. The primary cleanup activities that have taken place in the 300 Area include removal of contaminated soils and debris, treatment of the material to reduce the toxicity and mobility of the contaminants, and disposal of the material in an appropriate long-term waste management facility. Currently, the contaminated groundwater in the 300 Area is being monitored to ensure that the contamination levels are decreasing through natural processes. The uranium concentration is associated with contamination remaining in the deep vadose zone and smear zone, where the smear zone is the area where free product occurred in the soil and was then smeared across the soil when the water table fluctuated between historic high and low water table elevations.

In oxidizing groundwater conditions, soluble uranyl ion (UO_2^{2+}) creates strong complexes with carbonate. Wellman (2008) reported that at pH of ~8.5, uranyl ion form carbonate complexes: 27% as $UO_2(CO_3)_2^{2-}$ and 68% as $UO_2(CO_3)_3^{4-}$, 3% as $UO_2(OH)_2^{0}$ and 2% as $UO_2(OH)_3^{1-}$. The highly water soluble uranyl carbonate complexes can greatly increase the solubility of uranium minerals and facilitate uranium desorption reactions from soil and sediments (Langmuir, 1997). Serne (2002) reported that the uranium adsorption K_d values ranged from 7 to 2 mL/g in the presence of bicarbonate concentrations between 0.9 to 2.2 mM; however, K_d values were reduced to the 0 to 0.3 mL/g range when bicarbonate concentrations increased to 2.5 - 13 mM.

By changing the chemical speciation, toxic and mobile species can be converted to nontoxic and immobile species (Knox, Brigmon, Kaplan, & Paller, 2008). Uranium has a high affinity to form strong and the most stable complexes with phosphate amongst oxygen-containing ligands (Giammar D. , 2001) (Sowder, Clark, & Fjeld, Dehydration of Synthetic Autunite Hydrates, 2000). The presence of phosphate in groundwater can limit the mobility of the uranyl cation (UO_2^{2+}) in the subsurface due to the formation of sparingly insoluble autunite minerals. Injection of a soluble sodium tripolyphosphate amendment into the uranium contaminated groundwater and soil have been shown to effectively sequester uranium through the formation of insoluble uranyl phosphate minerals. The uranyl phosphates are a large family of minerals, $X_{1-2}[(UO_2)(PO_4)]_{2-1}\cdot nH_2O$, where X is any monovalent of divalent cation (Vermeul, et al., 2008).

Release of uranium from autunite takes place during slow dissolution of the mineral structure. The solubility products of uranyl phosphate, log K_{sp}, reported in the literature have been measured from 49 to 53 (Grenthe, et al., 1992) (Sandino & Bruno, 1992) which is slightly less soluble then other autunite phases such as calcium (log K_{sp}=45) or sodium (log K_{sp}=48) (Langmuir, 1997). Environmental factors, such as pH, temperature, dissolved organic matter, and redox potential, have tremendous effects on both uranium and polyphosphates. For example, hydrolysis of polyphosphates has been found to take place at lower pH ranges (Heyns, 1998), which in turn can influence its reaction rate with uranium. Similarly, pH and redox potential can

also have influence on these chemicals, either by changing their oxidation states (uranium) or by influencing hydrolysis (polyphosphates).

Information on the stability of uranyl-phosphate phases is limited to pH, temperature, and a few aqueous organic materials (Wellman, Icenhower, Gamerdinger, & Forrester, 2006). Kinetic dissolution studies of autunite conducted in the wide range of pH and temperatures in flow-through and batch experiments illustrated a strong dependency of dissolution rates on pH but were relatively insensitive to temperature variations (Wellman, Gunderson, Icenhower, & Forrester, 2007) (Wellman, Icenhower, Gamerdinger, & Forrester, 2006). Yet, limited data available about autunite stability relates to complexation with ligands

Carbonate/bicarbonate leaching solutions are traditionally used to extract uranium from contaminated soils. Manson (1997) examined carbonate leaching of uranium from contaminated soil at the Fernald Site, Ohio. The leach solution of $KHCO_3/K_2CO_3$ at 1:1 ratio and the total concentration of CO_3^{2-} 0.5 M effectively removed 80% of uranium from soil within 48h and an additional 5% over the next 288h in column experiments. Increases in the reaction temperature often enhance the solution reaction rate. However, no appreciable changes were noted in the removal rate at temperatures of 25, 45, and 65^oC using 0.5 M HCO_3^- as a leaching solution (Manson, Turney, Thomson, Lu, & Longmire, 1997).

TASK 1.3 OBJECTIVE

The objective of the experimental work was to quantify the effect of bicarbonate on the stability of synthetic meta-autunite created as a result of uranium stabilization through polyphosphate injection. The polyphosphate technology with the formation of autunite is identified as the most feasible remediation strategy to sequester uranium in contaminated groundwater and soil *in situ*. The experimental work will help to quantify the dissolution kinetics of meta-autunite minerals in the presence of bicarbonate and investigate the influence of factors such as temperature and pH on the dissolution kinetics.

A series of dissolution experiments were conducted in a single pass flow through (SPFT) reactor using a mixture of carbonate and TRIS buffer solution subjected to various temperatures. The parameters that were tested are carbonate concentrations in the range of 0.5 - 3.0 mmol/L, pH (6 - 11), and temperature (5 - 60^oC).

TASK 1.3 MATERIALS AND METHODS

Synthetic Sodium Meta-autunite

A modified direct precipitation method from Vochten, et al. (1980) described by Wellman, et al. (2005) was used for synthesis of Na-autuntie. The precipitation of Na-autunite was accomplished by mixing uranyl nitrate, $UO_2(NO_3)_2.6H_2O$ solution and sodium phosphate dibasic, $Na_2HPO_4{\cdot}7H_2O$ in a volumetric ratio of 1:7.5 while stirring at 70^oC. The overall reaction is as follows:

$$Na_2HPO_4.7H_2O + UO_2(NO_3)_2.6H_2O \text{ -----> } Na[UO_2PO_4]nH_2O + NaNO_3 + HNO_3 \quad (1)$$

Heating was terminated after a yellowish green precipitate was formed rapidly and stirring was continued until the solution returned to room temperature. The solids were allowed to cure at

room temperature for 24 hours without stirring. Solids were recovered from solution using vacuum filtration with a 0.45 μm disposable Nalgene filter; the solids were then washed with DI water heated to 70^{o}C followed by rinsing with isopropyl alcohol. Solids were dried at room temperature until a constant weight was achieved.

Characterization of Sodium Meta-Autunite

The synthesized and partially reacted autunite solids were characterized by JSM-5900-LV low vacuum scanning electron microscope (SEM) at 15kV for identification of particle size. Energy dispersive X-ray spectroscopy (EDS) was used to determine the composition and purity of the solids. The composition of the particles was analyzed using a Noran System Six Model 200SEM energy dispersive X-Ray spectroscopy (EDS). Pre-experimental surface area analysis was conducted following N_2-adsorbtion BET method (Brunauer, Emmett, & Teller, 1938) by using a micromeritics ASAP 2020 surface and porosity analyzer at Pacific Northwest National Laboratory (PNNL) and compositional analysis using Bruker 5000D XRD instruments.

Scanning Electron Microscopy (SEM)

SEM with EDS analysis was performed in the Advanced Materials Engineering Research Institute (AMERI) at Florida International University (FIU) by using a JSM-5900-LV low vacuum scanning electron microscope (SEM) at 15kV. The sample was mounted on a double-sided carbon tape as the mineral has a very low electrical conductivity and can be electrostatically charged during imaging. The compositional analysis was performed using EDS; composition of the solids was conducted at three (3) locations for sodium (Na), oxygen (O), phosphorous (P), nitrogen (N), and uranium (U), and the data is presented in Table 14. Average compositions of the elements were divided by molecular weight of the element to obtain molar quantities of the elements. Molar quantities of elements were divided with the lowest molar quantity to obtain the chemical formula of the mineral. Based on the data shown in Table 14, the chemical formula of the synthesized mineral's atomic ratio matches the atomic ratio of autunite and the chemical formula of the synthesized mineral is Na $[UO_2\ PO_4]$.

Table 14. Elemental Composition of Sodium Meta-Autunite After Washing

Element	Sample 1	Sample 2	Sample 3	Average	Molecular Wt.	Molar Quantity	Atomic Ratio
Na	5.14	6.29	6.91	6.11	23	0.27	1.08
O	20.37	21.93	25.11	22.47	16	1.40	5.69
P	7.3	7.77	7.87	7.65	31	0.25	1.00
U	65.25	62.1	56.54	61.30	238	0.26	1.04

X-Ray Diffraction (XRD)

X-ray diffraction analysis was performed on the synthesized autunite mineral at 40 kV and 40 mA using a Bruker 5000D XRD instrument. Diffraction patterns were obtained using a copper radiation source with a tungsten filter. The sample was analyzed in the range of 2 to 35^{o} for the 2-theta (2θ) with 0.04^{o} step increment and a two-second count time at each step. As shown in Figure 34, XRD patterns obtained for synthesized autunite matched, but at higher intensity, the diffraction patterns of the known autunite PDF obtained from PNNL for comparison.

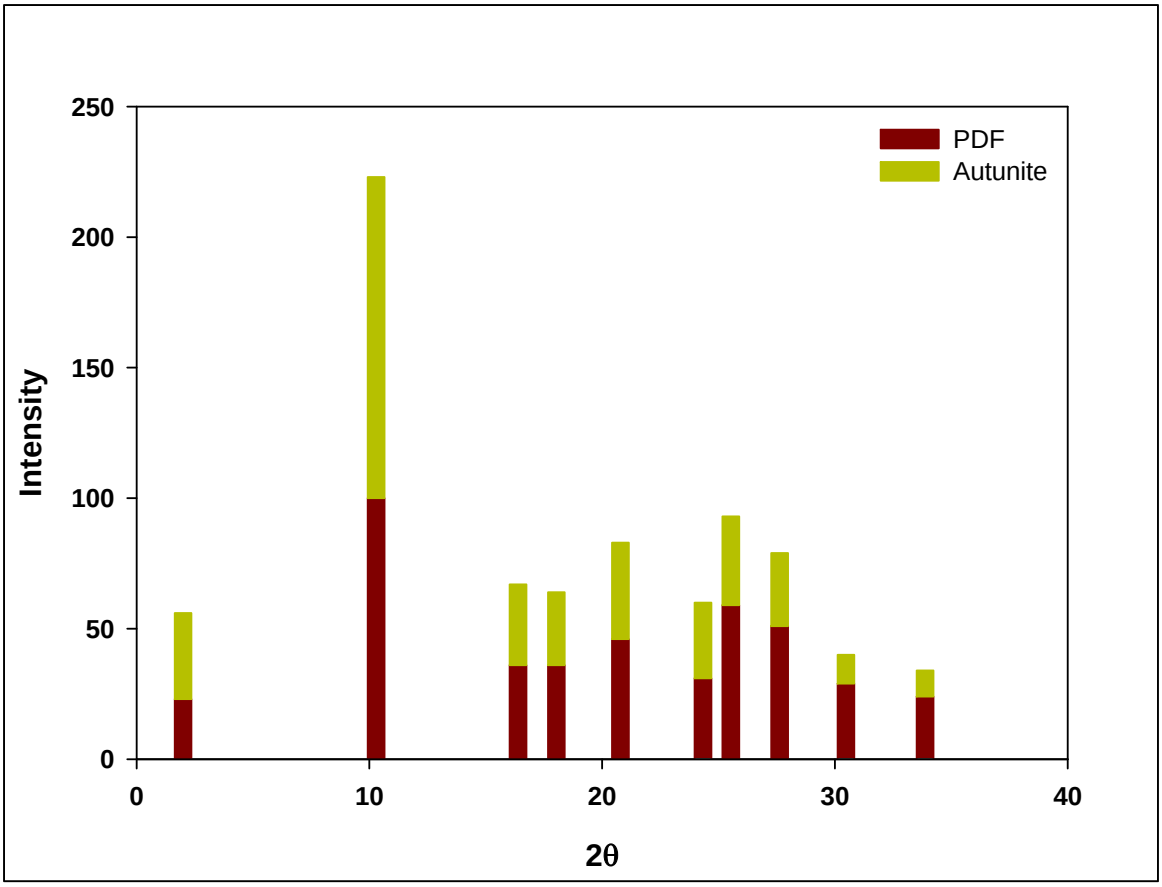

Figure 34. X-Ray diffraction patterns of synthetic Na-autunite mineral.

Carbonate Buffer Solutions

Buffer solutions were prepared with distilled de-ionized water (DDIW) consisting of 0.05 M *tris (hydroxymethyl) aminomethane* (TRIS, $(HOCH_2)_3CNH_2$) buffer and aqueous bicarbonate concentration in the range of 0.0005 to 0.003 M were used to investigate the uranium release from natural autunite mineral over a pH (23°C) interval of 6 to 11. The pH of the buffer solutions were adjusted using 0.1 M hydrochloric (HCl) acid and 0.1 M potassium hydroxide (KOH); composition of the buffer solutions are shown in Table 15.

Single-Pass Flow-Through (SPFT) Experiments

The SPFT test was designed to conduct experiments under controlled pH and temperature conditions with constant fresh water flowing through a reaction cell filled with a mineral sample. The well-mixed batch type reactor was used in the current study to measure the dissolution rates of autunite minerals under strictly controlled conditions. The most important feature of this test was to remove the ions released into solution as a result of autunite dissolution by continuously flowing fresh water into the system. This test has been widely used to measure reaction rates of minerals and could be easily adapted to operate with various flow rates, solution composition, and sample mass and temperature variations to ensure accurate rate determinations (McGrail, Ebert, Bakel, & Peeler, 1997) (Wellman, Icenhower, Gamerdinger, & Forrester, 2006).

Table 15. Composition of Solutions of Bicarbonate Concentrations Used

Solution	Composition	pH @ 23°C
1	0.05 M Tris + 0.0005 M HCO_3^- + 0.01096 M HCl	5.96
2	0.05 M Tris + 0.0005 M HCO_3^- + 0.0103M HCl	7.00
3	0.05 M Tris + 0.0005 M HCO_3^- + 0.00779 M HCl	8.01
4	0.05 M Tris + 0.0005 M HCO_3^- + 0.00256 M HCl	9.01
5	0.05 M Tris + 0.0005 M HCO_3^- + 0.000147 M HCl	10.02
6	0.05 M Tris + 0.0005 M HCO_3^- + 0.00083 M KOH	11.00
7	0.05 M Tris + 0.001 M HCO_3^- + 0.0112 M HCl	6.01
8	0.05 M Tris + 0.001 M HCO_3^- + 0.0103 M HCl	7.02
9	0.05 M Tris + 0.001 M HCO_3^- + 0.00654 M HCl	8.00
10	0.05 M Tris + 0.001 M HCO_3^- + 0.00265 M HCl	9.01
11	0.05 M Tris + 0.001 M HCO_3^- + 0.000147 M HCl	10.00
12	0.05 M Tris + 0.001 M HCO_3^- + 0.00116 M KOH	11.00
13	0.05 M Tris + 0.002 M HCO_3^- + 0.0118 M HCl	6.01
14	0.05 M Tris + 0.002 M HCO_3^- + 0.0108 M HCl	6.99
15	0.05 M Tris + 0.002 M HCO_3^- + 0.00798 M HCl	7.99
16	0.05 M Tris + 0.002 M HCO_3^- + 0.00267 M HCl	9.01
17	0.05 M Tris + 0.002 M HCO_3^- + 0.00006 M KOH	10.00
18	0.05 M Tris + 0.002 M HCO_3^- + 0.00192 M KOH	11.00
19	0.05 M Tris + 0.003 M HCO_3^- + 0.0125 M HCl	6.01
20	0.05 M Tris + 0.003 M HCO_3^- + 0.01077 M HCl	7.01
21	0.05 M Tris + 0.003 M HCO_3^- + 0.00784 M HCl	8.01
22	0.05 M Tris + 0.003 M HCO_3^- + 0.00240 M HCl	9.01
23	0.05 M Tris + 0.003 M HCO_3^- + 0.000379 M KOH	9.99
24	0.05 M Tris + 0.003 M HCO_3^- + 0.002747 M KOH	11.00

The SPFT system, shown in Figure 35, includes a programmable Kloehn V6 syringe pump (55022) that transferred carbonate buffered fresh solution from an influent reservoir (R) via Teflon lines into two-port (1/4") 60 mL capacity *perfluoroalkoxide* (PFA) Teflon reactor vessels (Re) obtained from Savillex (Minnetonka, MN). The transport of the influent solution from the reservoir to the reactors was accomplished via 1/16-inch Teflon tubing and the effluent solution was transported via 1/32-inch Teflon tubing. The reactors were kept in an oven and refrigerator under the temperature controlled conditions during continuous system operation to maintain them at a specific temperature in the range of 5 to 60°C. A thin sample solids layer resting at the bottom of the reactor interacted with solution flowing through the reactor. The solution flow rate was in the range of 1 - 2.5 L/day. A blank solution sample was collected prior to the addition of Na-autunite. The effluent solution was continuously collected until steady state conditions were attained, which was attained after the transfer of ~8 reactor volumes; aliquots samples were retained for pH measurements and concentrations analysis of the dissolved elements (mainly U, P and Na). The concentrations of sodium (Na) and phosphorus (P) were determined by inductively coupled plasma mass spectroscopy (ICP-MS) and the total uranium concentration was measured using a kinetic phosphorescence analyzer (KPA).

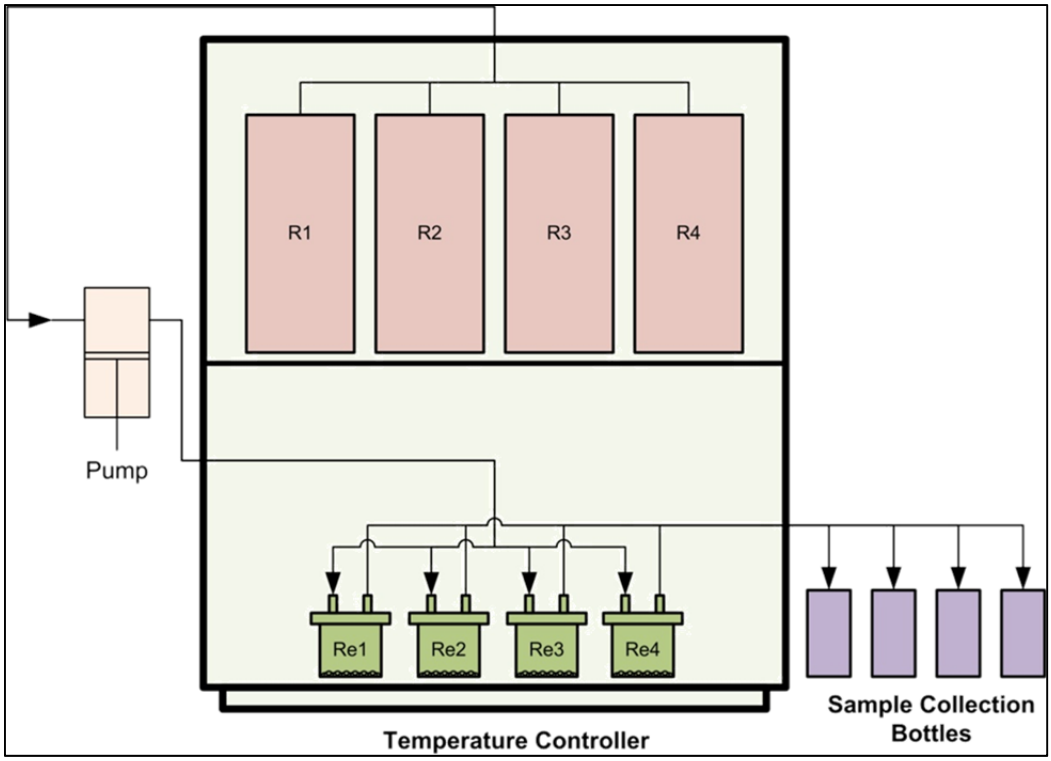

Figure 35. Graphical representation of experimental setup.

Dissolution Rate Calculations

Surface area measurements of autunite solids was carried out at PNNL by using the N_2-adsorption BET method (Brunauer, Emmett, & Teller, 1938). A micromeritics surface and porosity analyzer, Model ASAP 2020, was used to measure the surface area of the synthetic autunite samples. After the surface area was determined, the normalized dissolution rate was calculated for each component and at each sampling interval using the following formula:

$$R_i = (C_i - C_{ib}) \frac{q}{f_i S} \qquad (2)$$

Where:

R_i - the normalized dissolution rate for element i (g m^{-2} d^{-1}),

q- Flow rate, (L d^{-1}),

C_i- concentration of component i in the effluent (g L^{-1}),

C_{ib}- mean background concentration of component i (g L^{-1}),

f_i- the mass fraction of the element in the metal (dimensionless),

S - The surface area of the sample (m^2).

Flow rates, q, were determined gravimetrically by measuring fluid collected upon the sampling event. The background concentration of metals, C_{ib}, was determined by triplicate analyses of the influent. The value of f_i was calculated from the sample chemical composition.

Error Analysis

The lower limit of detection (LLD) of the instrument was used for the element where the element concentration is below the detection limit. The LLD of the instrument for an element is the lowest concentration of calibration standards that is reproducible within ±10% error.

The standard deviation of the dissolution rate is determined according to the uncertainty associated with each parameter shown in Equation 3. Standard deviation for uncorrelated random errors is given by:

$$\sigma_f = \sqrt{\sum_{i=1}^{n} \left(\frac{\partial f}{\partial x_i}\right)^2 \sigma_i^2} \quad (3)$$

Where:

σ_f = standard deviation of the function f;

x_i = parameter i;

σ_i = standard deviation of parameter i.

Substituting Equation 2 into 3 and converting to relative standard deviations, $\hat{\sigma}_r = {}^{\sigma_f}/_{\bar{x}}$, gives the following equation:

$$\hat{\sigma}_r = \sqrt{\frac{(\hat{\sigma}_c C_i^{out})^2 + (\hat{\sigma}_b C_i^{in})}{(C_i^{out} + C_i^{in})^2} + \hat{\sigma}_{fi}^2 + \hat{\sigma}_s^2 + \hat{\sigma}_q^2} \quad (4)$$

Relative errors include:

$\hat{\sigma}_c$= final concentration 10%;

$\hat{\sigma}_b$= background concentration 10%;

$\hat{\sigma}_{fi}$= mass distribution error 5%;

$\hat{\sigma}_s$= surface area error 15%;

$\hat{\sigma}_q$= flow rate error 5%.

Groundwater Modeling

Steady state concentrations were used to determine the aqueous speciation and saturation state of the effluent solution with respect to solid and liquid phases by using geochemical modeling software Visual MINTEQ version 3.0. Visual MINTEQ is a geochemical equilibrium speciation model capable of computing equilibria among the dissolved, adsorbed, solid, and gas phases in an environmental setting. Visual MINTEQ uses a well-developed thermodynamic database of the U.S. Geological Survey's WATEQ3 model and can be used to calculate the mass distribution between the dissolved, adsorbed, and multiple solid phases under a variety of conditions including a gas phase with constant partial pressure. MINTEQ has an extensive thermodynamic database that is adequate for solving a broad range of problems.

Sample Preparation

The presence of organic content in the leach solutions interfered with KPA; hence, samples collected during the experiments were pre-processed by wet ashing followed by dry ashing. A modified ashing technique described by John et al. (2000) was used to wet and dry ash the samples. One (1) ml of sample, 0.5 ml of concentration of nitric acid and 0.5 ml of 34% hydrogen peroxide were mixed and placed on a hot plate until white precipitate was obtained. Occasionally, some samples turned yellow while ashing; 0.5 ml of peroxide was added to those samples and the process continued until a white precipitate was obtained. After wet ashing was completed, samples were placed in a muffle furnace preheated to 450^{o}C for about 15 - 20 minutes to dry ash the samples. Samples were allowed to cool after the wet and dry ashing and 1 ml of 2 M nitric acid was added to bring the sample to the original volume, aliquots from the sample were used for analysis.

TASK 1.3 RESULTS AND DISCUSSION

Steady-State Concentrations

Concentrations used to calculate the dissolution rates were obtained when the system reached equilibrium. The results presented in Figure 36 are representative of the observations for all experiments and illustrate that steady-state conditions are met for different aqueous bicarbonate concentrations (0.0005 - 0.003 M) at the four temperatures (5, 23, 40, and 60°C) studied. For the pH range of 6-11, the graph shows the achievement of steady-state conditions, illustrated by the plateau region, after approximately six reactor volumes where the concentrations of uranium released from natural Na-autunite are invariant with respect to time. This figure also depicts the strong effect of pH in the dissolution rate of autunite, increasing uranium release as a function of pH; this is consistent with previous studies on dissolution rate of autunite minerals (Wellman, Icenhower, Gamerdinger, & Forrester, 2006).

Effect of Bicarbonate Concentrations

Bicarbonate concentrations ranging from 0.0005 to 0.003 M in 0.1 M TRIS buffer solutions were used to investigate the effect of bicarbonate, pH and temperature on the dissolution rate of synthetic Na-autunite. The solutions' pH values were varied from 6 to 11 at temperatures of 5, 23, 40, and 60^{o}C.

Figure 37 shows the rate of release of uranium from synthetic Na-autunite at pH 6 and across aqueous bicarbonate concentrations from 0.0005 to 0.003 M and temperature ranging from 5, 23, 40 and 60^{o}C. Under these conditions, the rate of releases of uranium increased by ~10 fold. The slope varied between 138.8±11 and 151±12, suggesting that the rate of release is dependent on the carbonate concentration. Figure 38 shows the rate of release of uranium from synthetic Na-autunite at pH 7, where the rate of release of uranium increased by ~10 fold and ~100 fold compared to the rate of release at pH 6. The increased rate of release of uranium varied between slope of 178.8±11 and 194±13.

Geochemical modeling results from visual MINTEQ at pH 6 and 7 indicate that the system is under saturated with respect to Schoepite and β-$UO_2(OH)_2$ and super saturated with respect to

$(UO_2)_3(PO_4)_2$(s) and K-autunite at bicarbonate concentrations of 0.0005 - 0.003 M, suggesting a potential for formation of $(UO_2)_3(PO_4)_2$(s) and K-autunite as secondary phases. The formation of these secondary phases indicates that the release of uranium is not attributed only to the dissolution of Na-autunite, but also to the secondary phase, controlling the net uranium concentration.

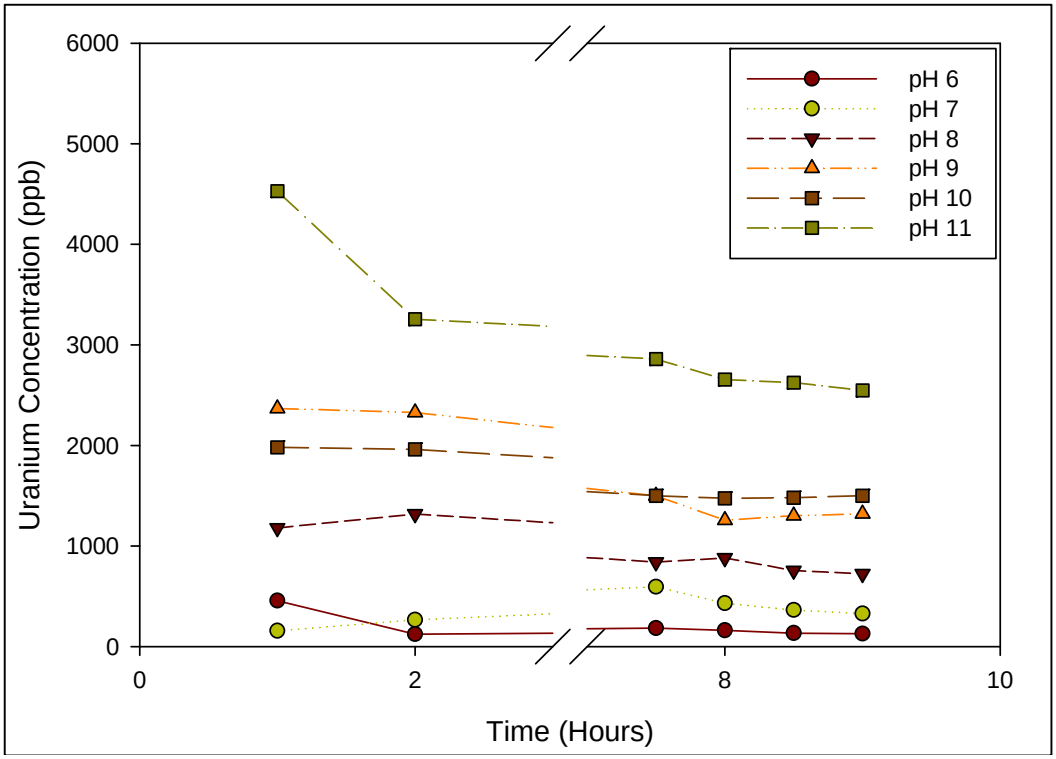

Figure 36. Change in the concentration of uranium over time for 0.003M bicarboante at 23°C.

Figure 39 shows the rate of release of uranium from synthetic Na-autunite at pH 8; the rate of release of uranium increased by ~10 times at pH 8 and increased by ~100 fold compared to the rate of release at pH 6. The increase in the rate of release of uranium varied between a slope of 196±12 and 210±11. The saturation indexes from geochemical modeling results at pH 8 suggest that the system is under saturated with respect to $(UO_2)_3(PO_4)_2$(s), Schoepite and β-$UO_2(OH)_2$ at high bicarbonate concentrations (0.001 - 0.003 M) while it is saturated at low bicarbonate concentration (0.0005 M) with respect to K-autunite, suggesting K-autunite is the only secondary mineral formed and contributing to the release of uranium.

The rate of release of uranium from synthetic Na-autunite at pH 9 is shown in Figure 40. The increase in the rate of release of uranium varied between a slope of 202±11 and 230±13. Saturation indexes (Table 16) from visual MINTEQ geochemical modeling at pH 9 shows that the system is saturated with respect to K-autunite but the degree of saturation is lower compared to the saturation at pH 8, contributing a lesser amount of uranium. The rate of release of uranium from Na-autunite at pH 10 and pH 11 and across bicarbonate concentrations of 0.0005 M and 0.003 M and at temperatures of 5, 23, 40 and 60°C are shown in Figure 41 and Figure 42. At pH 10, the increase in the rate of release is lower and varied between 90±11 and 102±12 and, at pH 11, the rate of release varied between 148±10 and 156±12.

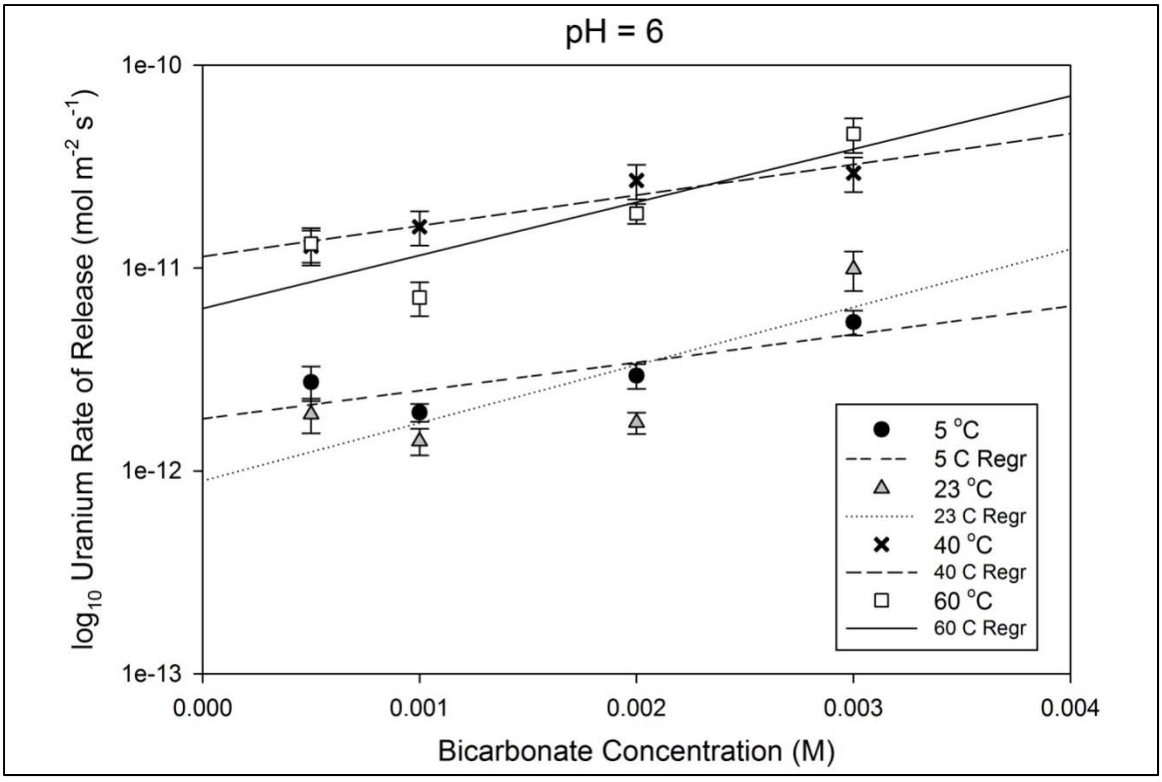

Figure 37. Uranium rate of release as a function of bicarbonate concentration at pH 6.

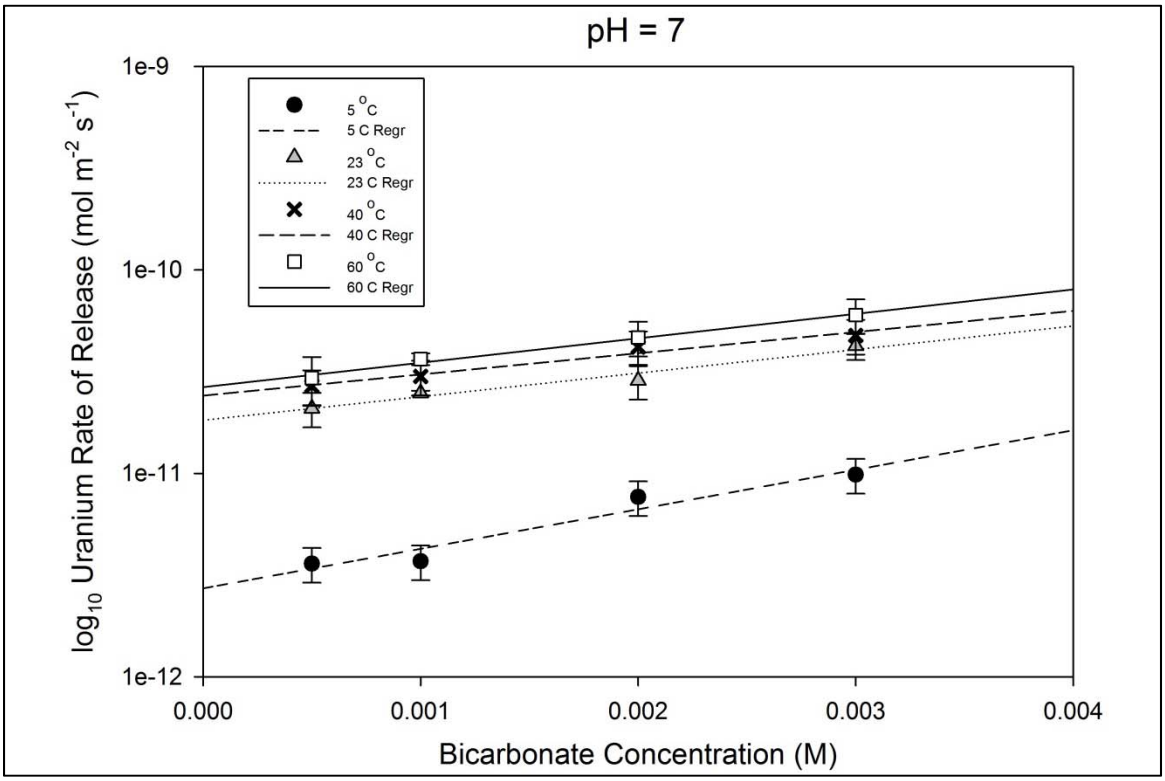

Figure 38. Uranium rate of release as a function of bicarbonate concentration at pH 7.

Table 16. Saturation Indices of Uranyl Compounds from Geochemical Model

pH	Bicarbonate (M)	$(UO_2)_3(PO_4)_2$(s)	K-Autunite	Schoepite	$UO_2(OH)_2$ (beta)
6	0.0005	5.079	7.906	-0.11	-0.338
	0.001	4.902	7.829	-0.206	-0.435
	0.002	4.572	7.683	-0.382	-0.61
	0.003	4.305	7.563	-0.522	-0.75
7	0.0005	3.388	7.915	0.189	-0.039
	0.001	2.799	7.632	-0.114	-0.342
	0.002	1.846	7.169	-0.595	-0.824
	0.003	1.224	6.867	-0.907	-1.136
8	0.0005	0.963	7.311	0.368	0.139
	0.001	-0.094	6.788	-0.163	-0.391
	0.002	-1.265	6.21	-0.748	-0.976
	0.003	-1.962	5.867	-1.096	-1.324
9	0.0005	-1.583	6.552	0.58	0.352
	0.001	-2.377	6.158	0.183	-0.045
	0.002	-3.543	5.58	-0.399	-0.627
	0.003	-4.242	5.236	-0.747	-0.975
10	0.0005	-4.609	5.536	0.569	0.341
	0.001	-4.738	5.474	0.505	0.277
	0.002	-5.147	5.275	0.302	0.074
	0.003	-5.678	5.015	0.037	-0.191
11	0.0005	-8.669	3.703	0.342	0.112
	0.001	-8.739	3.659	0.32	0.09
	0.002	-8.948	3.524	0.254	0.024
	0.003	-9.285	3.303	0.144	-0.086

Negative sign indicates under saturation

Geochemical modeling (Table 16) suggests that $(UO_2)_3(PO_4)_2$(s) is under saturated and the system is saturated with respect to K-autunite, Schoepite and β-$UO_2(OH)_2$ at both pH 10 and 11. The degree of saturation of $(UO_2)_3(PO_4)_2$(s) is much lower at these pH values indicating that $(UO_2)_3(PO_4)_2$(s) is not contributing to the release of uranium; thus, the rate of release of uranium with an increase in bicarbonate concentration (slope) is lower compared to that at lower pH values and is also evident from Figure 41 and Figure 42.

Figure 43 and Figure 44 depicts the dissolution rate of sodium at pH 6 and pH 11 across bicarbonate concentrations of 0.0005 M to 0.003 M and across a temperature range of 5 to 60^{o}C. As evident from the figures, there is no quantifiable change in the rate of release of sodium in the range of bicarbonate concentrations tested at different pH levels (6-11) and at different temperatures (5-60^{o}C). Similar behavior is observed for phosphate and data, presented in Figure 45 and Figure 46.

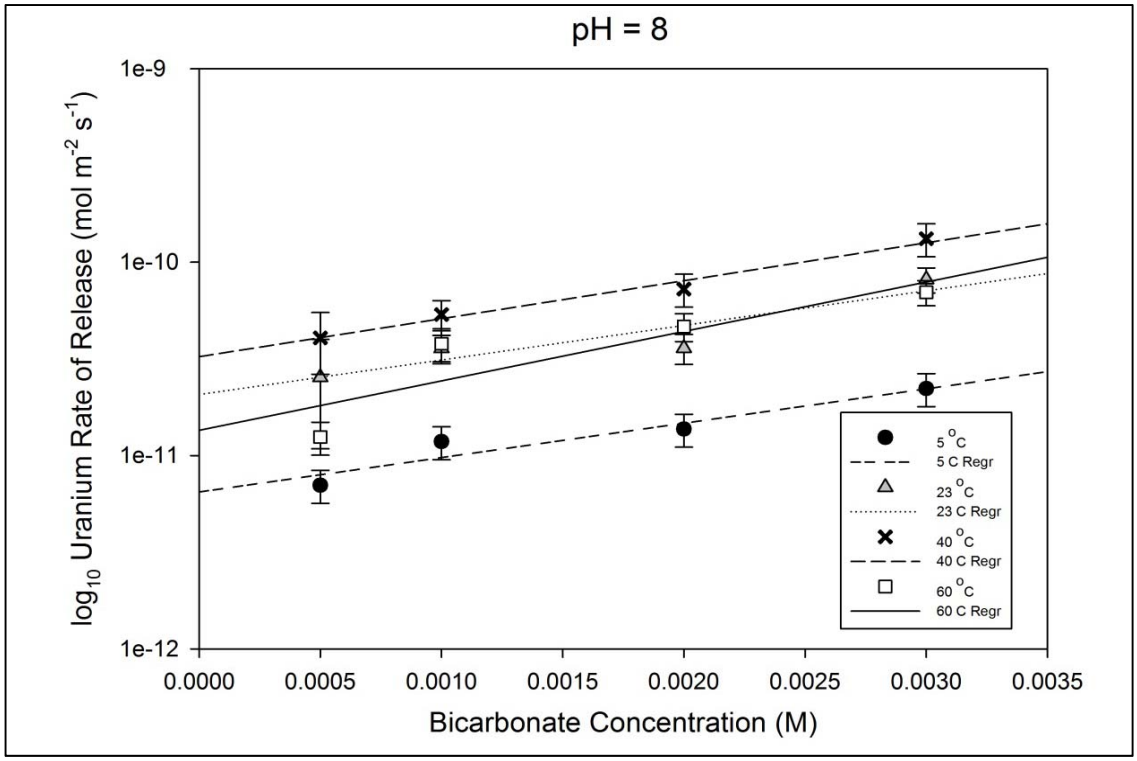

Figure 39. Uranium rate of release as a function of bicarbonate concentration at pH 8.

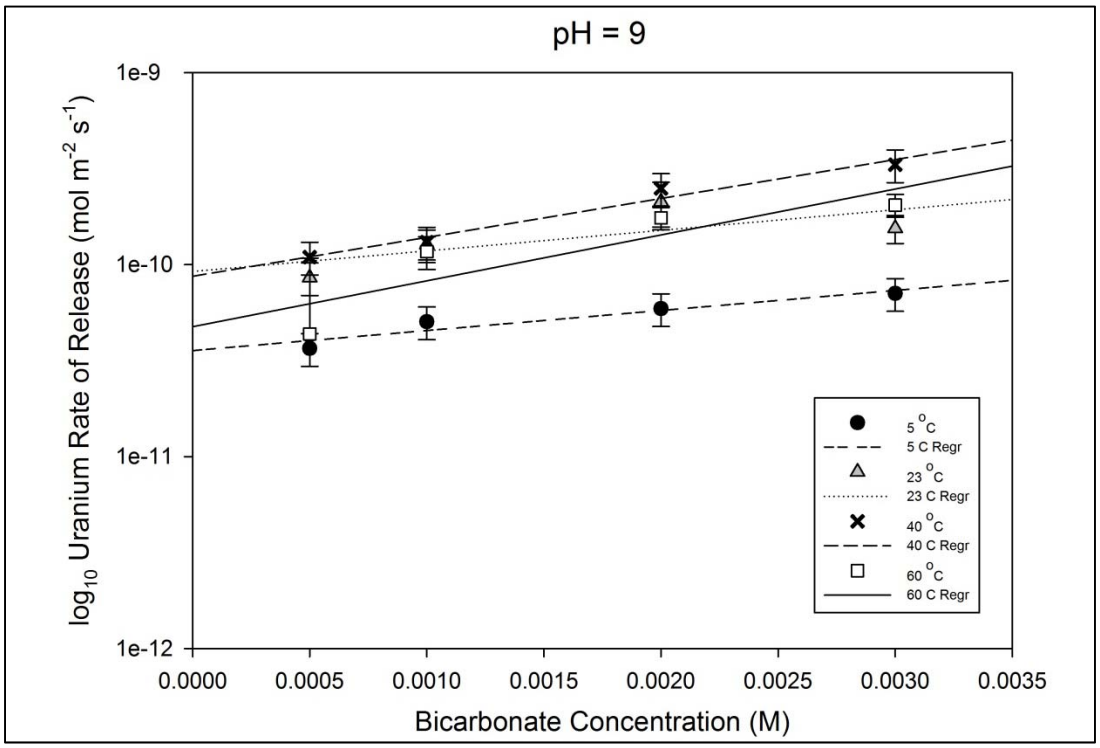

Figure 40. Uranium rate of release as a function of bicarbonate concentration at pH 9.

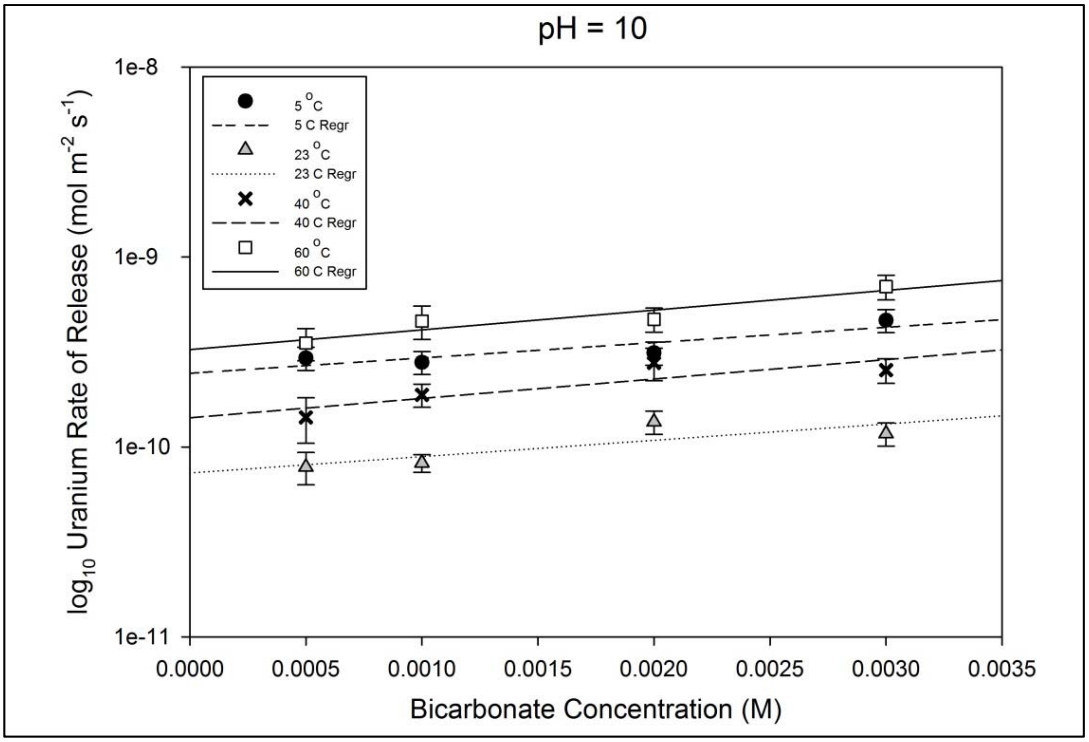

Figure 41. Uranium rate of release as a function of bicarbonate concentration at pH 10.

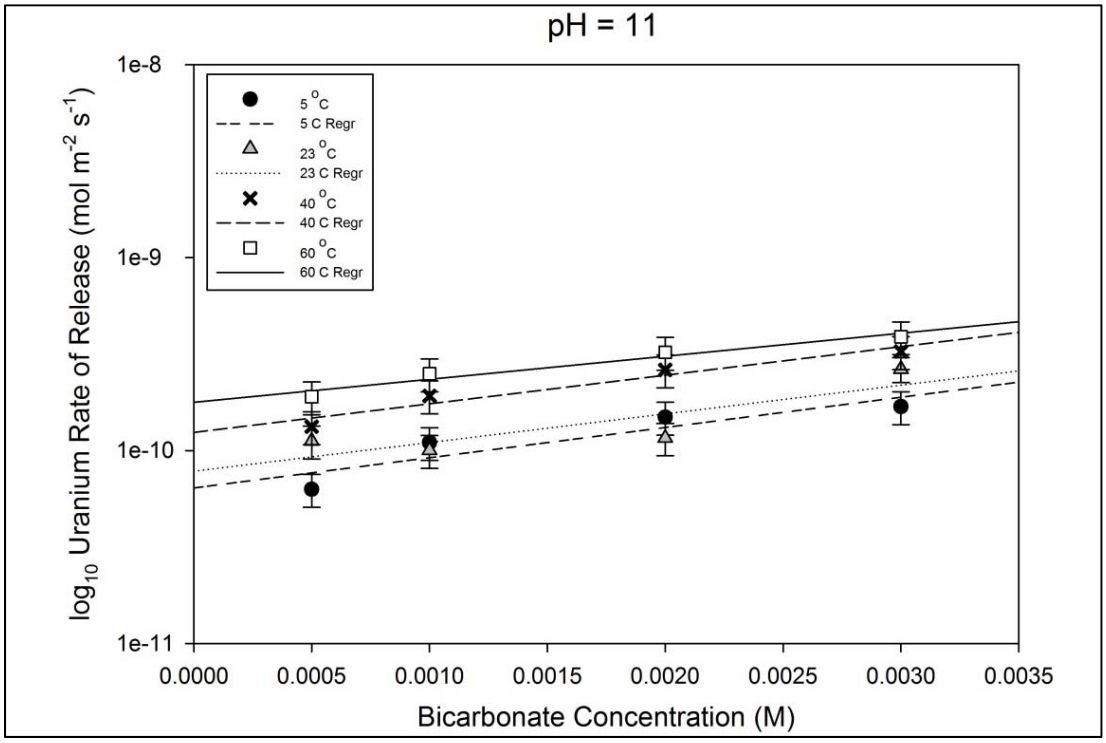

Figure 42. Uranium rate of release as a function of bicarbonate concentration at pH 11.

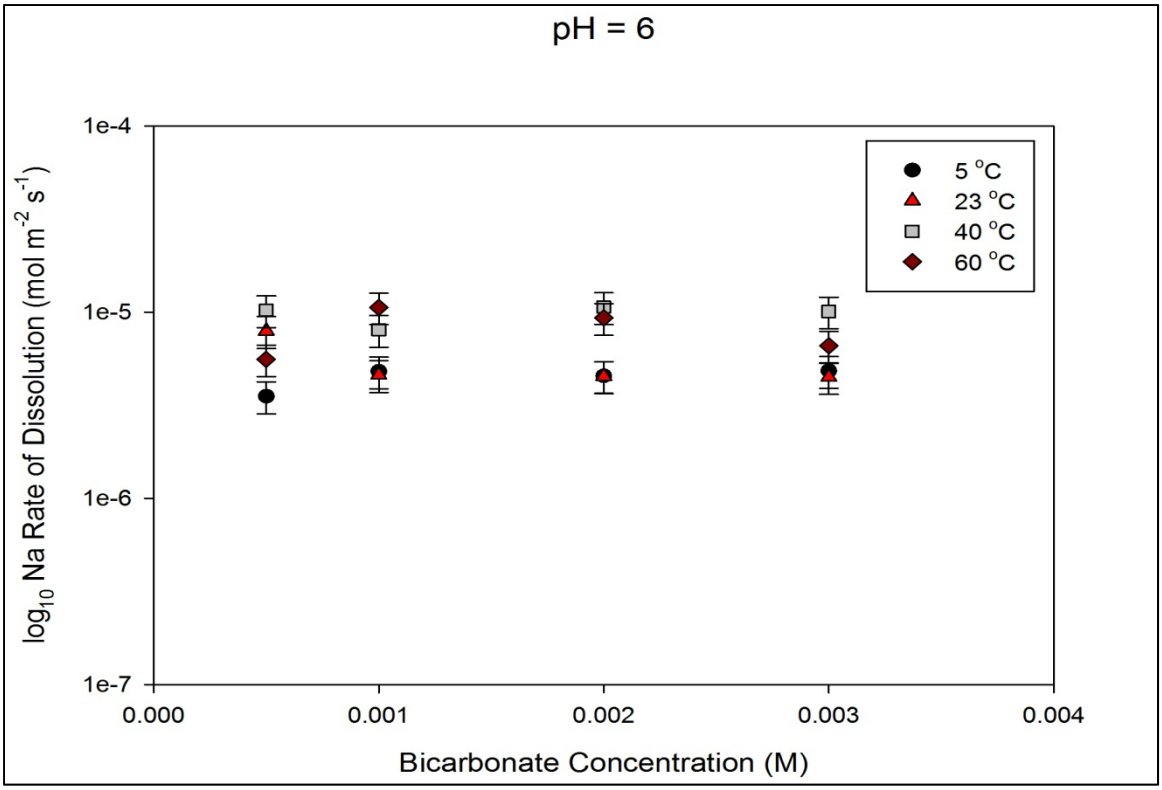

Figure 43. Sodium rate of release as a function of bicarbonate concentration at pH 6.

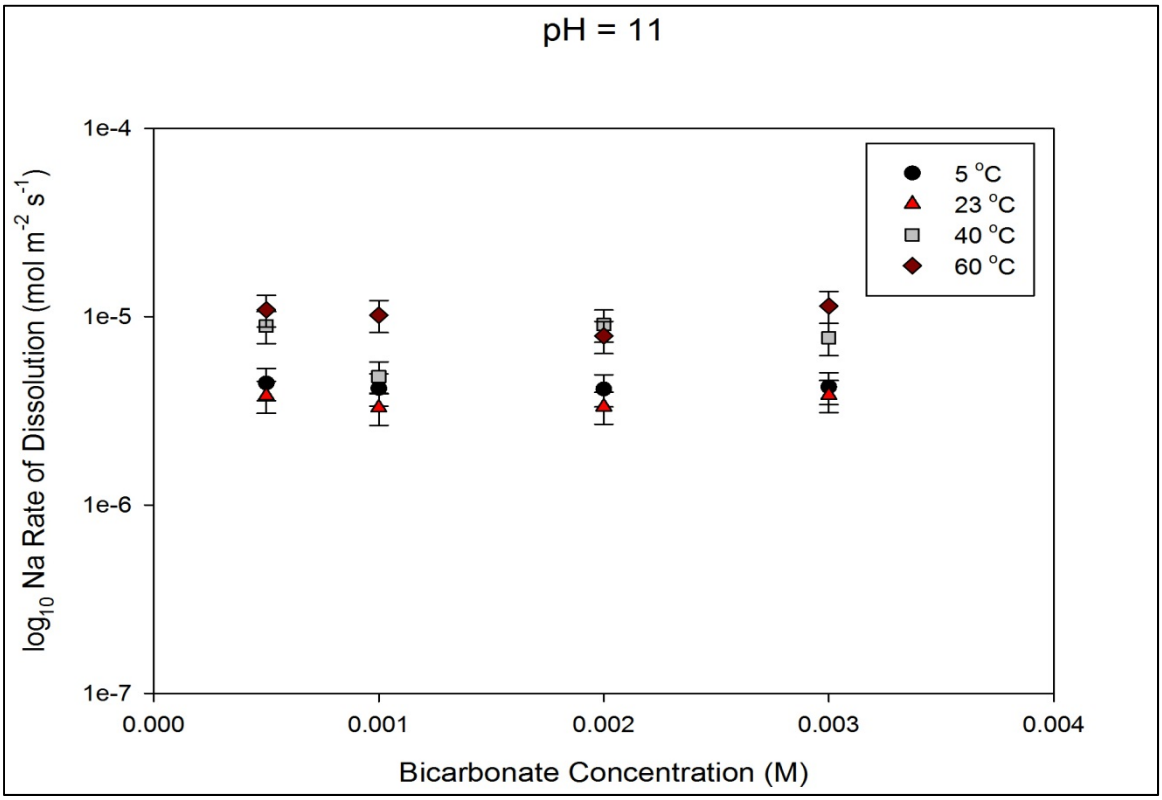

Figure 44. Sodium rate of release as a function of bicarbonate concentration at pH 11.

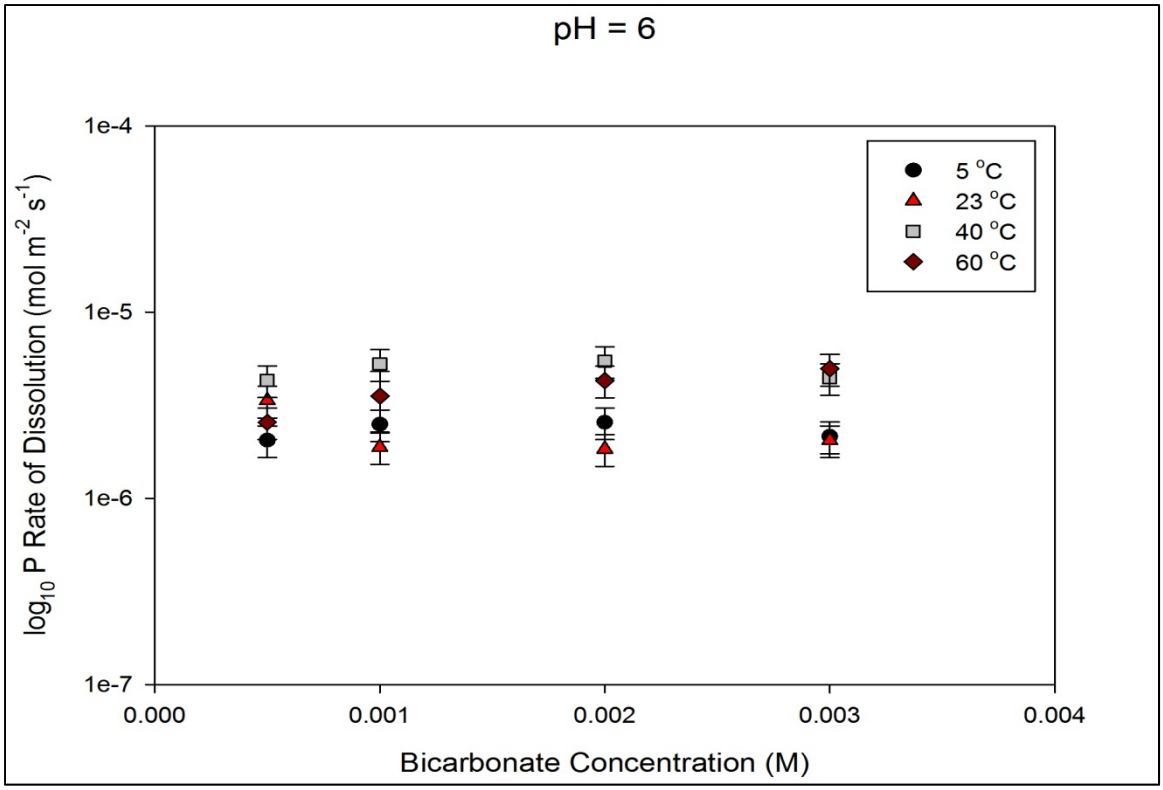

Figure 45. Phosphate rate of release as a function of bicarbonate concentration at pH 6.

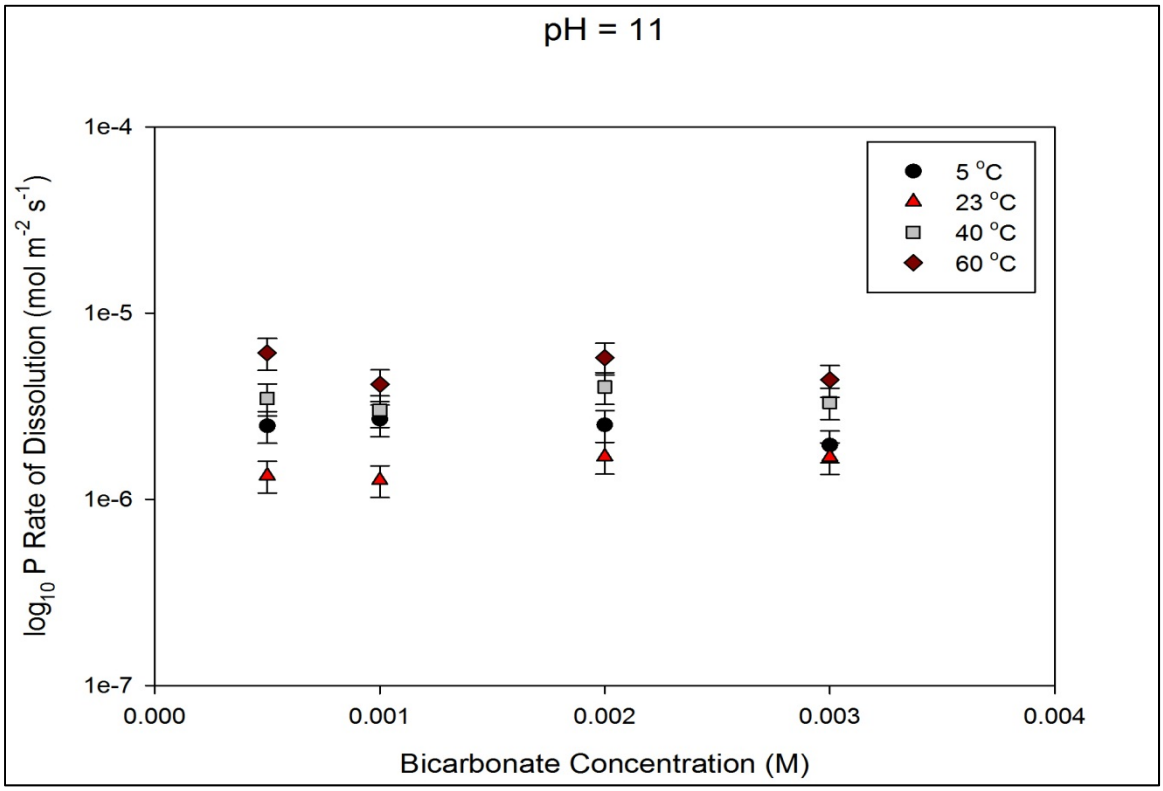

Figure 46. Phosphate rate of release as a function of bicarbonate concentration at pH 11.

TASK 1.3 CONCLUSIONS

The rate of dissolution of Na-autunite was evaluated under different bicarbonate concentrations ranging from 0.0005 M to 0.003 M via single-pass flow through cell experiments, which provide insight to the geochemical cycle of the uranium system, the hydro-geochemical parameters that affect the mobility of uranium. The experiments conducted were designed to evaluate the effects of pH (6-11) and temperature (5 to 60^{o}C) on the carbonate promoted dissolution of synthetic Na-autunite.

The rate of release of uranium from Na-autunite is directly correlated to the concentration of bicarbonate. The bicarbonate ion has a tendency to form soluble complexes with uranium, thus releasing uranium from Na-autunite. Results from these experiments shows that the rate of release of uranium is lower at pH 6 to 7; however, at pH 8 – 11, the rate of release increases. The rate of release of uranium at 23^{o}C in the concentration of bicarbonate studied ranged from 1.90 x 10^{-12} at pH 6 to 2.64 x 10^{-10} at pH 11 and tended to increase as the bicarbonate concentration increased.

The geochemical modeling data from Visual MINTEQ shows that, at low pH (pH 6 and pH 7), some of the possible secondary phases that contain uranium are saturated and some are unsaturated; however, at pH 8 and pH 9, the system is mostly unsaturated, suggesting an increase in the rate of release of uranium from Na-autunite and secondary phase minerals. At pH 10 and 11, the system is saturated with respect to possible secondary phases, resulting in the lower release of uranium at high pH.

The rate of release of sodium and phosphate shows no differentiable change with the change in the concentration of bicarbonate. The geochemical modeling data showed that the amount of sodium and phosphate dissolved is lower than the amount of sodium and phosphate precipitated.

ACKNOWLEDGMENTS

Funding for this research was provided by U.S. DOE grant number DE-EM0000598. We would like to thanks DOE EM12 (Office of Soil and Groundwater Remediation and Dr. Dawn Wellman (PNNL) for their guidance and support. We would like to thank Dr. Patricia Sobecky and Dr.Robert J. Martinez from the Univ. of Alabama, Tuscaloosa, AL, for providing us with the *Arthrobacter* sp. strains and to acknowledge Dr. Yanqing Liu and John Barchi from the FIU AMERI facilities for their assistance with the SEM/EDS analysis. We are grateful to research engineer Kirk Scammon from Materials Characterization Facility, University of Central Florida, for his help with the XPS analysis. We finally wish to thank Mr.Varun Penmatsa for his assistance with FTIR and Mr. Kent Parker from PNNL for his help with the surface area analysis of autunite mineral.

REFERENCES

Amayri, S., Reich, T., Arnold, T., Geipel, G., Bernhard, G., 2005. Spectroscopic characterization of alkaline earth uranyl carbonates. Journal of Solid State Chemistry, 178, 567–577.

Arnson, T. R., 1982. The chemistry of aluminum salts in papermaking. Tappi J., 65, 3, 125-128.

Balkwill, D. L., Reeves, R. H., Drake, G. R., Reeves, J. Y., Crocker, F. H., Baldwin K, M., and D. R. Boone, 1997. Phylogenetic characterization of bacteria in the subsurface microbial culture collection," FEMS microbiology reviews, vol. 20, pp. 201-216.

Bernhard, G., Geipel, G., Reich, T., Brendler, V., Amayri, S., Nitsche, H., 2001. Uranyl(VI) carbonate complex formation: validation of the $Ca_2UO_2(CO_3)^3$(aq.) species. Radiochim. Acta 89, 511–518.

Boylen, C.W., 1973. Survival of Arthrobacter crystallopoietes during prolonged periods of extreme desiccation. Journal of Bacteriology, vol. 113, pp. 33.

Brunauer Stephen, Emmett P H and Teller Edward Adsorption of Gases in Multimolecular Layers, Journal of the American Chemical Society. - 1938. - 2 : Vol. 60. - pp. 309-319.

Buck, B.J., Brock, A. L., William H.J., Ulery, A. L., 2004, Corrosion of Depleted Uranium in an Arid Environment: Soil-Geomorphology, SEM/EDS, XRD, and Electron Microprobe Analyses, Soil & Sediment Contamination, 13:545–561.

Burns, P.C., Miller, M.L. and R.C. Ewing, 1996. U^{6+} minerals and inorganic phases: a comparison and hierarchy of crystal structures, The Can. Mineralogist 34, p. 845–880

Coates, J. "Interpretation of Infrared Spectra, A Practical Approach." Encyclopedia of Analytical Chemistry. Chichester: John Wiley & Sons, 2000. 10815-0837.

Cotton, Simon. "Coordination Chemistry of the Actinides."Lanthanide and actinide chemistry. Chichester, England: Wiley, 2006. 173-199. Print.

Crocker, F. H., Fredrickson, J. K., White, D. C., Ringelberg, D. B. and D. L. Balkwill, 2000. Phylogenetic and physiological diversity of Arthrobacter strains isolated from unconsolidated subsurface sediments, Microbiology, vol. 146, pp. 1295.

Devivo, B., Ippolito, F., Capaldi, G., Simpson, P. R. (Eds), Uranium Geochemistry, Mineralogy, Exploration and Resources. The Institution of Mining and Metallurgy, London, 1984, p. 43.

Ejnik John W. [et al.] Optimal sample preparation conditions for the determination of uranium in biological samples by kinetic phosphorescence analysis (KPA), Journal of Pharmaceutical and Biomedical Analysis, 2000. - pp. 227-235.

Ekwere, A.S. and Edet, A., 2012, Distribution and Chemical Speciation of Some Elements in the Ground Waters of Oban Area (South-Eastern Nigeria), Res. J. Environ. Earth Sci., 4(3): 207-214.

EPA Radiation Protection EPA. - EPA, July 2011. http://www.epa.gov/radiation/radionuclides/uranium.html.

EPA Recovery Act of 2009 Hanford. - 2011. - http://www.hanford.gov/page.cfm/FAQ.

Fiedor, J. N., Bostick W. D., Jarabek R. J. , Farrell J., 2003, Understanding the Mechanism of Uranium Removal from Groundwater by Zero-Valent Iron Using X-ray Photoelectron Spectroscopy, Environ. Sci. Technol. 1998, 32, 1466-1473.

Fredrickson, J. K., Zachara, J. M., Balkwill, D. L., Kennedy, D., Li, S. W., Kostandarithes, H. M., Daly, M. J., Romine, M. F. and Brockman, F.J. , 2004. Geomicrobiology of high-level nuclear waste-contaminated vadose sediments at the Hanford Site, Washington State, Applied and Environmental Microbiology, vol. 70, pp. 4230.

García-Ruiz, JM, 1998. Carbonate precipitation into alkaline silica-rich environments. Geology, 26, 9, 843–846

García-Ruiz, JM, Melero-García, E., Hyde, S.T., 2009. Morphogenesis of self-assembled nanocrystalline materials of barium carbonate and silica. Science, V. 323

Gasc, F., Thiebaud-Roux, S., and Mouloungui , Z., 2009, Methods for synthesizing diethyl carbonate from ethanol and supercritical carbon dioxide by one-pot or two-step reactions in the presence of potassium carbonate, The Journal of Supercritical Fluids, vol. 50 (n°1). pp. 46-53.

Gasteiger, H.A., Frederick, W.J., Streisel, R.C.,1992. Solubility of aluminosilicates in alkaline solutions and a thermodynamic equilibrium model. Ind. Eng. Chem. Res. 31, 1183-1190.

Giammar Daniel E and Hering Janet G Time Scales for Sorption-Desorption and Surface Precipitation of Uranyl on Goethite - Pasadena : Environmental Science and Technology, 2001. - 35. - pp. 3332-3337.

Giammar Daniel Geochemistry of Uranium At Mineral-Waterinterfaces: Rates Of Sorption-Desorption And dissolution-Precipitation Reactions - Pasadena 2001.

Gorman-Lewis D., Skanthakumar, S., Jensen M.P., Mekki S., Nagy K.L., Soderholm L., 2008, FTIR characterization of amorphous uranyl-silicates, Chemical Geology 253, 136–140.

Grenthe, I., Fuger, J., Konings, R.J.M., Lemire, R.J., Muller, A.J., Nguyen-Trung, C., Wanner, H., 1992. Chemical Thermodynamics of Uranium. Elsevier, Amsterdam.

Guillaumont, R., Fanhänel, T., Fuger, J., Grenthe, I., Neck, V., Palmer, D.A., Rand, M.H., 2003. Chemical thermodynamics. OECD Nuclear Energy Agency, vol. 5. Elsevier.

Heyns Henk-Jan De Jager and Anton M. Study of the Hydrolysis of Sodium Polyphosphate in Water Using Raman Spectroscopy, Applied Spectroscopy. - 1998. - 6 : Vol. 52. - pp. 808-814.

Ilton, E. and P. Badus, P, 2011. XPS determination of uranium oxidation states. Surf. Interface Anal., 43, 1549–1560.

Ivanova, R., Bojinova, D., Nedialkov, K., 2006. Rock phosphate solubilization by soil bacteria. Journal of the University of Chemical Technology and Metallurgy, 41, 3, 297-302

Kalmykov, SN, Choppin GR., 2000. Mixed Ca^{2+}/UO_2^{2+} /CO_3^{2-} complex formation at different ionic strengths. Radiochim Acta, 88,603–606.

Karberg, N.J., KS. Pretziger, J.S. King, A.L. Friend, and J.R. Wood, 2005, Soil carbon dioxide partial pressure and dissolved inorganic carbonate chemistry under elevated carbon dioxide and ozone, Oecologia, 142, p. 296-306.

Katsenovich, Y.P., Carvajal, D.A., Guduru, R., Lagos, L.E., 2012b. Assessment of the Resistance of Hanford Site *Arthrobacter* Isolates to Uranium (VI) Exposure. Geomicrobiology Journal. DOI:10.1080/01490451.2011.654376

Katsenovich, Y.P., Carvajal, D.A., Wellman, D.M., Lagos, L.E., 2012a. Enhanced U(VI) release from autunite mineral by aerobic *Arthrobacter* sp. In the presence of aqueous bicarbonate. Chemical Geology,V. 308-309, p. 1-9.

Kellermeier, M., Melero-Garcıa, E., Glaab, F., Klein, R., Drechsler, M., Rachel, R., Garcıa-Ruiz, JM and W. Kunz, 2010. Stabilization of amorphous calcium carbonate in inorganic silica-rich environments. J. AM. CHEM. SOC. 132, 17859–17866

Knox A S [et al.] Interactions among phosphate amendments, microbes and uranium mobility in contaminated sediments, Science of the Total Environment. - 2008. - pp. 63-71.

Lakshtanov, LZ., and S.L.S. Stipp, 2010. Interaction between dissolved silica and calcium carbonate: 1. Spontaneous precipitation of calcium carbonate in the presence of dissolved silica, Geochimica et Cosmochimica Acta, 74, 2655–2664.

Langmuir Donald Aqueous environmental geochemistry, Prentice Hall, 1997.

Langmuir, D., 1978. Uranium solution–mineral equilibia at low temperatures with application to sedimentary ore deposits. Geochimica et Cosmochimica Acta 42, 547–569.

Manson C. F. [et al.] Carbonate Leaching of Uranium from Contaminated Soils, Environmental Science & Technology. - 1997. - pp. 2707-2711.

McGrail B. P. [et al.] Measurement of kinetic rate law parameters on a Na□Ca□Al borosilicate glass for low-activity waste, Journal of Nuclear Materials, 1997. - pp. 175-189.

Miravete, A., Proceedings of the Ninth International Conference on Composite Materials (ICCM/9), Composites Behaviour, vol. 5. University of Zaragosa, Madrid: Woodhear Publishing Limited, 1993. Print.

Qafoku NP, Ainsworth CC, Szecsody JE, Qafoku OS, 2003. Aluminum Effect on Dissolution and Precipitation under Hyperalkaline Conditions: I. Liquid Phase Transformations. J Environ Qual. 32, 6, pp.2354-63.

Sandino Amaia and Bruno Jordi The solubility of (UO2)3(PO4)24H2O(s) and the formation of U(VI) phosphate complexes: Their influence in uranium speciation in natural waters, Geochimica et Cosmochimica Acta. - [s.l.] : Geochimica et Cosmochimica Acta, 1992. - pp. 4135-4145.

Schlosser, F., Moskaleva, LV., Kremleva, A., Kruger, S and Rosch,N., 2010. Comparative density functional study of the complexes $[UO_2(CO_3)_3]_4^-$ and $[(UO_2)_3(CO_3)_6]_6^-$ in aqueous solution. *Dalton Trans.*, 39, 5705–5712. DOI: 10.1039/c002788j

Serne R. J. [et al.] 300 Area Uranium Leach and Adsorption Project [Report]. - Richland : Pacific Northwest National Laboratory, 2002.

Serne RJ, MJ Lindberg, SR Baum, GV Last, RE Clayton, KN Geiszler, GW Gee, VL LeGore, CF Brown, HT Schaef, RD Orr, MM Valenta, DC Lanigan, IV Kutnyakov, TS Vickerman, CW Lindenmeie, 2008. Characterization of Vadose Zone Sediment: Borehole 299-E33-45 Near BX-102 in the B-BX-BY Waste Management Area. 2002. PNNL-14083. Contract DE-AC06-76RL01830.

Sheng, Z., Tokunaga, TK., WAN, J., 2003. Influence of calcium carbonate on U(VI) sorption to soils. Environ. Sci. Technol. 37, 5603-5608.

Sherman Hsu. C.P., "Infrared Spectroscopy." Handbook of Instrumental Techniques for Analytical Chemistry. By Frank A. Settle. Upper Saddle River, NJ: Prentice Hall, 1997. 247-83. Print.Su, C and D. L. Suarez, 1997. In situ infrared speciation of adsorbed carbonate on aluminum and iron oxides. Clays and Clay Minerals, V. 45, 6, 814-82.

Skoog, D A., Holler, F. J., and Stanley R. Crouch, 2007. Principles of instrumental analysis. 6th ed. Belmont, CA: Thomson Brooks/Cole, Print.

Smeaton,C.M., Weisener,C.G., Burns,P.C., Fryer,B.J. and Fowle,D.A., 2008. Bacterially enhanced dissolution of meta-autunite. American Mineralogist, 93, 1858-1864.

Sowder A. G. The formation, transformation, and stability of environmentally relevant uranyl mineral phases. - 1998.

Sowder A. G., Clark Sue B. and Fjeld R. A. Dehydration of Synthetic Autunite Hydrates, Radiochimica Acta. - 2000. - pp. 533-538.

Sparks, D. Kinetic and mechanisms of soil chemical reactions at the soil mineral/water interface.-, 1999. In: D.L Sparks, Editor, Soil Physical Chemistry.

Stumm W and Wollast R Coordination chemistry of weathering: Kinetics of the surface-controlled dissolution of oxide minerals, Rev. Geophys. 1990. - pp. 53-69.

Stumm Werner and Morgan James J Aquatic Chemistry: Chemical Equilibria and Rates in Natural Waters, New York : John Wiley & Sons, 1996.

Su, C and D. L. Suarez, 1997. In situ infrared speciation of adsorbed carbonate on aluminum and iron oxides. Clays and Clay Minerals, V. 45, 6, 814-82.

Szecsody, JE, MJ Truex, L Zhong, MD Williams, CT Resch, JP McKinley, 2010. Remediation of Uranium in the Hanford Vadose Zone Using Gas-Transported Reactants: Laboratory-Scale Experiments. PNNL-18879. Contract DE-AC05-76RL01830.

Um, W., Serne, R.J., Brown, C. F., Last, GV., 2007b. U(VI) adsorption on aquifer sediments at the Hanford Site. Journal of Contaminant Hydrology 93, 255–269.

Um, W., Serne, R.J., Krupka, KM, 2007a. Surface Complexation modeling of U(VI) sorption to Hanford sediment with varying geochemical conditions. Environ. Sci. Technol., 41, 3587-3592.

Van Waasbergen, L.G., Balkwill, D. L., Crocker, F. H., Bjornstad, B. N., and R. V. Miller, 2000. Genetic diversity among Arthrobacter species collected across a heterogeneous series of terrestrial deep-subsurface sediments as determined on the basis of 16S rRNA and recA gene sequences. Applied and environmental microbiology, vol. 66, pp. 3454.

Vazques, P., Holguin, G., Puente, ME., Lopez-Cortes, A., Bashan, Y, 2000. Biol. Fertil. Soil, 460-468.

Vermeul V. R. [et al.] In-Situ Uranium Stabilization Through Polyphosphate Injection: Pilot-Scale Treatability Test at the 300 Area, Hanford Site, Waste Management, Phoenix 2008.

Vermeul, VR., Bjornstad, BN., Fritz, B.G., Frutcher, JS., Mackley, RD., Mendoza, D.P., Newcomer, D.R., Rochhold, ML., Wellman, DM., Williams, M.D, 2009. 300 Area Uranium Stabilization Through Polyphosphate Injection: Final Report. PNNL-18529. Prepared for the U.S. Department of Energy under Contract DE-AC05-76RL01830.

Vochten R and Deliens M Transformation of curite into metaautunite paragenesis and electrokinetic properties, Physics and Chemistry of Minerals. - 1980. - pp. 129-143.

Voinescu, A.E., Kellermeier, M., Bartel, B., Carnerup A.M., Larsson, A., Touraud, D., Kunz, W., Kienle, L., Pfitzner, A., and Hyde, S.T., 2008, Inorganic Self-Organized Silica Aragonite Biomorphic Composites, Crystal Growth & Design, vol. 8(n°5). pp. 1515-1521.

Wellman D. M. [et al.] Uranium Stabilization Through Polyphosphate Injection 300 Area Uranium Plume Treatability Demonstration Project [Report]. - Richland : PNNL, 2007.

Wellman Dawn M [et al.] Synthesis and characterization of sodium meta-autunite, $Na[UO_2PO_4]\cdot 3H_2O$, Radiochimica Acta. - 2005. - pp. 393-399.

Wellman Dawn M [et al.] Uranium Plume Treatability Demonstration at the Hanford Site 300 Area: Development of Polyphosphate Remediation Technology for In Situ Stabilization of Uranium, WasteManagement 2008. - Phoenix, 2008.

Wellman Dawn M. [et al.] Dissolution kinetics of meta-torbernite under circum-neutral to alkaline conditions, Environmental Chemistry. - 2009. - pp. 551-560.

Wellman, DM., Gunderson, KM, Icenhower, JP., Forrester, S.W., 2007. Dissolution kinetics of synthetic and natural meta-autunite minerals, $X_{3-n}^{(n)+}[(UO_2)(PO_4)]_2 \cdot xH_2O$, under acidic conditions. Geochemistry, Geophysics, Geosystems, V. 8, 11

Wellman, DM., Icenhower, JP., Gamerdinger, A.P., Forrester, S.W., 2006. Effects of pH, temperature, and aqueous organic material on the dissolution kinetics of meta-autunite minerals, $(Na, Ca)_{2-1}[(UO_2)(PO_4)]_2\cdot 3H_2O$. American Mineralogist, V. 91, p. 143-158.

Yang, C.S., Kannan, M., Choi, C.K., 2005, Studies on the low dielectric SiOC(–H) thin films deposited using MTMS and oxygen as precursors by UV source assisted PECVD, Surface & Coatings Technology 200, 1624– 1628.

APPENDIX

ARC-2004-C032-207-29

PROGRESS REPORT ON RESULTS OF U(VI) BIOSORPTION IN THE PRESENCE OF BICARBONATE AND CALCIUM IONS

Project 2: Rapid Deployment of Engineered Solutions to Environmental Problems

CONTRACT NO. DE- EM0000598

Submitted to:

U.S. Department of Energy
Program Services Division, ME-643.1
1000 Independence Avenue, SW
Washington, D.C. 20585

Submitted by:

Leonel E. Lagos, Ph.D & David Roelant, Ph.D, Principal Investigators
Leonel Lagos, Ph.D., P.M.P®, Project Manager
Yelena Katsenovich, PhD
Denny A.Carvajal, MS, DOE Fellow
Bryant Thompson, DOE Fellow

Applied Research Center
Florida International University
10555 W. Flagler Street, EC2100
Miami, FL 33174

Submitted on:

January 11, 2012

FIU | Applied Research Center
FLORIDA INTERNATIONAL UNIVERSITY

TABLE OF CONTENTS

LIST OF FIGURES

LIST OF TABLES

INTRODUCTION

Uranium (U) is the most abundant actinide element found throughout the environment; it is well known as a health hazard for both its toxicity and radioactivity. Understanding its fate and transport behavior in the subsurface is important in evaluating the environmental effects of U at contaminated sites such as U mining, processing, and nuclear waste disposal facilities where the accidental releases of radioactive materials have directly impacted the subsurface. Uranium (VI) is the most stable valence of uranium under oxidizing conditions and is primarily found in oxic circumneutral-to-mildly-basic geochemical conditions, where U(VI) dominates as the highly soluble and stable uranyl ion, UO_2^{2+} (Langmuir1997, Murphy and Shock 1999). Due to complicated chemical behavior in natural systems, it readily forms uranyl complexes with a variety of ligands (e.g. carbonate, phosphate, silicate) (Grenthe et al. 1992; Langmuir 1997). These complexation reactions often result in the formation of mobile aqueous species or the precipitation of insoluble U-bearing minerals (Finch and Murakami 1999).

Microbial activities in many environmental systems contaminated with actinides can profoundly affect U(VI) mobility due to the secretion of protons, various ligands, and organic acids into their immediate surroundings (Knox et al. 2008). In addition, microorganisms tend to interact with their aqueous environment by metabolism-independent reactions. The Gram-positive bacteria cell wall component is mainly comprised of peptidoglycan (PG), which contains several acidic groups and teichoic acids, in which phosphate groups are important elements. The main reactive groups on the cell surface that contribute to metal uptake are the carboxylic, phosphate, and hydroxyl groups with a calculated pK_a value of 4.82 ± 0.14, 6.9 ± 0.5, and 9.4 ± 0.6, respectively (Fein et al. 1997). The value of the log stability constants for the uranyl ion that forms surface complexes with the phosphate functional groups and the

deprotonated carboxyl functional groups of the bacterial cell wall were calculated as log K =11.8 ± 0.2 and log K = 5.4± 0.2, respectively (Fowle et al. 2000). These stability constants are high enough to affect U(VI) mobility in aqueous systems.

Bicarbonate is a predominant complexing agent for U(VI) in oxidized environments, forming several soluble stable carbonate complexes with uranium (VI). Their mobility in aquifers under circumneutral pH conditions is explained by the formation of highly soluble and stable uranyl-carbonato complexes, $UO_2CO_3^0$, $UO_2(CO_3)_2^{2-}$ and $UO_2(CO_3)_3^{4-}$(Langmuir 1978; Guillaumont et al. 2003). Strong binding of U with carbonates in soil and aqueous systems can interfere with the complexation by bacterial surfaces.

Calcium (Ca) is a common aqueous cation found in equilibrium with calcite in porewater and groundwater at many sites contaminated with U. Ca can complex with U(VI) in bicarbonate solutions to form calcium-uranyl-carbonate species such as $Ca_2UO_2(CO_3)_3^0$(aq) and $CaUO_2(CO_3)_3^{2-}$. Their large formation constants (Guillaumont et al. 2003) suggest that Ca can affect U(VI) accumulation and toxicity on cells of *Arthrobacter* sp. due to the formation of soluble and stable calcium uranyl carbonate complexes in aqueous solution. Recent studies have demonstrated that calcium, through the formation of a ternary aqueous calcium-uranyl-carbonate species, increased the rate of U solid phase sample dissolution and U(VI) bioavailability for the microbial reduction (Liu et al. 2007).

Of interest to our investigation was the aerobic Gram-positive *Arthrobacter* sp., which comprises a very diverse group known for their ability to survive in extreme conditions. These bacteria are one of the most common groups in soils and are found in fairly large numbers in Hanford soil as well as other subsurface environments contaminated with heavy metals and radioactive materials (Boylen 1973, Balkwill et al. 1997, Van Waasbergen et al. 2000, Crocker et

al. 2000). Balkwill et al. (1997) reported the predominance of the genus *Arthrobacter* among the culturable aerobic heterotrophic bacteria from the Hanford Site sediments with this group accounting for roughly up to 25% of the subsurface isolates. In addition, *Arthrobacter*-like bacteria were the most prevalent in the highly radioactive sediment samples collected underneath the leaking high-level waste storage tanks and accounted for about of one-third of the total soil isolatable bacterial population (Fredrickson et al. 2004). The objectives of this study are to: (i) report results from uranium biosorption experiments with *Arthrobacter* strain G975, previously isolated from the Hanford subsurface; (ii) study the potential role of aqueous bicarbonate, which is an important complexing ligand for U(VI), and (iii) report the effect of calcium on uranium biosorption. These observations can provide insight into important microbiological processes affecting the fate and transport of uranium in Ca-rich carbonate-bearing subsurface environments, common to the semi-arid areas of western U.S.

MATERIALS AND METHODS

Arthrobacter Strains and Growth Culture Conditions

G975 *Arthrobacter* strains, isolated from Hanford soil, were obtained from the Subsurface Microbial Culture Collection (SMCC) (Florida State University, Tallahassee). Detailed descriptions of site geology, sample collection procedures, and methods of bacteria isolation are available from Van Waasbergen et al. (2000). The strain identification, previously confirmed by 16S rDNA phylogeny, was *Arthrobacter oxydans* G975 (Balkwill et al. 1997, Van Waasbergen et al. 2000). The strain was cultured in PYTG medium consisting of 5 g/L peptone, 5 g/L tryptone, 10 g/L yeast extract, 10 g/L glucose, 0.6 g/L $MgSO_4.7H_2O$, 0.07 g/L $CaCl_2.2H_2O$ and 15 g/L agar. The *Arthrobacter* strain was aerobically grown in 250 mL foam-stoppered

sterile Erlenmeyer glass flasks amended with 50 ml of 5% PYTG media at 29˚C in the shaker/incubator.

The cell density (cells/mL) was calculated with the help of INCYTO C-Chip disposable hemocytometers. In addition, cell density was determined by measuring the absorbance at 660 nm by means of spectrophotometer (UV-1601, Shimadzu) and relating them to known cell numbers counted via the use of the hemocytometer.

Synthetic Groundwater

The U(VI) biosorption experiments were conducted with carbonate-free and carbonate-amended synthetic groundwater (SGW). Treatments, bearing carbonate with or without calcium additions, were amended with $KHCO_3$ and $CaCl_2{\cdot}2H_2O$, respectively, followed by a pH adjustment to 7.3 by 0.5M HCL or 0.5M NaOH, as required. The carbonate-free SGW formulation was made up from 0.6 mM of $CaCl_2{\cdot}2H_2O$, 0.21 mM of $MgCl_2$, 0.07 mM of KCl, and 2 mM of HEPES buffer, dissolved in DIW (Zachara 2004). The content of calcium, which served as an inorganic nutrient for bacterial cells in SGW solution, was too small to substantially affect the adsorption process compared to the 5 mM Ca used in the Ca-rich solution.

Biosorption Kinetics

The U biosorption rate was studied by measuring the bacterial uranium biosorption as the dependent variable and the uranium concentrations at equilibrium, bicarbonate concentrations, and time as the three independent variables. The U(VI) concentrations spiked to SGW, 1.26 μM and 61.76 μM, were made by the addition of the appropriate aliquots from 100 mg/L uranyl nitrate $[UO_2(NO_3)_2{\cdot}6H_2O]$ stock solution prepared in DIW. Two concentrations of bicarbonate were used in the experiments: SGW solutions without the addition of $KHCO_3$ but at equilibrium with atmospheric CO_2 and 2.5 mM of $KHCO_3$. Sampling was conducted at 0.25, 0.75, 2, 4, 6, 24,

and 48 hour intervals. Samples were centrifuged for 5 min at 3000 rpm and then cell-free supernatants were analyzed for U(VI) using a Kinetic Phosphorescence Analyzer (KPA-11) (Chemcheck Instruments, Richland, WA). Experiments were conducted in triplicate using 4 mL of SGW inoculated with 4E+10 cells of G975 strain in 15 ml polypropylene sterile tubes. The tubes were kept in the incubator shaker at 60 rpm and 25°C for 48 hours. The metal uptake, q (mg ion metal / g bacteria), was determined by solving the mass balance equation presented in eq. 1.

$$q = \frac{(C_0 - C_t) * V}{m} \quad (1)$$

Where C_0 and C_t are the initial and final metal ion concentrations (mg/L), respectively, V is the volume of solution (mL), and m is the bacteria dry weight (g).

Adsorption Isotherm

The equilibrium U(VI) adsorption was carried out at different initial concentrations of U(VI) ranging from 2.1 µM to 84 µM while maintaining the dry weight of *Arthrobacter* sp. G975 at 0.24 ± 0.05 mg in each treatment. The dry weight of bacteria was indirectly estimated by relating the direct cell count obtained by a hemocytometer and the bacterial mass acquired by following the modified EPA method 340.2 for the same number of cells. The role of bicarbonate ions and their impact on U(VI) adsorption by bacteria was investigated using SGW amended with 0, 0.5, 2.5, and 5 mM of $KHCO_3$. In addition, select vials were enriched with calcium (5 mmol/L $CaCl_2$) to investigate its effects on biosorption. Sample preparations, with regards to the cell concentrations, pH, and sample volume were performed identically to the biosorption kinetic experiments. In addition, abiotic controls were prepared to account for any U(VI) losses due to adsorption on tube walls and caps. Uranium biosorption was calculated with eq. 1. Sorption isotherms were created by plotting the amount of metal uptake (q) against the equilibrium concentration of metal ions detected in the solution (C_e). The slope of this correlation is the

partition coefficient, K_d, that corresponds to the distribution of metal ions between the aqueous and solid phases. The Linear, Freundlich, and Langmuir sorption isotherms were used to simulate the adsorption capacity of uranium by *Arthrobacter* sp. G975 at equilibrium (Chang and Wang 2002, Schluter 1997, Xie et al. 2008, Aksu 2001, Benguella and Benaissa 2002).

Desorption Experiments

After biosorption experiments, G975 cells were harvested to further analyze the amount of U(VI) adsorbed and accumulated inside the cells. Cells were rinsed in DIW and re-suspended in 10 mL of 10 mM Ethylenediaminetetra-acetic acid disodium salt (Na_2EDTA) solution, a strong uranium chelating agent, with the pH adjusted to 7.2 (Acharya 2009). After 10 min of gentle agitation, the samples were centrifuged and the U(VI) concentrations in the supernatant were determined with the KPA-11 instrument. This process allowed U(VI), bound to the cell membrane, to desorb back into solution. The mass of U(VI) recovered from cell walls, assumed to be equal to the mass recovered during the EDTA washing procedures, was calculated using eq. 2.

$$\mathbf{U(VI)_{adsorbed\ (recovered)}(\mu g) = C_{desorbed}\left(\frac{\mu g}{L}\right) * EDTA\ volume\ (L)} \quad (2)$$

The initial mass of uranium added and the mass of uranium in solution at equilibrium was calculated in the same fashion, using initial (C_0) and equilibrium (C_e) U(VI) concentrations considering 4 mL of the solution volume used in the biosorption experiments. Thus, the mass of internally accumulated U(VI) was estimated by solving the mass balance equation 3.

$$[U]_{Internal\ Accumulation} = [U]_{initial} - [U]_{in\ solution} - [U]_{\ adsorbed} \quad (3)$$

Cell Viability

After 24 hours exposure to U(VI) in the biosorption experiment, cells were tested for viability by counting the colony forming units (CFU), the growing cell density and the reduction

of the total organic carbon (TOC) after U-loaded G975 cells were seeded to the 5% PTYG growth media. Cell viability in CFU was assayed by inoculating a homogeneous aliquot (0.01 mL - 0.1 mL) of cells suspension prepared in serial dilutions in agar plates containing 5% PTGY medium. Serial dilutions helped to obtain colony numbers on each plate ranging between 30-300. The colony-forming units were then calculated using eq. 4.

$$\frac{CFU}{ml} = \frac{CFU * Dilution\ Factor}{Sample\ volume\ (ml)} \quad (4)$$

G975 cell growth in 5% PTYG media was monitored via spectrophotometric (UV-1601, Shimadzu) optical density at 660 nm wavelength in a separate time-based experiment conducted in triplicate. The TOC values obtained via Shimadzu TOC-VCSH analyzer were compared to the corresponding values in the U-free controls.

Microscopy Analysis

Cell morphology and surface composition analysis were examined after the biosorption experiments via an atomic force microscope (AFM) and a scanning electron microscope coupled with energy dispersive X-ray spectroscopy (SEM/EDS). Three concentrations of bicarbonate were employed in the SEM/EDS analysis: 0 mM, 5 mM, and 10 mM. After 24h of equilibration time, cells were harvested by centrifugation at 4000 rpm for 5 min and washed twice with a 50 mM of HEPES-Na prepared in deionized water (DIW). Then, the cells were fixed in the 5 mL of 2% glutaraldehyde in 0.1 M HEPES-Na buffer at pH 7.2 for 2 h at 4^{o}C. The fixative was changed at least two times. The material was removed by centrifugation and washed with 50 mM HEPES-Na buffer three times for 10 min. The rinsed cells were then dehydrated in ethanol/water solutions of 35% (v/v), 70% (v/v), and 90% (v/v) each for 10 min, and two times in 100% (v/v) for 10 min. Dehydrated samples were immersed for 10 min each in 50% and 100% pure hexamethyldisilazane (HMDS) (Pierce Biothechnology, Inc) followed by 10 min of air-drying to

allow liquid to evaporate from the sample (Fratesi et al. 2004). The dehydrated specimens were then kept in the desiccator until time of the EDS assay. Uranium- treated and control samples were mounted on aluminum stubs with double-sided sticky carbon tape. The cell surface composition was analyzed using a SEM-Energy-Dispersive-Spectrometry (SEM-EDS) Noran System Six Model 200 at magnifications of 2000.

Sample preparation procedures for AFM samples require firmly attached bacterial cells on silicon wafer substrates, such that the cells remain stable when subjected to tip forces. Bacterial samples, prewashed with DIW to remove residual U(VI), were immobilized onto the 3-aminopropyltrimethoxysilane coated silicon wafer substrates. A concentrated bacterial suspension of 5 μL was dropped onto a silanized silicon wafer (Dorobantu et al. 2008). Samples were dried under a low pressure nitrogen gas flow until excess moisture was completely evaporated. The substrates were fixed onto metallic discs using epoxy glue and transferred to the AFM stage for imaging. A Multimode Nanoscope IIIa system from Veeco Instruments (Santa Barbara, California) was used for all AFM imaging analysis. Phase imaging was performed by using Si_3N_4 soft tapping tips (BudgetSensors, Bulgaria) to ensure minimum sample damage with a force constant 7.4 N/m and resonating frequency of 150 kHz. To ensure cells viability, the complete AFM analysis was performed within two hours after the sample was prepared.

Speciation Modeling

The equilibrium speciation modeling was performed by means of Visual MINTEQ (v. 3.0, maintained by J. Gustafsson at KTH, Sweden, available at http://www.lwr.kth.se/English/OurSoftware/vminteq/ updated with the Nuclear Energy Agency's thermodynamic database for uranium) to identify the predominant uranium species in aqueous media solutions from the applied treatments. The model was run with the described

concentrations of the aqueous SGW and amended concentrations of calcium and bicarbonate. In bicarbonate-free solutions, a CO_2 partial pressure (pCO_2) was assumed to be $10^{-3.5}$ atm.

Statistical Analysis

Results with multiple experimental groups and independent factors, such as the effects of various bicarbonate, calcium, and uranium concentrations on the biosorption of U(VI), were examined with ANOVA statistics. The Holm-Sidak multiple comparison test was performed when significant differences were found between samples. All statistical tests were carried out by Sigma plot 11.2 (Systat Software Inc.). Significant levels were set to $\alpha = 0.05$.

RESULTS AND DISCUSSION

Kinetics Analysis

The dry weight of bacteria was calculated indirectly from the relationship between cell weight and cell count taken in their exponential growth phase by means of a hemocytometer. This relationship between cell numbers and dry cell weight is outlined in eq. 5 ($R^2 = 0.90$, n=2).

$$\boldsymbol{Dry\ cell\ weight\ (mg) = 6^{-10}\ \frac{mg}{cell} \cdot Cell\ Numbers} \quad (5)$$

The weight of a single G975 *Arthrobacter* cell was estimated as 600±115 fg; this value is comparable with 628±770 fg/cell obtained for E.coli (Loferer-Krößbacher et al. 1998). The ability of the *Arthrobacter* species to undergo marked changes in form during their growth was observed during the course of this study and confirmed with the literature (Van Waasbergen et al. 2000).

The biosorption rate of U(VI), $\frac{mg}{g*min}$, under various environmental conditions, provides insight on the mechanisms of the process and establishes the exposure time required for soluble U(VI) to reach sorption equilibrium, characterized by the unchanging U(VI) concentration in the solution.

The bioadsorption experiments conducted with carbonate-free SGW solutions showed that G975 *Athrobacter* sp. can effectively remove soluble U(VI). In aqueous solutions at equilibrium with CO_2 atmospheric pressure, the total U(VI) biosorption rises to 90±19% and 83±21% for 1.26 μM and 61.76 μM of initial U(VI) concentrations, respectively. At equilibrium, the same system amended with 2.5 mM of bicarbonate exhibited a significant decrease in adsorption ranging between 30±2% - 47±4%. The low removal efficiency of U(VI) in the presence of aqueous carbonate is expected in these conditions considering the strong binding affinity of actinides toward carbonate ligands. U(VI) adsorption was recorded between 12-32% across the studied concentration range within the initial 25 minutes of bacterial exposure to uranium. After the initial fast period of U(VI) adsorption, the process was gradually slowed until it reached equilibrium at 24 hours for all treatments (Figure 1). Henceforth, biosorption samples were analyzed at 24 hours for all experiments. During this time, the pH remained unchanged in all tested batches.

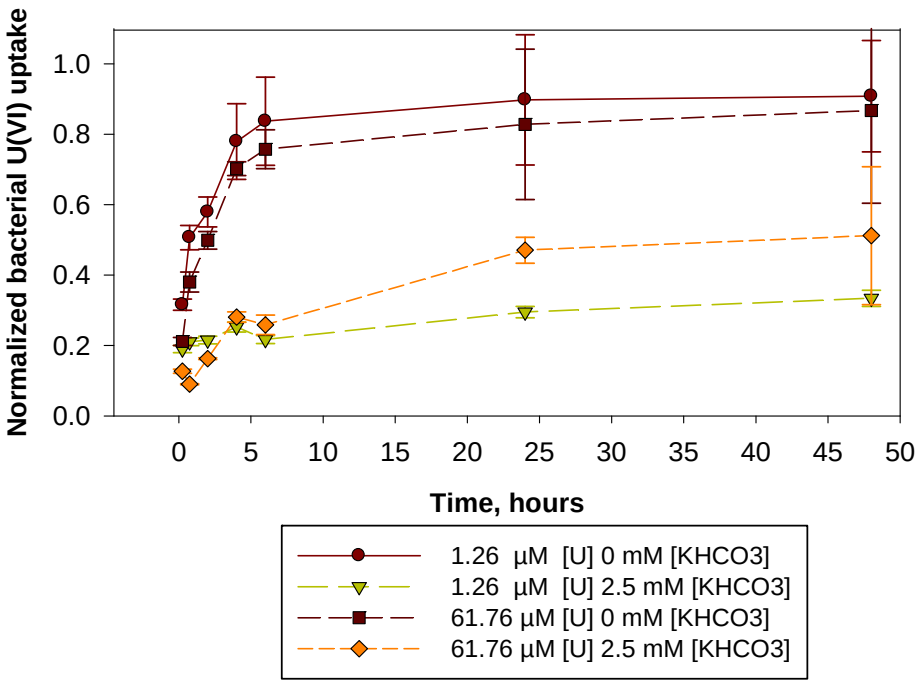

Figure 1. Normalized U(VI) uptake by *Arthrobacter* sp. G975 vs. Time, under low (1.26 µM U(VI) and high (61.76 µM U(VI)) concentrations and 0 and 2.5 mM of bicarbonate in SGW, pH 7.3, 25°C.

The controlling mechanisms of biosorption kinetics were better understood by applying the first-order, second-order, and the pseudo-second-order kinetic models to the experimental data (Benguella and Benaissa 2002, Aksu 2001). Only the pseudo-second-order model adequately describes the kinetics of uranium biosorption with the experimental data showing very little error (R^2>0.99) (Table 1); its equation is expressed as:

$$dq_t/d_t = k_2(q_e - q_t)^2 \quad (6)$$

Integration leads to

$$[1/ (q_e - q_t)] = (1/q_e) + k_2t \quad (7)$$

Or

$$(t/q_t)=(1/k_2q_e^2)+(1/q_e)\ t \quad (8)$$

Where q_e is the equilibrium adsorption capacity and q_t represents the adsorption capacity of time t (mg g^{-1}). The plot of t/q_t (mg/g) against time, t, gives a linear relationship and the k_2 and q_e was obtained from the intercept and slope, respectively (Table 1).

We can conclude from the pseudo second-order model that biosorption may be the rate limiting step and the rate is proportional to the square of the number of unoccupied sites (Aksu 2001).

Table 1. Pseudo 2nd-Order Model Simulation Sorption Kinetic Rates
k rate constant (mgU(VI)/g/min) and equilibrium adsorption capacity (Qe=mgU(VI)/g) for Arthrobacter sp. G975 in carbonate amended SGW at pH 7.3, 25°C

		Bicarbonate	
	Pseudo 2nd Order $\frac{dQ_t}{dt} = k(Q_e - Q_t)^2$ $\frac{t}{Q_t} = \frac{1}{kQ_e^2} + \frac{t}{Q_e}$	**[$KHCO_3$] 0 mM**	**[$KHCO_3$] 2.5 mM**
Uranium	**[U(VI)] 1.26 µM**	**k=0.014 ± 0.01 Q_e=3.76 (R^2=0.997)**	**k =0.012 ± 0.01 Q_e=1.37 (R^2=0.997)**
	[U(VI)] 61.76 µM	**k =7.16E-5 ± 1E-5 Q_e=213.7 (R^2=1)**	**k =3.24E-5 ± 8E-6 Q_e=132.6 (R^2=0.991)**

U(VI) Biosorption at Equilibrium in the Presence of Aqueous Bicarbonate and Ca Ions

The non-linear response surface plots (Figure 2) depict the effect of bicarbonate, calcium, and uranium concentrations at equilibrium on the U biosorption process (mg/g). Results show sharp changes in the metal biosorption, which increases with an increase in U(VI) concentration at equilibrium, and decreases by increasing values of the bicarbonate content in solution (Figure 2A). In SGW amended with 5 mM of Ca and 2.5 mM of HCO_3, U(VI) biosorption increased by 42% compared to values obtained in SGW modified merely by 2.5 mM HCO_3.

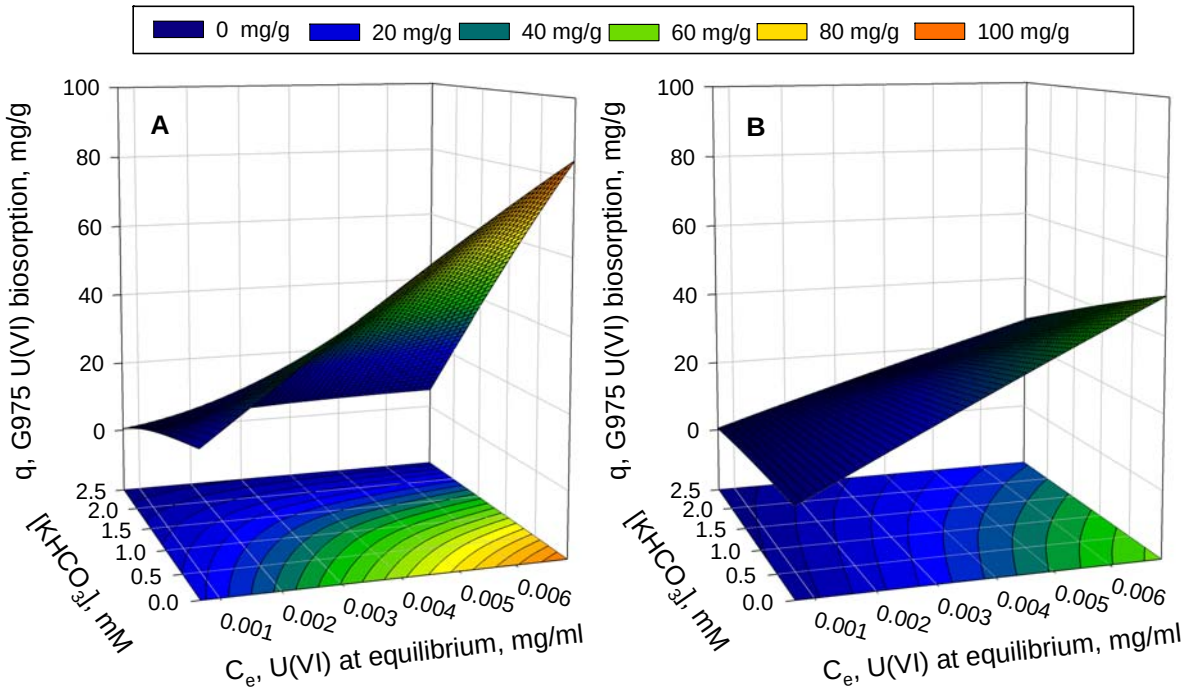

Figure 2. Response surface model, *Arthrobacter* sp. G975 uranium uptake (mg/g) by U(VI) and $KHCO_3$ concentrations at equilibrium (24 hours) in SGW, pH 7.3, 25°C with: A (Left) 0mM Ca. B (Right) 5mM Ca.

To examine the relationships between G975 adsorbed U(VI) (q) and U(VI) concentrations at equilibrium (C_e), the Langmuir, Freundlich, and Linear isotherms were fitted to the experimental data. Although the entire studied isotherm models showed a fairly good fit to the experimental data, based on higher correlation coefficients, the data can be preferably fitted with the Langmuir model. Based on the K_d values of the linear isotherms (Table 2), the adsorption capacity exponentially decays (R^2=0.998) as the bicarbonate concentration is increased in solution. Therefore, we can assume that there exists a limit close to 5 -10 mM of HCO_3 at which point carbonate-bearing experiments exhibit little or no measurable U uptake onto the bacterial surface. A summary of the results fitted to the simulated models are shown in Table 2.

Table 2. Simulated Results of Biosorption Isotherm with Langmuir, Freundlich, and Linear Equations Arthrobacter sp. G975 at various bicarbonate concentrations in SGW, pH 7.3, 25°C, 24 hours (n=3)

Ca, mM	$KHCO_3$, mM	K_L, mL/mg	S_{max}	R^2	K_F, mL/g	n	R^2	K_d, mL/g	R^2
0	0	526.3 ± 106.5	76.9 ± 15.3	0.990	1,932.0± 57.4	1.524	0.977	10,195.8 ± 791.9	0.954
0	0.5	200.0 ± 128.6	46.3 ± 29.6	0.990	2,904.0 ± 247.4	1.142	0.970	6,378.0 ± 613.9	0.982
0	2.5	23.3 ± 16.5	42.0 ± 29.7	1.00	3,288.5 ± 305.8	0.840	0.943	1,301.7 ± 63.4	0.995
0	5	130.5 ± 216.6	1.9 ± 2.9	0.550	13,152.2 ± 3,946.6	0.527	0.820	378.2 ± 52.1	0.946
5	0	92.2 ± 0.004	93.5 ± 37.4	0.998	1,845.0± 21.3	1.256	1.00	9,542.3± 1,875.5	0.928
5	2.5	27.2 ± 8.5	17.8 ± 3.9	0.910	20,749.1 ± 6,118.5	0.628	0.810	2,384.6 ± 639.5	0.874

The bacterial U(VI) uptake capacity at equilibrium with 0.0069 mg/mL of U(VI) and atmospheric CO_2 partial pressure in SGW was calculated at 84.34 ± 0.72 mg/g (Figure 2). At these conditions, 40-50% of U(VI) was removed by the bacteria. The percentage of U(VI) uptake, observed between 70-90%, tends to increase as the U(VI) concentration at equilibrium was decreased. The 5 mM addition of bicarbonate limited U(VI) adsorption to no greater than 5%. This low percent value was supported by EDS analysis, which indicates that samples with increasing bicarbonate concentrations have less U(VI) content on the cell walls compared to the control ($P<0.004$) (Table 3). Additionally, in the absence of bicarbonate, higher exposure of U(VI) to the cells resulted in higher weight % of U(VI) on the bacterial cell surface.

Table 3. Average U(VI) Bioaccumulation by G975 Arthrobacter Cells (n=3)

Strain	G975				
U(VI), mg/L	9.5	20	20	20	27
[$KHCO_3$], mM	0	0	5	10	0
U weight, %	0.52±0.25	2.29±0.88	0.58±0.37	0.29±0.24	2.82±0.8

AFM scans specified cell surface localized precipitation of uranium. As depicted on Figure 3, uranium crystalline deposits are distinctly visualized on the cell surface of uranium treated samples, while the surfaces of the control samples show no precipitation.

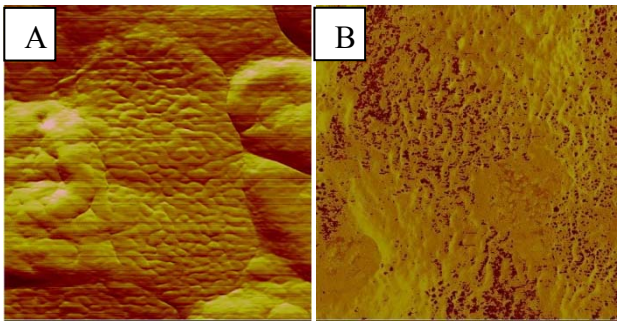

Figure 3. A) G975 control sample (scan size 2.94 × 2.94 µm^2) showing its unusual wrinkled surface morphology. B) G975 amended with 10ppm uranium (scan size 1.45 × 1.45 µm^2). Image clearly shows crystalline deposition on the cell surface.

To statistically interpret the effects of calcium ions, aqueous bicarbonate, and soluble U(VI) on the biosorption process, several combinations of various parameters were analyzed by a 3-way ANOVA model (Table 4). The ANOVA analysis concludes that a significant difference exists ($p<0.001$) between the interaction of calcium and bicarbonate. This difference is supplemented by the different K_d values for treatments with 0 and 5 mM of calcium amendments in 2.5 mM of bicarbonate-amended solutions, 1,301.7± 63.4 vs. 2,384.6 ± 639.5, respectively (Table 2). However, interactions between calcium and uranium do not make a statistically significant change to U(VI) biosorption ($p=0.448$). This statistic is supported by comparing the K_d values for 0 and 5 mM of Ca without bicarbonate ion added, 10,195.8± 791.9 vs. 9,542.3 ± 1,875.5, respectively. Due to these interactions, it is not possible to provide an unambiguous interpretation on isolated factors, such as calcium, whose effects on biosorption response depends on the amount of bicarbonate and uranium present in solution.

Table 4. 3-Way Analysis of Variance

Source of Variation for U(VI) Biosorption	**DF**	**SS**	**MS**	**F**	**P**

Ca	1	208.327	208.327	184.275	<0.001
Ce, U(VI)	1	6029.784	6029.784	5333.640	<0.001
$KHCO_3$	1	4708.991	4708.991	4165.333	<0.001
Ca, x Ce, U(VI)	1	0.688	0.688	0.608	0.448
Ca, x $KHCO_3$	1	1467.674	1467.674	1298.229	<0.001
Ce, U(VI) x $KHCO_3$	1	1856.056	1856.056	1641.773	<0.001
Ca x Ce, U(VI) x $KHCO_3$	1	533.412	533.412	471.829	<0.001
Residual	14	15.827	1.131		
Total	21	17036.209	811.248		

Normality Test (Shapiro-Wilk) Passed (P = 0.104)

Desorption Experiments

Desorption experiments were conducted to differentiate the amount of U(VI) externally adsorbed on the cell surface from that taken up by cells for internal accumulation. The results shown on Figure 4 revealed the presence of U(VI) accumulation inside the cell across the experimental range of studied U(VI) concentrations (0.005 μM-0.247 μM). The percentage of U(VI) uptake accumulated inside the cell was found comparable to the externally adsorbed U(VI) on the cell walls. Previous studies via TEM/EDS confirmed the presence of bioaccumulated U inside the cells (Choudhary and Sar 2011). The addition of 2.5 mM of bicarbonate resulted in limited adsorption (Figure 4).

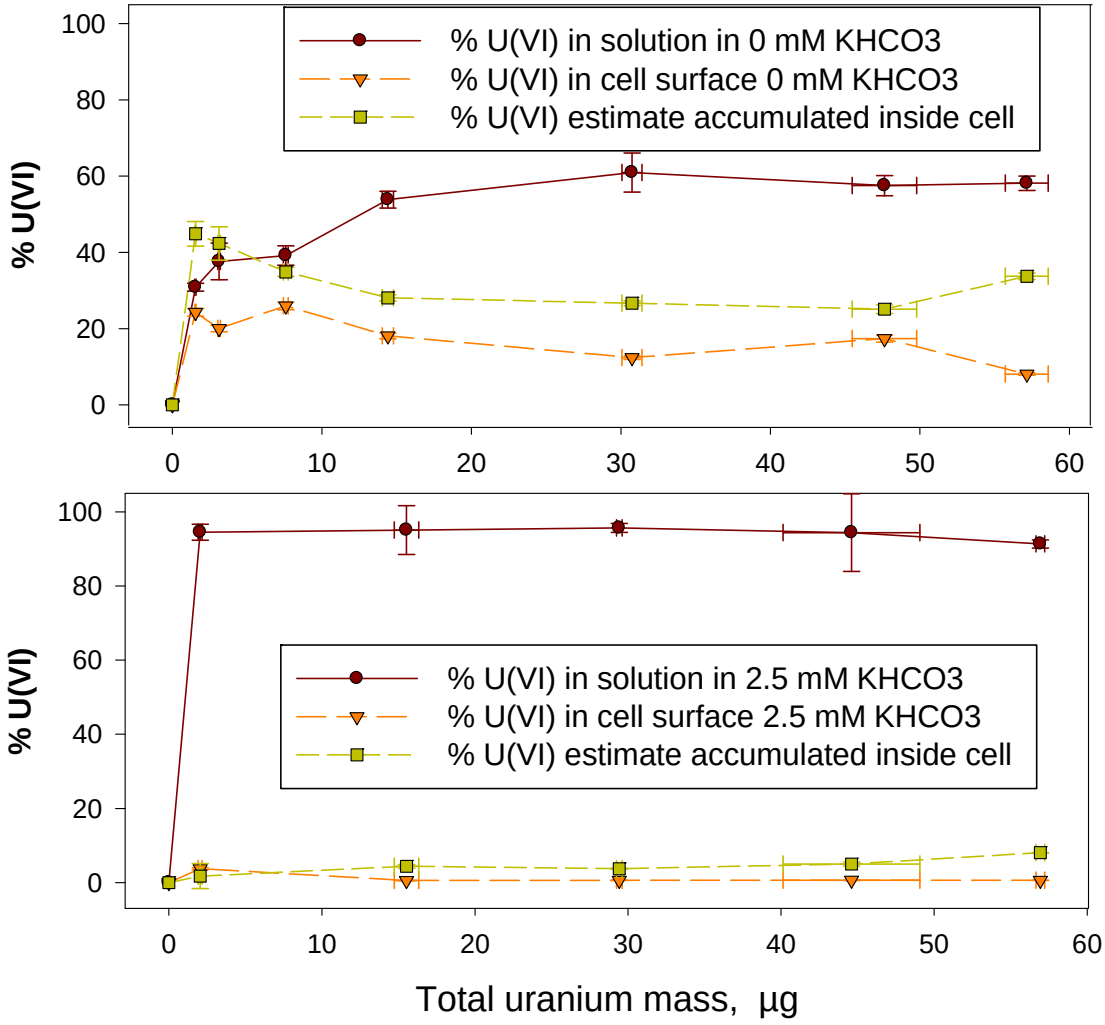

Figure 4. Calculated percentages of U(VI) distribution in SGW solution, adsorbed on bacterial cell, and accumulated inside cells at 0 and 2.5mM bicarbonate concentrations (at pH 7.3, 25°C, 24 hours).

Cell Viability

The total number of surviving cells, after the 24 hours exposure to U(VI) in selected treatments, were differentiated from dead cells by the number of CFU grown. The number of cells able to resume growth activity after exposure to U(VI) compared to the initial cell density (approximately 8.85E+10±8.61E7 CFU) provides a gauge of the U(VI) toxicity and its effects on G975 cells. It is observed that, at 84 µM of U(VI) in SGW amended with 5mM Ca, the number of surviving cells is increased by 68%, and by 1,166% in the presence of 2.5 mM of $KHCO_3$

(Figure 5). The combination of 5 mM Ca with 2.5 mM of $KHCO_3$ yielded 23% fewer viable cells than the treatment with 2.5 mM of $KHCO_3$ alone, which could be a result of the larger U(VI) sorption observed (Figure 2), leading to an increased effect of U(VI) toxicity on the living cells. Overall, based on the grown CFU, the presence of Ca and KHCO3 inhibit the capability of U to damage the cells ability to grow.

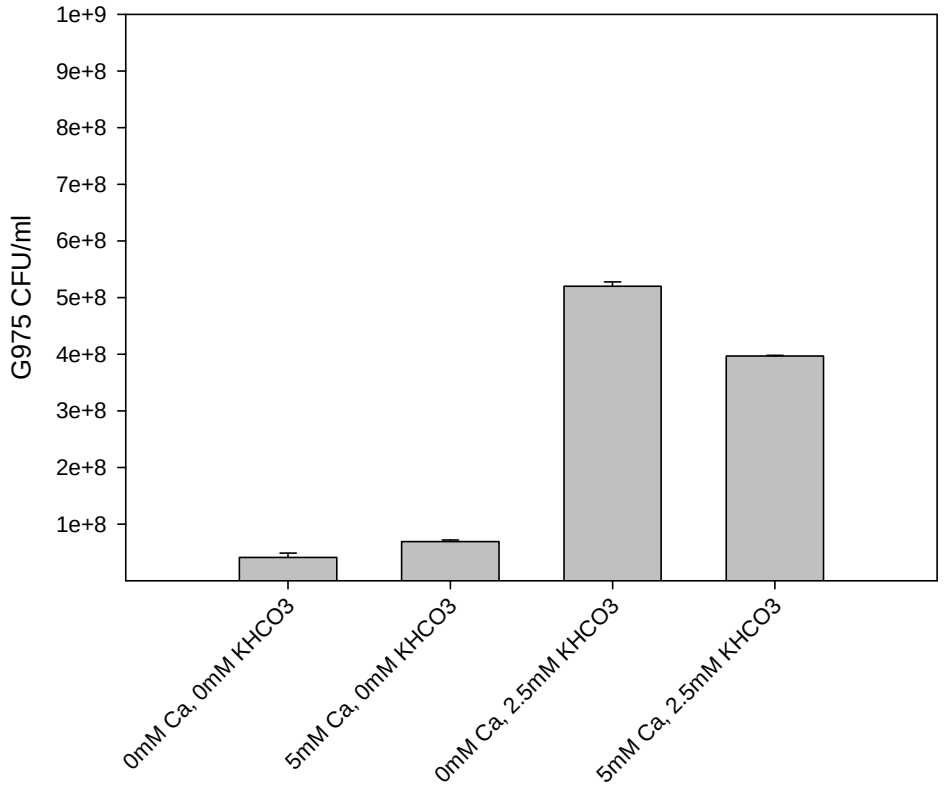

Figure 5. Observed changes in G975 CFU grown in 5% PTYG agar plates after 24 h exposure to 84µM U(VI)-bearing SGW amended with bicarbonate (0 and 2.5 $KHCO_3$), and calcium (0 and 5 mM) at pH 7.3, 25°C.

Cells previously treated with 84 µM of U(VI) in bicarbonate-free solution consumed 5.2±0.2% of the initial TOC value of 818.8±59 mg/L when seeded in the fresh 5% PTYG media. In contrast, samples exposed to the same concentration of U(VI) in solutions bearing 5 and 10 mM of bicarbonate consumed 41±13% and 48±13% of TOC, respectively (Figure 6). Samples with 5 mM of added Ca showed a 0.2% and 5% difference in TOC consumption in

solutions amended with 0 and 2.5 mM of bicarbonate, respectively. Uranium in the presence of bicarbonate forms highly soluble U(VI)-carbonate complexes that lessen U(VI) toxicity on bacterial cells. In Ca-rich solutions, Ca binds with U(VI) and bicarbonate, creating strong Ca-uranyl-carbonate complexes which would dominate the aqueous U(VI) budget (Kalmykov and Choppin 2000). In addition, since Ca is a structural component within the cell wall of Gram-positive bacteria (Beveridge and Koval 1981) it has a relatively small amount of adsorption onto the bacterial surface (Fowle and Fein 1999). However, irreversible Ca binding to specific functional groups can compete with U, making these sites unable to adsorb U(VI) and, as a consequence, reduce the toxic effects of U(VI) on bacterial cells. Nevertheless, the shielding effect created by bicarbonate against U toxicity was observed to be much stronger than that of calcium; there were no observable differences found between the control treatments without U(VI) and those amended with U(VI) at 5-10 mM of HCO_3 in solution (Figure 6).

The liner relationship (R^2>0.997) between the optical density and the number of cells in bacterial suspension was utilized to monitor the cells ability to multiply over time (Figure 7):

$$\text{Cell density, cell/mL} = (\text{ABS} - 0.00873)/4.85\text{E-}10 \quad (9)$$

At 48 hours the absorbance changes in U(VI)- free controls showed that the addition of bicarbonate did not affect cell densities, which converged at 8.7E8 cells/mL. The G975 cells exposed to 84μM of U(VI) in bicarbonate-free and 5 mM bicarbonate solutions averaged 62.5%, and 35.1% reduction in cells density, correspondingly, while growing over the same time period in 5% PTYG (Figure 7). Compared to experiments using SGW, the addition of 5 mM of calcium increased the cell density by 27.8% and 1.7% for the solutions amended with 0 and 2.5 mM of bicarbonate, respectively.

Inhibition of bacteria activity appears to be associated with the binding of U(VI) to the cell envelope. The passive binding of uranyl to cell surfaces reduces membrane fluidity and

permeability limiting media nutrient uptake. However, the presence of carbonate can mitigate this effect by stripping uranyl from the cell surface and forming uranyl-carbonate complexes in solution (Bencheikh-Latmani and Leckie 2003). These observations support our results showing that the cell metabolism is being impaired by uranium, but mitigated in the presence of bicarbonate (Figure 5, Figure 6). Triggered by the addition of U(VI) to the media, a decrease in TOC consumption was found consistent with the loss in cell density.

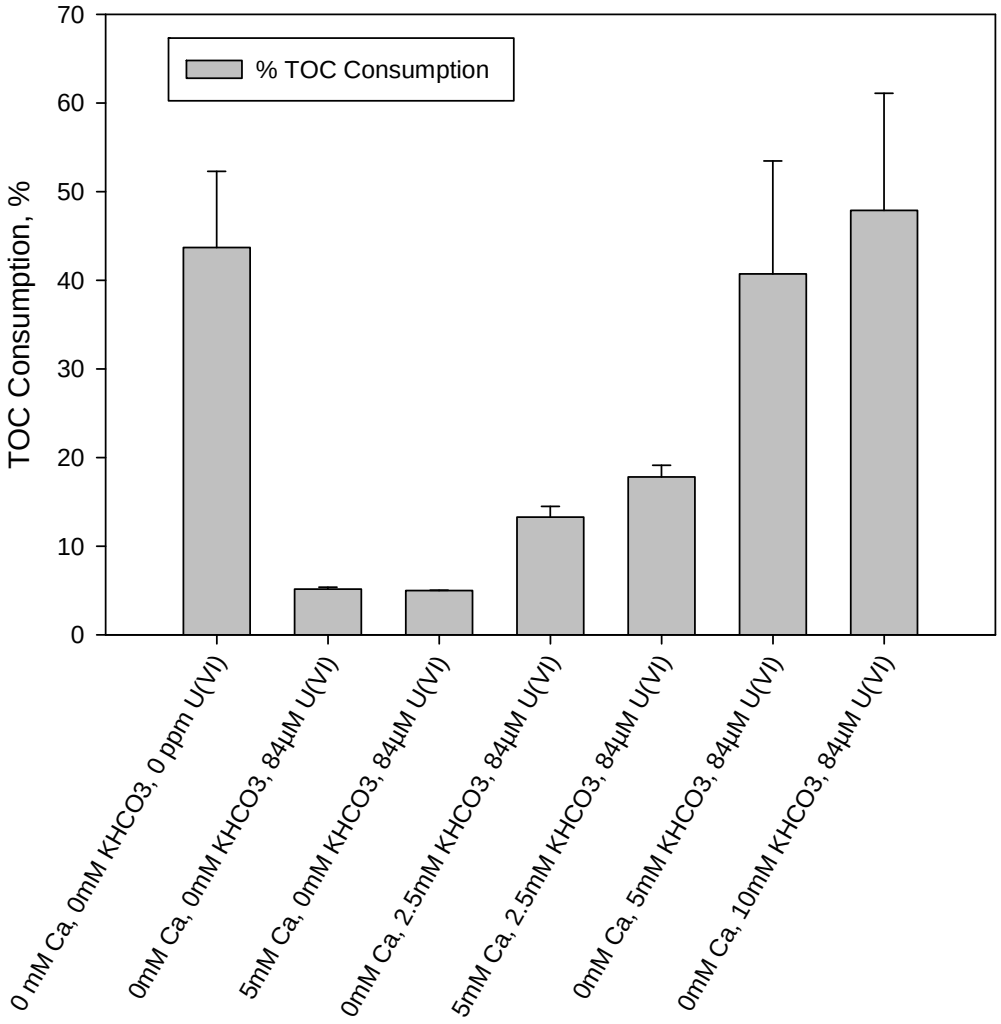

Figure 6. Observed changes in TOC consumption of G975 cells grown in 5% PTYG media after exposure to U(VI)-free and 84µM U(VI)-bearing SGW amended with bicarbonate (0, 5, and 10 of KHCO3), and calcium (0 and 5 mM) at pH 7.3, 25°C for 24 h.

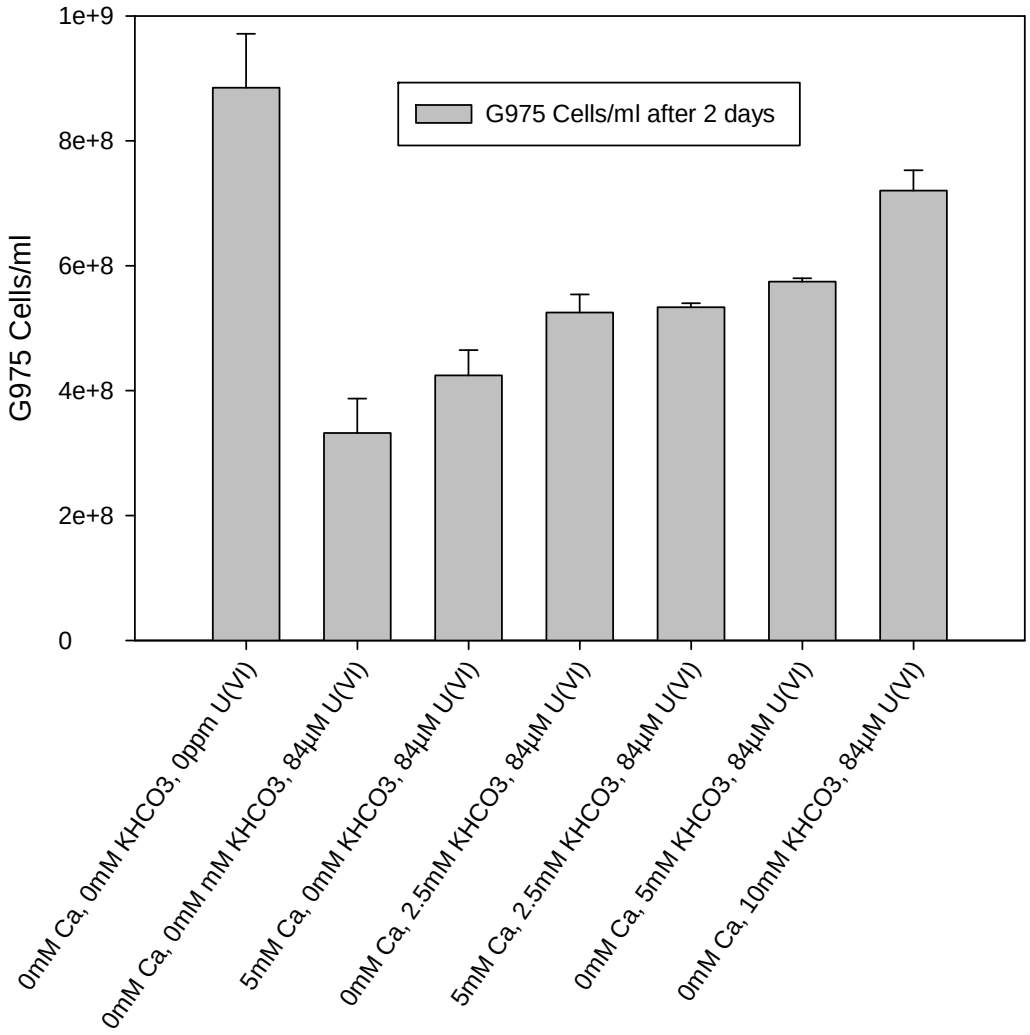

Figure 7. Observed changes in G975 cells population density grown in 5% PTYG after exposure to U(VI)-free and 84µM U(VI)-bearing SGW amended with bicarbonate (0, 2.5, 5, 10 mM KHCO3) and calcium (0 and 5 mM) at pH 7.3, 25°C for 48 h.

Visual MINTEQ Speciation Modeling

The mitigation effect of bicarbonate on the toxicity of cells exposed to U (VI) can be partially explained using Visual MINTEQ-based speciation modeling (Figure 8). Based on the modeling predictions, it is likely that the $(UO2)_3(OH)^{5+}$ species plays an important role on U(VI) toxicity since its concentration undergoes the largest changes in the presence of bicarbonate ions for 0.32 µM and 84 µM of U(VI). In fact, the trimetric form of uranium, $(UO2)_3(OH)^{5+}$, is the most positive species and has the most potential to interact or damage negatively charged cell

walls. The MINTEQ model predicted that increasing the bicarbonate concentrations in solution causes accumulation of negatively-charged uranium-carbonate complexes, thus reducing the concentration of the total positive species in the solution. At 84µM of U(VI), as the carbonate concentration increases from 0 to 10 mM, the total U(VI) concentration of $UO_2(CO_3)_3^{-4}$ species increases. This change in soluble bicarbonate concentrations makes negatively charged ions containing U to be less interactive with the negatively charged cell surfaces.

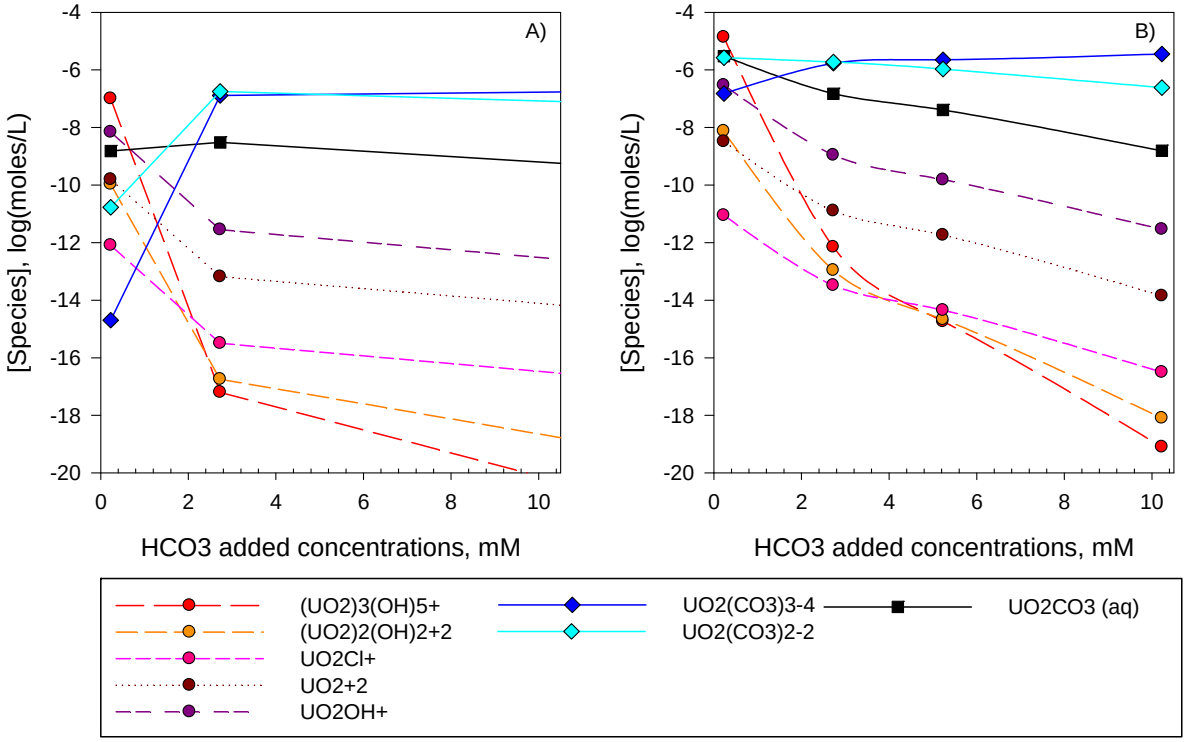

Figure 8. Visual MINTEQ U(VI) speciation modeling summary for U species in SGW at A) 0.32 µM U B) 84 µM U at pH 7.3, 25°C for different bicarbonate concentrations.

In the case where no Ca or bicarbonate was present in solution, U(VI) speciation is dominated by more positive species (Figure 9). The MINTEQ model shows that when 5 mM of Ca is present in the SGW matrix, the $Ca_2UO_2(CO_3)_3$ (aq) uranium-bicarbonate species grow the fastest as U(VI) concentrations are increased. Combining both, 5 mM of Ca and 2.5 mM of $KHCO_3$, generates $Ca_2UO_2(CO_3)_3$ (aq) as the major species of uranium followed by $UO_2(CO_3)_3^-$

^{4}. The negligible amount of positive species and high concentrations of neutral and negative U(VI) species justifies our previous results showing lower percentages of biosorption and stimulation of bacterial viability.

The biosorption results are in agreement with the MINTEQ modeling results. Uranium sorption is greatest in the absence of both Ca and $KHCO_3$, which can be attributed to the high affinity between the positively charged U species and the negatively charged cell membrane. Ca by itself produces unsubstantially less positive U(VI) species that slightly reduces the percent of U(VI) sorption. However, in the presence of $KHCO_3$ or in combination with Ca, negative and neutral U species are predominant. These species do not strongly interact with the negatively charged bacteria surface compared to positively charged species and, as a result, these treatments produce the least amount of U sorption. These finding confirm the results of previous studies, where U(VI) toxicity was mitigated by the presence of bicarbonate species (Hogan et al. 2005, VanEngelen et al. 2010).

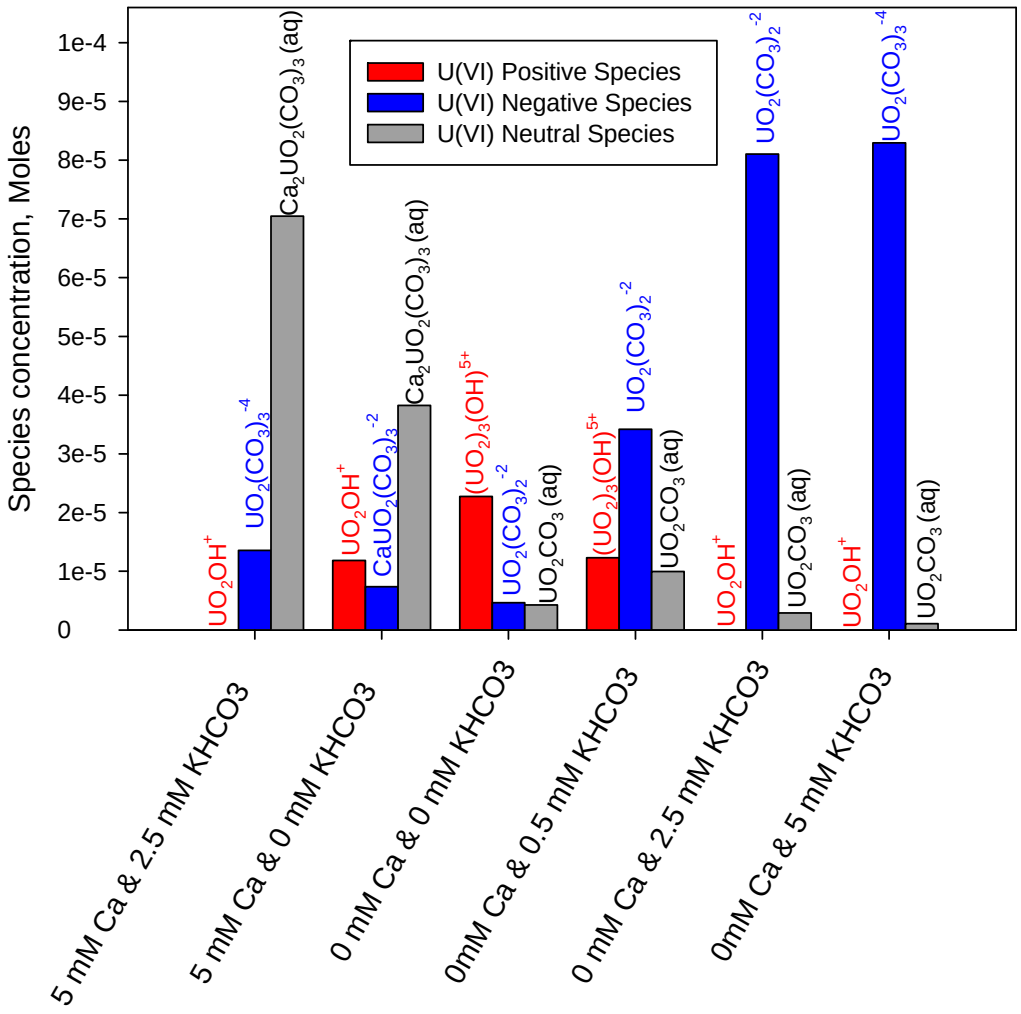

Figure 9. Visual MINTEQ U(VI) speciation modeling summary in SGW with 0 or 5 mM of Ca, 0,0.5,2.5, and 5 mM of bicarbonate at 84 µM, pH 7.3, 25°C.

CONCLUSION

The *Arthrobacter* G975 strain, which roughly accounted for up to 25% of subsurface isolates, was used in the experiments. The study confirmed that *Arthrobacter* sp. G975 can effectively remove soluble U(VI) ions from aqueous solution. The U(VI) bioaccumulation was measured up to 83-90% for the aqueous solutions at equilibrium with CO_2 atmospheric pressure. Kinetics data analysis confirmed that the process follows a pseudo second-order kinetics model (R^2>0.991). It was conclusively proven that the presence of aqueous bicarbonate and Ca ions can

affect the sorption behaviors of U(VI). The maximum biosorption capacity of U(VI) ions in the studied U(VI) concentration range at 25°C by *Arthrobacter* sp. G975 was observed at 99.7±2.95, 42.4±4.5, 20.6±6.5, and 5.5±5.2 mg/g for 0, 0.5, 2.5, 5 mM bicarbonate-bearing solutions, respectively. The incremental increase in aqueous bicarbonate concentrations exponentially reduced the U(VI) microbial bioaccumulation compared to values obtained in carbonate-free SGW. Experimental data indicates that increasing bicarbonate concentrations to 0, 0.5, 2.5 and 5 mM reduced the maximum U(VI) bioaccumulation by approximately 0%, 57±5%, 79±7% and 94±5%, respectively. The Langmuir isotherm models produced a higher correlation coefficient with the experimental data than the Linear and Freundlich adsorption models. Despite the large biosorption capacity, there is experimental evidence to suggest that some U(VI) is accumulated inside the cell. In the presence of bicarbonate, when highly soluble and mobile carbonate complexes dominate the aqueous speciation of U(VI), the viability of cells treated with U(VI) was increased. Although the highest U(VI) biosorption by A. G975 strain was obtained in bicarbonate-free SGW, this bacterial strain remained very effective across all bicarbonate and calcium concentrations tested. These results are a strong affirmation that bacterial adsorption/bioaccumulation can significantly affect the mobilities of uranyl species in Ca-rich carbonate-bearing subsurface environments.

ACKNOWLEDGEMENTS

Funding for this research was provided by US DOE Grant Number: DE- EM0000598. We would like to thank Dr. David Balkwill for providing us with *Arthrobacter* sp. strains and acknowledge Dr. Yanqing Liu and Rakesh Guduru for their assistance with the AFM, SEM images and EDS analysis of bacterial surface composition.

REFERENCES

Balkwill, D. L., Reeves, R. H., Drake, G. R., Reeves, J. Y., Crocker, F. H., Baldwin K, M., and D. R. Boone, 1997. Phylogenetic characterization of bacteria in the subsurface microbial culture collection," FEMS microbiology reviews, vol. 20, pp. 201-216.

Beveridge, T.J., Koval, S.F., 1981. Binding of metals to cell envelopes of Escherichia coli K-12. Appl. Environ. Microbiol. 42, 325–335.

Boylen, C.W., 1973. Survival of Arthrobacter crystallopoietes during prolonged periods of extreme desiccation. Journal of Bacteriology, vol. 113, pp. 33.

Choudhary, S., Sar, P., 2011. Uranium biomineralization by a metal resistant Pseudomonas aeruginosa strain isolated from contaminated mine waste. Journal of Hazardous Materials 186, p. 336–343.

Crocker, F. H., Fredrickson, J. K., White, D. C., Ringelberg, D. B. and D. L. Balkwill, 2000. Phylogenetic and physiological diversity of Arthrobacter strains isolated from unconsolidated subsurface sediments, Microbiology, vol. 146, pp. 1295.

Fein, J.B., Daughney, C.J., Yee, N., Davis, T.A., 1997. A chemical equilibrium model for metal adsorption onto bacterial surfaces. Geochim. Cosmochim. Acta 61, 3319–3328.

Finch R.J. and Murakami, T., 1999. "Systematics and paragenesis of uranium minerals. in" Uranium: Mineralogy, Geochemistry and the Environment", PC Burns & B. Finch, eds," Rev. Mineral. Geochem, vol. 38, pp. 91–179.

Fowle, D A. and Fein, J B.,1999. Competitive adsorption of metal cations onto two gram positive bacteria: Testing the chemical equilibrium model. Geochimica et Cosmochimica Acta, Vol. 63, No. 19/20, pp. 3059–3067.

Fowle, D.A., Fein, J.B., Martin, A.M., 2000. Experimental study of uranyl adsorption onto Bacillus subtilis. Environ. Sci. Technol, V. 34, pp. 3737–3741.

Fredrickson, J. K., Zachara, J. M., Balkwill, D. L., Kennedy, D., Li, S. W., Kostandarithes, H. M., Daly, M. J., Romine, M. F. and Brockman, F.J. , 2004. Geomicrobiology of high-level nuclear waste-contaminated vadose sediments at the Hanford Site, Washington State, Applied and Environmental Microbiology, vol. 70, pp. 4230.

Grenthe I., Fuger J., Konings R. J. M., Lemire R. J., Muller A. J., Nguyen-Trung C., and Wanner H, 1992. Chemical Thermodynamics of Uranium. Elsevier, Amsterdam.

Guillaumont, R., Fanhänel, T., Fuger, J., Grenthe, I., Neck, V., Palmer D.A. and M.H. Rand, 2003. Chemical Thermodynamics, OECD Nuclear Energy Agency vol. 5, Elsevier, 919 pp.

Hogan AC, vanDam RA, Markich S, Camilleri C. 2005. Chronic toxicity of uranium to a tropical green alga (Chlorella sp.) in natural waters and the influence of dissolved organic carbon. Aquatic Toxicol 75:343–353.

Kalmykov, SN., and G.R. Choppin, 2000. Mixed Ca2+/UO22+/CO32- complex formation at different ionic strengths. Radiochimica Acta: Vol. 88, pp. 603.

Knox, A. S., Brimon, R. L., Kaplan, D. I., and M. H. Paller, 2008. Science of the Total Environment 395:63

Langmuir, D., 1978. Uranium solution-mineral equilibria at low temperatures with applications to sedimentary ore deposits. Geochimica et Cosmochimica Acta, 42, pp. 547-569.

Langmuir, D., 1997. Aqueous environmental geochemistry Prentice Hall. Upper Saddle River, NJ.

Liu, C., Jeon, B., Zachara, J.M., Wang, Z., 2007. Influence of Calcium on Microbial Reduction of Solid Phase Uranium (VI). Biotechnology and Bioengineering, 97, 6, p.1415-1422.

Loferer-Krößbacher, M., Klima, J. and R. Psenne, 1998. Determination of Bacteria Cell Dry Mass by transmission Electron Microscopy and Densitometric Image Analysis. r. s.l. : Appl Environ Microbiol, 64,2, pp. 688-694.

Montgomery, D. C. (2008). The 2k Factorial Design . In D. C. Montgomery, *Design and Analysis of Experiments* (7th edition ed., pp. 207-229). New York : John Wiley & Sons, INC.

Murphy W. M. and Shock E. L., 1999. Environmental Aqueous Geochemistry of Actinides. In Uranium: mineralogy, geochemistry and the environment, Vol. 38 (ed. P. C. Burns and R. Finch), pp. 221-254. Mineralogical Society of America.

Van Waasbergen, L.G., Balkwill, D. L., Crocker, F. H., Bjornstad, B. N., and R. V. Miller, 2000. Genetic diversity among Arthrobacter species collected across a heterogeneous series of terrestrial deep-subsurface sediments as determined on the basis of 16S rRNA and recA gene sequences. Applied and environmental microbiology, vol. 66, pp. 3454.

VanEngelen, MR., Field, EK., Gerlach, R., Lee, BD, Apel, WA and Peyton, BM., 2010. UO_2^{+2} speciation determines uranium toxicity and bioaccumulation in an environmental Pseudomonas sp. isolate. Environmental Toxicology and Chemistry, Vol. 29, No. 4, pp. 763–769.

Zachara, J.M., Smith, S.C, 2004. Groundwater Sampling and Characterization of 300-FF-5 Uranium Plume Sediments and Groundwaters. Pacific Northwest National Laboratory.